NASA CR 120821

118

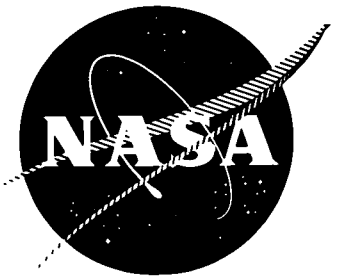

DESIGN AND DEVELOPMENT OF A SMALL STRUCTURALLY INTEGRATED ION THRUSTER SYSTEM

CONTRACT NAS 3-14129

OCTOBER 1971

PREPARED FOR

NASA LEWIS RESEARCH CENTER
CLEVELAND, OHIO 44135

SHIGEO NAKANISHI, PROJECT MANAGER

HUGHES RESEARCH LABORATORIES
A DIVISION OF HUGHES AIRCRAFT COMPANY
3011 MALIBU CANYON ROAD
MALIBU, CALIFORNIA 90265

1. Report No.	2. Government Accession No.	3. Recipient's Catalog No.
CR-120821		

4. Title and Subtitle	5. Report Date
DESIGN AND DEVELOPMENT OF A SMALL STRUCTURALLY INTEGRATED ION THRUSTER SYSTEM	October 1971
	6. Performing Organization Code
7. Author(s)	8. Performing Organization Report No.
Julius Hyman, Jr., (see Program Participation Page)	
	10. Work Unit No.
9. Performing Organization Name and Address	11. Contract or Grant No.
Hughes Research Laboratories 3011 Malibu Canyon Road Malibu, California 90265	NAS 3-14129
	13. Type of Report and Period Covered
12. Sponsoring Agency Name and Address	Contractor Report
National Aeronautics and Space Administration Washington, D.C. 20546	14. Sponsoring Agency Code

15. Supplementary Notes

16. Abstract

A 5 cm Structurally Integrated Ion Thruster (SIT-5) has been developed for attitude control and station keeping of synchronous satellites. With 2-D vectorable grids (±10°), thrust is 0.56 mlb at beam voltage V_B = 1200 V ($I_{sp,eff}$ = 2220 sec), total mass efficiency η_m = 64%, and electrical efficiency η_E = 46.8%. Nonvectoring thrust of 0.41 mlb has also been demonstrated at very low specific impulse ($I_{sp,eff}$ = 1665 sec) with dielectric coated grids at V_B = 650 V, η_m = 65%, and η_E = 40%. Structural integrity is demonstrated with dielectric coated grids for shock (30 G), sinusoidal (9 G), and random (19 G^2/Hz) accelerations. System envelope is 31.6 cm long by 14 cm flange B.C. with a mass of 8.5 kg including 6.2 kg mercury propellant.

17. Key Words (Suggested by Author(s))	18. Distribution Statement
Mercury Propellant Electron Bombardment Ion Propulsion System Vibration Test Performance Test 5 cm Diameter	Unclassified - Unlimited

19. Security Classif. (of this report)	20. Security Classif. (of this page)	21. No. of Pages	22. Price*
Unclassified	Unclassified	145	$3.00

* For sale by the National Technical Information Service, Springfield, Virginia 22151

PROGRAM PARTICIPATION

Contributions by members of the HRL technical staff who participated in the program are acknowledged below.

PROGRAM MANAGEMENT	J. Hyman, Jr.
DESIGN	S. Kami
THERMAL ANALYSIS	J.R. Bayless and J.W. Ward
DYNAMIC ANALYSIS	H.H. Cooley, Jr.
STRESS ANALYSIS	M.M. Frisman
STRUCTURAL TESTING	J.R. Bayless, P.E. Burnell, and W.J. Davis
SUBASSEMBLY TESTING	J.R. Bayless and J.D. Thompson
THRUSTER TESTING	J.R. Bayless and C.R. Dulgeroff

TABLE OF CONTENTS

LIST OF ILLUSTRATIONS

LIST OF TABLES

ABSTRACT

A 5 cm Structurally Integrated Ion Thruster (SIT-5) has been developed for attitude control and station keeping of synchronous satellites. With 2-D vectorable grids (±10°), thrust is 0.56 mlb at beam voltage V_B = 1200 V ($I_{sp,eff}$ = 2220 sec), total mass efficiency η_m = 64%, and electrical efficiency η_E = 46.8%. Nonvectoring thrust of 0.41 mlb has also been demonstrated at very low specific impulse ($I_{sp,eff}$ = 1665 sec) with dielectric coated grids at V_B = 650 V, η_m = 65%, and η_E = 40%. Structural integrity is demonstrated with dielectric coated grids for shock (30 G), sinusoidal (9 G), and random (19 G^2/Hz) accelerations. System envelope is 31.6 cm long by 14 cm flange B.C. with a mass of 8.5 kg including 6.2 kg mercury propellant.

SECTION I

SUMMARY

A 5-cm Structurally Integrated ion Thruster system (SIT-5) was developed under Contract NAS 3-14129. Extensive analysis accompanied the design of this thruster system to insure compatibility of the propulsion device both with the launch environment and with the thermal and mechanical environments imposed by the host spacecraft. The completed thruster system underwent a comprehensive test program, including vibration testing to demonstrate structural integrity and performance testing both with dielectric coated grids and with thrust vectoring double grid optics. Thruster tests were complemented by an accompanying program of component testing, including separate tests of the Cathode Isolator Vaporizer (CIV) subassembly and the Neutral Vaporizer (NV) subassembly, and the Reservoir Feed System (RFS) subassemblies. These tests serve to confirm the basic viability of the thruster system and define its limits of performance.

In design of the SIT-5 system, emphasis was placed on both structural and thermal integration of all components to achieve minimum size, maximum structural strength, and maximum over-all efficiency. Structural design centered about the concept that the thruster system should be supported at the point of maximum mass concentration. On this basis the propellant reservoir is supported by a mounting flange at the equator of the spherical mercury tank. The thruster itself is cantilevered from that location by a main support structure and insulated from that structure by four ceramic insulators. The neutralizer is attached to the ground screen

enclosing the thruster assembly which is also cantilevered from the main mounting flange. The main cathode was designed as part of an integral combination with the isolator and the main vaporizer. In this subassembly minimum separation is provided between the various elements. This allows the cathode, isolator, and vaporizer to be coupled closely to one another, thereby minimizing the over-all extent and also permitting heat transfer between several elements. In this way, cathode heat (which is conducted from the cathode tip) is used effectively to maintain the downstream end of the isolator assembly at the required temperature. Similarly the heat rejected from the main vaporizer assembly is conducted toward the upstream end of the isolator so that no separate heater is required for the isolator assembly. The same philosophy was used in design of the neutralizer-vaporizer subassembly. The vaporizer was placed as close to the neutralizer cathode as permitted by the requirements of avoiding thermal runaway.

Elements of the thermal design were checked against a comprehensive computer-aided thermal analysis, in which the temperatures of the thruster were calculated under varying environmental conditions, including exposure to full sunlight or spacecraft shadow, operation at full power or with discharge extinguished, and location of thruster near to or within the spacecraft as opposed to far from the spacecraft. Temperatures were calculated under various combinations of these conditions to assure that all temperatures remain within acceptable boundaries, set, for instance, by the requirement that mercury propellant not be allowed to freeze within the reservoir of the feed lines and that the temperature of the reservoir should not exceed the maximum allowable values for the butyl rubber bladder which forms part of the reservoir system. The coupling characteristics of the two

vaporizers with their associated cathodes were also checked with this thermal analysis to see that the coupling was kept to as high a value as permissible within the constraint of maintaining thermal control over vaporizer temperature by the vaporizer heater and not having its temperature rise uncontrollably in response to thermal coupling with the cathode.

Comprehensive mechanical and dynamic analysis was also carried out. The analysis was initiated by a mathematical model of the thruster system in which it is represented as a matrix of lumped masses joined by spring tensors. By means of the MARS computer program, this model was subjected mathematically to the dynamic environment of thruster launch. System responses to the dynamic environment are generated by this program and expressed in terms of amplitude displacement. Displacement amplitudes in turn are related to material stresses, which permit stress analysis of the thruster system subject to the dynamic environment. Where structural weaknesses were identified by this procedure, corrective action was taken. Similarly, regions that appeared to be over designed were reduced in size in order to minimize over-all system mass. The final proof of structural integrity was indicated by a dynamic test in which the thruster was subjected to shock (30 G), sinusoidal (9 G) and random (19 G^2/Hz) vibrations. This test demonstrated a high degree of structural integrity and only minor changes were required to insure a satisfactory launch capability.

The CIV, NV, and RFS subassemblies were tested to establish their performance before assembly and testing of a complete thruster system. Generally, satisfactory results were demonstrated in each of these tests. The CIV demonstrated a capability for operation throughout the range of parameters anticipated in thruster operation. The isolator

was shown to be capable of holding off voltages to 1 kV with current leakage less than 5 μA. Temperature profiles from the cathode tube, the isolator, and the vaporizer were found to be generally satisfactory with no cold spots developing and over-all power close to the minimum anticipated values. Similar satisfactory performance was obtained with the NV subassembly. A general characteristic was identified which indicated decreasing coupling voltage between the neutralizer cathode and a screen collector with increasing current to the keeper associated with that cathode. Testing with the RFS subassembly served to establish the pressure retention capability of the positive expulsion propellant reservoir and to establish the long term capability for vaporizer phase separation under steady state and cyclic conditions. The same mercury propellant reservoir feed line and vaporizers were used in this test as had earlier been subjected to the dynamic environment imposed by the structural integrity tests.

Two 50 hour and one 100 hour tests were conducted to document performance of the SIT-5 propulsion system. An initial 50 hour performance test with a laboratory type feed system utilizing dielectric-coated optics was carried out to demonstrate the effectiveness of discharge chamber optimization. In this test the contractual goal for thruster operation, with an over-all efficiency of η_T = 26.6% was approximated. The best over-all performance was obtained with the electrical efficiency at η_E = 40% and the propellant utilization efficiency of η_m = 65%, including neutralizer losses which averaged about 9% of total propellant flow. The thruster system performance test was concluded with a cyclic test consisting of 10 cycles of startup and shutdown. The objective of the cyclic test was to provide performance data for the SIT-5 to go from a low level standby condition to a state of full power and return to the low level condition.

The low level condition, with a standby power of 10.3 W and total mercury flow rate equivalent of $I_{T,Hg}$ = 3.8 mA, was consistent with low power and low propellant consumption while maintaining the main cathode-to-keeper and neutralizer-to-cathode keeper discharges. Transition from the standby condition to full beam operation lasted about 10 min. After 20 min the thruster was operating under full normal conditions, with the exception that the main keeper current held at 300 mA to avoid extinction of the main discharge. After 40 min the main keeper current could be set to the normal operating value of 100 mA. When cathode-to-keeper discharges were extinguished, re-ignition was assured by utilization of a keeper discharge power supply with an open circuit voltage of 460 V. Starting from an extinguished condition with a vaporizer temperature at T_V = 100°C, ignition of the main cathode was acquired after 8 min with a main cathode heater power of 32 W, and of the neutralizer after 6 min with a neutralizer cathode heater power of 28.5 W.

In a second test, the complete SIT-5 thruster assembly was operated with its dielectric-coated ion extraction system to verify operation and conformance with design criteria. Conformance with electrical performance criteria was obtained from a 50 hour test of the S/N 101 thruster system with an electrical efficiency η_E = 38%. Anomalous behavior of the main cathode vaporizer subassembly, however, prevented meaningful measurement of the mass utilization efficiency.

The 13 month development of the SIT-5 thruster system was culminated with completion of the final 100 hour durability test. This operation served to evaluate the level of system performancy (including its ±10° thrust vectoring capability) when paired with the beam deflection device developed at the Hughes Research Laboratories (HRL) under Contract NAS 3-14058. In this configuration, the system

was operated at an electrical efficiency η_E = 46.8% with a propellant utilization efficiency η_m = 64% (including neutralizer losses).

SECTION II

INTRODUCTION

Mission and systems analyses have demonstrated the suitability of electron-bombardment ion thrusters for attitude control and station keeping of synchronous satellites where low system mass and long life are major requirements. This suitability is furthered by component improvements found in research thruster tests with beam voltages considerably below those previously required. Research both at the Lewis Research Center of NASA and at the Hughes Research Laboratories has demonstrated the feasibility of high performance, low specific impulse electron-bombardment thrusters in sizes from 5 to 30 cm anode diameter. It is expected that thrusters sized for station keeping functions will be about 5 cm in anode diameter.

Under Contract NAS 3-14129, Hughes has analyzed, designed, fabricated, and tested a lightweight, structurally integrated, electron-bombardment mercury ion thruster system which is suitable for attitude control station keeping of a synchronous satellite. The system includes a 5 cm electron-bombardment thruster combined with a main Cathode Isolator Vaporizer (CIV) subassembly, a Neutralizer Vaporizer (NV) subassembly, and a gas pressurized mercury propellant reservoir. The mass of the thruster system is 8.5 kg, including the propellant mass of 6.2 kg.

Construction of the 5 cm Structurally Integrated Thruster (SIT-5) system relied heavily on technology available from the NASA development of the SERT-II ion propulsion system. The configuration of the discharge chamber was (to first approximation) scaled from that of the 15 cm SERT-II Thruster[1,2] developed at the Lewis Research Center (LeRC) of Nasa. Design

of the feed system and packaging structure conformed to criteria of low system mass and long life, which are major requirements in the proposed application with synchronous satellites.

The dependence in the subject program of each new task upon successful completion of preceding tasks set a high premium on the reliability and integrity of designs and techniques of fabrication. Although sufficient time was allotted for complete testing and minor modifications in all of the system components, major redesign of any of these components would have jeopardized the successful completion of the entire program. Careful control was exercised in the design, therefore, to insure close compliance with desired component characteristics. Attention to all power losses in the system was of particular importance in this program as compared with the development of larger systems where discharge power is of overriding magnitude. Complete and detailed structural and thermal analysis was employed to anticipate and eliminate all significant problem areas. Attention was given to integration of the thruster system within an over-all satellite system, and to the effects of the space environment (e.g., space cold soak, solar incidence, etc.) The capability for thrust system restart after emerging from the earth's shadow was given special consideration.

Because of the broad based nature of the design and analysis, the SIT-5 system is of flight-type status with regard to system reliability from the standpoint of structural integrity and firm control over the operation of each component. All elements of the thruster system are structurally and thermally matched with one another and also with respect to the spacecraft with which it will be ultimately associated.

SECTION III

TECHNICAL PROGRAM

A technical program is described below which led to development of the SIT-5 ion propulsion system. A detailed description of the system is given in terms of its design and fabrication, its level of structural qualification, and current level of operating performance. The system description facilitates detailed discussion of the comprehensive program of structural and thermal analysis which preceded hardware fabrication. Subassembly tests and developments are described which precede integrated operation of the SIT-5 system. The discussion is concluded by a summary tabulation of system performance both for steady state and cyclic operation with a dielectric-coated ion extraction system, and for design point operation of the thruster when paired with an ion extraction system having a two-dimensional capability for electrostatic ion beam deflection.

A. THE SIT-5 ION PROPULSION SYSTEM

A mercury-bombardment ion propulsion system has been developed with an anode diameter of 5 cm. This system makes use of the technology established by NASA in development of the SERT II ion propulsion system and extends it to a range of thrust level which is suitable for attitude control and station keeping of a synchronous satellite.

1. System Design and Fabrication

Figure 1 is a photograph of the Structurally Integrated Thruster System (SIT-5) shown attached to a display stand. The system includes a 5 cm electron-bombardment thruster, which delivers 0.41 mlb of thrust at a net accelerating voltage of 650 V (when operated with dielectric-coated ion extraction system) with a propellant utilization efficiency in excess of 65% (including neutralizer losses) and a system electrical efficiency of 40%. The mass of the completed thruster system is 8.5 kg, including the propellant mass of 6.2 kg. The system operates at somewhat higher efficiency when operated with a net accelerating voltage of 1200 V when paired with a thrust-vectorable extraction system developed under Contract NAS 3-14058.

An engineering drawing of the SIT-5 system is shown in Fig. 2. The propellant reservoir is fabricated by welding thin hemispherical shells (4 in. in diameter) to separate flanges which are grooved on the mating faces to accept a sealing ring of the butyl rubber bladder. The circular cross-section of the sealing ring is molded as an integral part of the bladder edge. The hemispherical shell, which is upstream of the thruster assembly, is perforated to allow passage of the pressurizing nitrogen gas to drive the mercury supply to the main and neutralizer cathodes. The gas reservoir is fabricated from a thin stainless steel plate which is drawn into a cylindrical shell and welded to the upstream mounting flange. To increase its pressure-holding capability, the upstream end of the gas reservoir is formed to a concave radius. The gas reservoir is fitted with a gas fill valve of the type commonly used in aircraft medium-pressure gas storage tanks.

M 7635

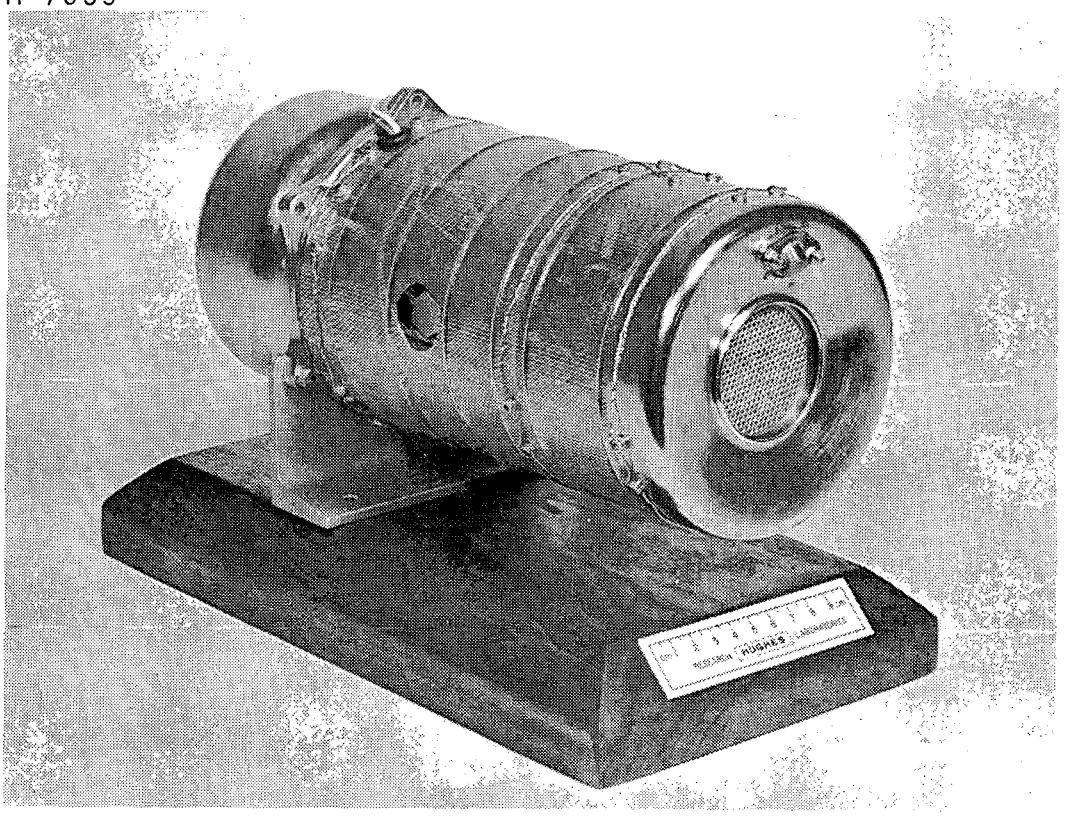

Fig. 1. Structurally Integrated Thruster System (SIT-5) Shown Attached to a Display Stand.

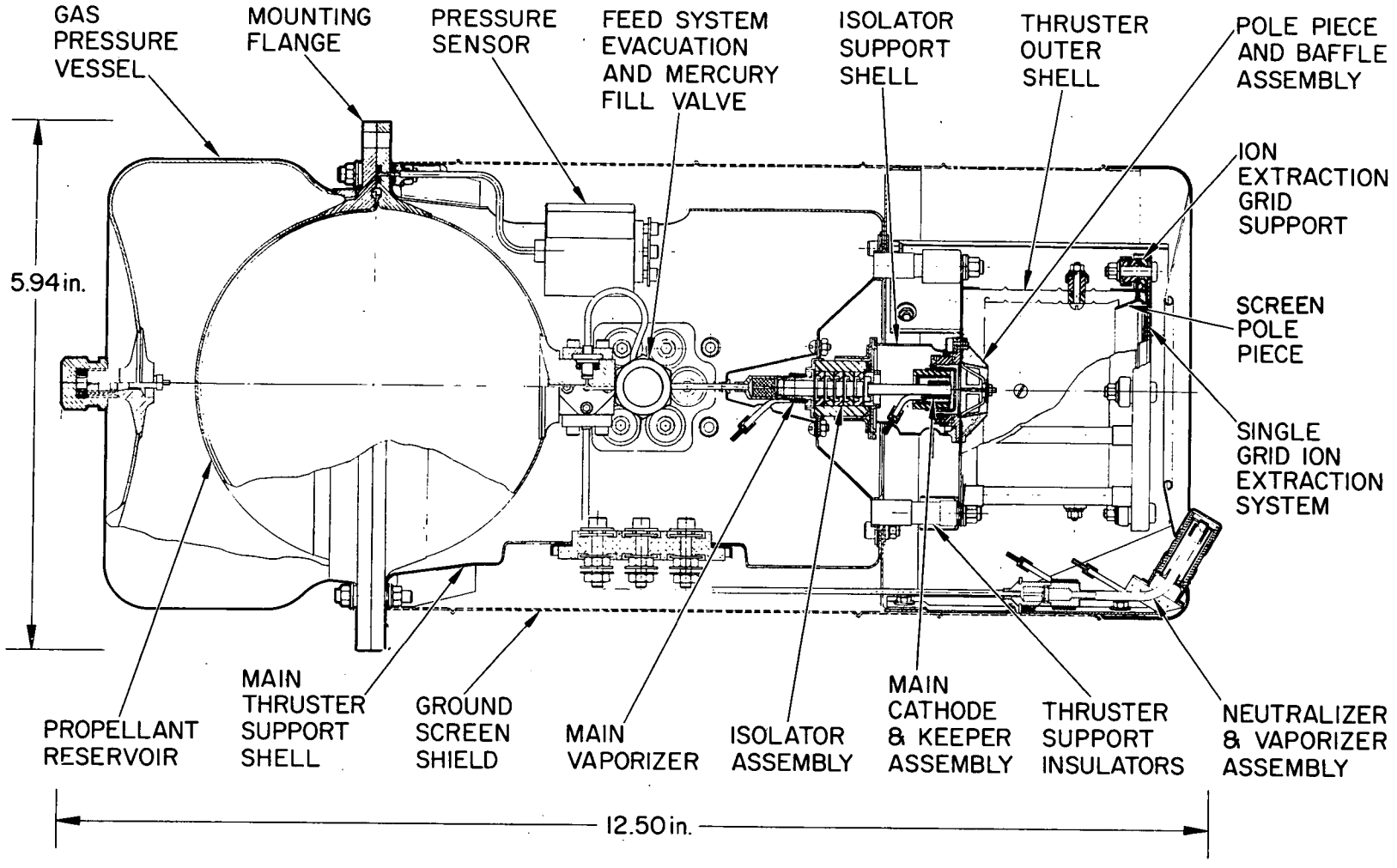

Fig. 2. Engineering Drawing of the SIT-5 System.

The downstream end of the propellant reservoir is fitted with a stainless steel manifold with rubber O-rings providing the required seals for connecting propellant lines from a propellant fill valve and to the main and neutralizer cathodes.

With the butyl rubber diaphragm in position, the reservoir halves are assembled and held together by twelve bolts around the perimeter of the flange. Lock-nuts are used to insure proper attachment during vibration. The reservoir sealing flange projects by 0.5 in. beyond the system envelope, and the same flange is provided with additional mounting holes to provide attachment for the thruster system to the spacecraft. Interface mounting at the equator of the propellant reservoir is considered an optimum position due to the high mass concentration at this location, which is represented by the mercury propellant. Mounting at this location provides the structural stiffness which is required to avoid low frequency response of the reservoir to vibrations encountered during launch, which could otherwise result in high amplitude deformations.

The main thruster support shell is attached to the downstream mounting flange by the same twelve bolts which clamp the reservoir halves. Four insulator assemblies are welded to the thruster support shell to provide electrical isolation of the thrust chamber from spacecraft ground. The cylindrical wall of the main support shell provides a convenient mounting surface for electrical terminations. Midpoint support of the ground screen and front shield, and partial support point for the neutralizer feed line is also provided.

The neutralizer cathode and vaporizer assembly is supported by a thin-walled bracket which is attached to the ground screen shield. Appropriate heat shielding provides thermal isolation of the neutralizer assembly and insures that no condensation of the mercury vapor occurs in the region between the vaporizer and the cathode.

The thruster endplate (formed from mild steel) is attached to the four support insulators which are welded and brazed to the support shell structure. The baffle and the cathode pole-piece assembly are bolted (with lock-nuts) to the inside face of the thruster endplate. An isolator support shell is attached to the upstream side of the thruster endplate.

The thruster outer shell is fabricated by rolling thin stainless steel sheet stock to a cylindrical shape 6.4 cm in diameter by 4.8 cm long. The joint is seam-welded and the assembly is spot-welded to identical iron rings which interface with the iron endplate and front pole-piece. The anode is formed and seam-welded in a similar manner and attached to the thruster outer shell by insulator assemblies. Stiffening ribs are rolled into the thruster and anode shells to strengthen the structures.

The main cathode design employs a 1/8 in. diameter hollow cathode of the enclosed type. The cathode is integrated with a 0.27 in. diameter vaporizer-isolator assembly. This assembly is mounted with a detachable flange to the isolator support shell, and the mercury feed tube is mated with the reservoir through a detachable connector as described previously. Heat shielding is provided around the main cathode. A strain-relief loop is formed in the feed line between the reservoir and the main vaporizer to reduce stresses which might result from relative motion between these components during launch. The neutralizer cathode is a 1/8 in. enclosed hollow cathode with integrally welded 0.27 in. vaporizer and associated tubulation. The mercury feed line of the neutralizer assembly is also attached with a detachable connector to the propellant reservoir. The neutralizer, main cathode, and vaporizer housings are fabricated from seamless thin wall tantalum tubing.

The dielectric-coated ion extraction system consists of a perforated molybdenum plate with an insulated coating of high electrical resistivity which combines to form a single grid system. This coating is of sufficient strength to resist fracture under launch conditions. The hole pattern of the ion extraction system is a hexagonal close-packed array of 0.193 cm diameter holes located on 0.254 cm centers. The molybdenum substrate is 0.055 cm thick with the coating applied to a thickness of approximately 0.125 cm. The grid is mounted on a toroidal ring insulator, and the assembly is held by four supports.

This design incorporates features which add to structural integrity while maintaining minimum mass. No conflict exists between these requirements because the degree of strength which is necessary is, in many cases, no greater than the amount which is required to support the structural element. Portions of the system which bear only their own load have been rolled, stamped, or otherwise formed from thin-walled sheet metal to achieve maximum strength with minimum mass. Ribs, heads, channels, and other stiffening elements are formed as integral parts of these structures. Necessary massive elements are located such as to transmit the load directly to the thrust system mounting flange in order to reduce the length of the supports and to reduce bending moments at the mounting points. The major concentration of load occurs at the propellant reservoir which is supported directly at the equator of the spherical vessel.

In order to minimize weight, type 304 stainless steel was chosen for most structural elements, because it is known to resist attack by mercury and can readily be welded to the soft-iron components of the thruster. No mass penalty was associated with the use of stainless steel, because it may be used in thin sections while still maintaining structural integrity.

2. Structural Qualifications

The structural integrity of the SIT-5 system has been proven by a series of shock and vibration tests. This system satisfied design expectations with only minor exceptions. These have been corrected by straightforward component design modifications.

The system was subjected to shock, sinusoidal, and random accelerations in each of the three mutually perpendicular axes in order to simulate the conditions encountered during rocket launching.

a. Shock Tests – In these tests, the SIT-5 system was subjected to three half-sine pulses in the positive and negative directions along each of the primary axes. The pulse amplitude was 30 G and the duration was 8 msec. The applied shock pulses were monitored by means of an accelerometer with a resonant frequency of approximately 20 kHz.

b. Sinusoidal Vibration Tests – The system was also subjected to sinusoidal vibration along the three primary axes at levels defined in Table I below.

TABLE I

Sinusoidal Vibration Test Levels

Frequency	Level
5 to 19 Hz	0.5 in. double amplitude
19 to 2000 Hz	9 G (0-peak)
Sweep Rate: 2 octaves/min.	

T176

c. Random Vibration Tests – The SIT-5 system was subjected to random vibrations along each axis at levels defined in Table II.

TABLE II

Random Vibration Test Levels

Frequency Band	Power Spectral Density
20 to 340 Hz	0.11 G^2/Hz
340 to 400 Hz	Up 12 dB/octave
400 to 2000 Hz	0.22 G^2/Hz
Over-all Level: 19.9 G rms Duration: 5.4 min/axis	

T276

3. Performance With Thrust-Vectorable Extraction System

As a final task of Contract NAS 3-14129, the thruster system was mated with a thrust-vectorable ion extraction system developed under NASA Contract NAS 3-14058. That extraction system, shown in Fig. 3, is capable of high angle (±10°) thrust vector control by electrostatic deflection. Prior to use in the subject contract, this extraction system was tested successfully under NASA Contract NAS 3-14058 for 100 hours at thrust vector angles up to the contractually required value of 10°. Post-test inspection showed only minimal electrode erosion.

Testing under the NAS 3-14129 program has demonstrated operation of the SIT-5 system at levels approaching design goals. In completion of the final goal under the subject contract, the SIT-5 thruster was operated in combination with the thrust-vectorable extraction system for a 100 hour

durability test. Thruster performance data for the 100 hour test is listed in Table III. In this configuration, the system operated at an electrical efficiency η_E = 46.8% with a propellant and utilization efficiency η_m = 64% (including neutralizer losses).

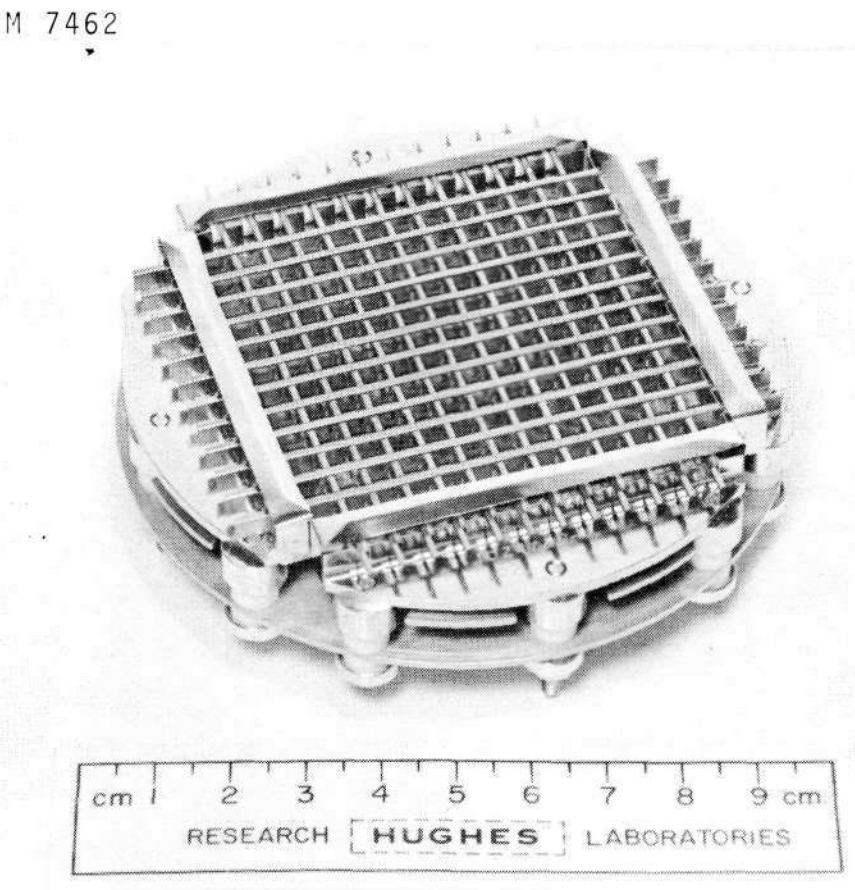

Fig. 3. Thrust-Vectorable Extraction System.

TABLE III

SIT-5 System Performance Profile

Nominal Operating Parameters	Operating Values (Test 101-TV-9)
Net Accelerator Voltage, V	1200
Beam Current, mA	33.5
Accelerator Voltage, V	-1180
Accelerator Drain Current, mA (at 0° deflection)	0.17
Discharge Voltage, V	42.0
Discharge Current, A	0.4
Cathode	
Keeper Voltage, V	0.0
Keeper Current, A	0.0
Keeper Power, W	0.0
Heater Power, W	0.0
Vaporizer Voltage, V	4.25
Vaporizer Current, A	1.78
Vaporizer Heater Power, W	7.5
Neutralizer	
Keeper Voltage, V	24.0
Keeper Current, A	0.64
Keeper Power, W	15.4
Heater Power, W	0.0
Vaporizer Voltage, V	3.35
Vaporizer Current, A	1.4
Vaporizer Heater Power, W	4.7
Coupling Voltage, V	38.0
Output Beam Power, W	40.1
Total Input Power, W	86.0
Thruster Propellant Flow Equivalent, mA (cathode flow)	51.2
Neutralizer Propellant Flow Equivalent, mA	1.2
Propellant Utilization Efficiency (including neutralizer)	64.0
Electrical Efficiency, %	46.8
Over-all Efficiency, %	29.8
Discharge Loss, eV/ion	500
Thrust, mlb	0.56
Specific Impulse, sec	2220
Power-to-Thrust Ratio, W/mlb	154

T277

B. DESIGN ANALYSIS AND STRUCTURAL TEST

Throughout the development of the SIT-5 thruster system, particular attention has been directed toward assuring thermal and structural compatibility with the host satellite. To study the appropriate interactions, a set of mathematical models of the thruster system were generated and employed to predict the equilibrium temperature distribution and to analyze the dynamic responses of the thruster system. These analyses were conducted concurrently with the system design so that the effects of design variation could be accurately assessed. The techniques and results of these analyses are described in the following.

1. Thermal Analysis

To guarantee design effectiveness, detailed thermal analysis was carried out to minimize power losses and to insure that temperatures of critical components did not vary beyond allowable limits for materials employed in the thruster system. Both the steady state and transient thermal analysis were accomplished by representing the 5 cm thruster system by a lumped parameter network of 45 nodes connected by radiation and conductance resistors.

As a result of this analysis, the temperature distribution of the SIT-5 thruster system has been shown to vary over a wide range, as a consequence of extensive variations in environmental and operational conditions. These variations result from the continuous alternation of exposure to direct solar radiation due to orbit motion of the spacecraft, thermal interaction of the thruster system with its host satellite, and intermittent operation of the thruster system. Precision techniques have also been derived for exact balancing of thermal fluxes to achieve optimum control over thruster subassemblies.

a. Steady State Thermal Analysis – The steady state thermal analysis was carried out with the aid of digital computer program TAS-1B, which solves for the steady state temperature distribution in a lumped parameter network of temperature points (nodes) and heat flow paths (resistors). A node is provided for each portion of the system being modeled which is at a uniform temperature. The network may contain up to 80 nodes, and each node may be connected to any or all of the others. Any two nodes may be connected by two resistors, one representing conduction and/or convection and the other representing infrared radiation. In addition to exchanging heat with other nodes, each node may receive radiation and/or a direct heat input (as from internal dissipation of electtical energy). The inputs to TAS-1B which are required to model a device are the power inputs, nodal areas, radiant emissivities, radiation view factors, and thermal conductances.

A total of eight cases (representing a wide variety of operating conditions) were analyzed using the TAS-1B digital computer program in conjunction with the thermal model consistint of 45 nodes mentioned above. Particular attention was directed toward achieving thermal control of the two critical areas in the thruster system.

- Maintaining thermal control of the vaporizers which are heated partially by cathode – discharge power in order to minimize vaporizer power requirements.
- Maintaining the temperature of the propellant reservoir above the freezing point of mercury (-39° C) and below the maximum permissible bladder temperature (120°C).

(1) Vaporizer Temperature Control – A significant difference which separates the 5 cm electron-bombardment thruster from larger sizes is the extreme dependence of over-all system performance on the performance of individual component subassemblies. This dependence derives from the fact that discharge power constitutes only a fraction of the total source energy required to produce a beam ion. Rather, the major power losses are those required to maintain the keeper discharges and to heat the cathodes, vaporizers, and the isolator. Experience gained during experimental testing now confirms that significant reduction of subassembly losses can be realized by careful matching of thermal exchanges between adjacent component elements. The basic challenge is that of operating the cathode subassemblies with minimum over-all power while maintaining control over vaporizer temperature. This requires an ideal balance of thermal coupling between the cathodes and their associated vaporizers. This balance is achieved when – with zero vaporizer power – heat from the operating cathode, is sufficient to raise vaporizer temperature to a value just below that required to achieve the desired mercury flowrate.

The main cathode-isolator-vaporizer (CIV) subassembly received particular attention in the thermal analysis, because of its central significance to system performance and because of the close thermal coupling between the cathode tip and the main propellant vaporizer. The close coupling results from their close mechanical proximity, which is made necessary by demands of structural strength and by constraints on the over-all length of the subassembly. The thermal considerations which influence this design are described in the following as a typical example of the processes involved in component development.

Node temperatures are indicated in Fig. 4, which represent the equilibrium values predicted by computer program TAS-1B for the CIV subassembly. This equilibrium condition was calculated for the case of a thruster operating near the spacecraft and in sunlight. The power inputs correspond to a case in which (for efficient operation) the thruster is being operated at the maximum power level anticipated by the study, with 5.3 W of heater power applied to the cathode and 4.5 W of power dissipated by the keeper discharge. Initial calculations for operation under these conditions indicated a temperature at the vaporizer far in excess of the 250°C required by the vaporizer subassemblies to produce the desired value of 40 mA neutral flowrate equivalent. High thermal fluxes predicted initially between the cathode tip and the vaporizer prompted reducing the wall thickness of the tantalum cathode tube from 0.015 to 0.010 in. in order to reduce the thermal conduction along this heat flow path. This design modification resulted in a significant decrease in the computer-predicted vaporizer temperature. For thruster operation at maximum power in full sunlight it is still necessary, however, to use a thermally emissive coating* on the surfaces of both the vaporizer support cone and the isolator support cylinder to promote thermal radiation and thereby reduce vaporizer temperature below the desired value of 250°C, while still maintaining control over vaporizer temperature by dissipation of a finite amount ($\sim$2 W) of heater power at the vaporizer.

Having bracketed the possibilities of vaporizer temperature, no further design modifications were considered in the analysis, because the approximations used in the computerized

*This coating has earlier been used successfully in HRL development of a 20 cm LM cathode thruster system. It is applied as a water solution mixture of potassium silicate and titanium dioxide in a dry weight one-to-four ratio.

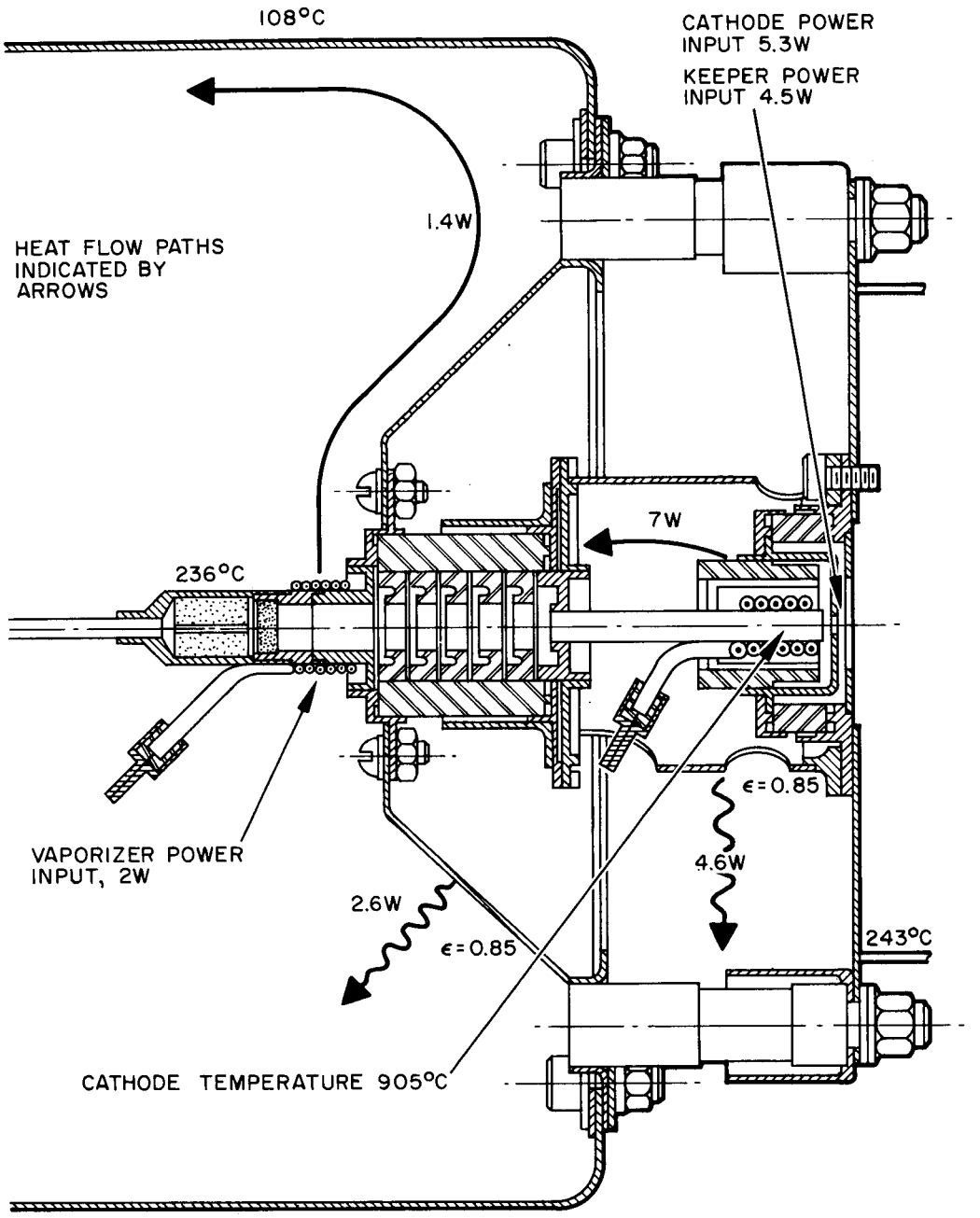

Fig. 4. Node Temperatures and Heat Fluxes Near the CIV of the SIT-5 System.

calculations were too great to permit a more exacting balance. The approximations relate not only to geometrical modeling factors but also to uncertainties in the necessary power levels for efficient thruster operation, the exact vaporizer flow calibration, and startup and shutdown requirements in conformance with mission profiles.

(2) Propellant Reservoir Temperature – As a result of the thermal analysis, techniques were also established to insure maintenance of the SIT-5 propellant reservoir within acceptable temperature limits. When the system is operated far away from the warmth of the spacecraft and in its shadow, a heater that consumes 5 W of electrical power is required at the reservoir location to prevent the stored mercury from freezing. This requirement prevails even though the thruster is operating at full power. To simultaneously provide for the case in which the system is exposed to sunlight, use of the thermal control coating is also necessary at the reservoir location. The coating increases the emissivity of the reservoir outer surface in order to maintain its temperature below the value of 120°C, which is the maximum allowable for butyl rubber (the bladder material).

b. Transient Thermal Analysis – Thermal transients were analyzed also to determine the critical thermal relaxation times of various components. This analysis was executed with the TAP-3 digital computer program to determine the thruster operating temperatures as a function of time after the system enters a zone of solar eclipse subsequent to operation under steady state conditions in sunlight. The TAP-3 digital computer program uses finite difference methods to calculate the transient temperatures in a lumped parameter network consisting of thermal capacitors, heat sources, and heat flow paths.

The steady state operating temperatures used as input to the transient analysis were determined using the TAS-1B digital computer program for the operating condition of minimum power, far from the spacecraft, in sunlight and with the propellant reservoir empty. The results of the transient analysis show that the shortest time constant (and hence the most critical component) occurs at the feed line adjacent to the neutralizer. It has a time constant of 52 min to reach the freezing point of mercury (-39°C) with no input power. However, a minimal heat input to the neutralizer cathode of only 1 W is sufficient to prevent freezing. The next most critical area is the main vaporizer feed line, which has a slightly longer time constant of 1.2 hours. The reservoir flange region has a time constant of 2.1 hours, and the main reservoir has a time constant of about 10 hours. Since the steady state thermal analysis has already shown a possible requirement for 5 W of heater power at the reservoir location, this last result did not impose an additional constraint on system design.

2. Structural Analysis and Test

For purposes of structural integration the set of shock and vibration specifications defined in Section A-2 were used to define the satellite-to-thruster interface. A mathematical model was generated, and the dynamic responses of the thruster system to the specified environment were determined by a computer simulation. From these responses, the dynamic loads and stress levels were analyzed for the purpose of identifying overstressed regions of the structure so that corrective design could be initiated. Conclusive proof of the accuracy of the structural analysis has now been demonstrated by a series of shock and vibration tests of the actual structure.

a. Structural Analyses – The entire structure was represented by lumped masses which correspond to structural elements and components. These are connected by massless flexible elements that represent the structural load paths of the thruster. A set of coordinates was chosen which is referenced to the center of the mercury reservoir. The X-axis was chosen along the thruster center line, and Y and Z were positioned in a standard right-hand coordinate system. The elements of the thruster system were broken down into symmetrical conical and cylindrical sections, nonsymmetrical beams, and flat plates. The masses for these elements were determined and their appropriate center-of-gravity coordinates were identified.

To generate the dynamic responses, a stiffness matrix for the over-all system was formed using in-house computer programs in conjunction with the GE 635 digital computer (the program calculates the frequencies and mode shapes for the complete structure). The programs which were used are called the MARS (Matrix Analysis Routine for Structures) structural analysis and response routines, which consist of two separate programs. MARS 1 solves for the eigenvalues and eigenvectors of the system and was used to calculate the static shear and bending moments in the structure that are imposed by a steady state gravitational load. MARS 2 was used to determine dynamic response of the structure to the specified dynamic environment.

Using the dynamic analysis results, a stress analysis was carried out to assess the structural strength of the thruster system. During this analysis, several possible design weaknesses were identified and the following corrective action was taken prior to construction of the system.

- The flanges leading to the hemispherical propellant tank were provided with tapered extensions which blend with the 0.030 in. tank wall thickness over a distance of approximately one-half inch.

- The thickness of the thruster endplate was increased from 0.020 to 0.050 in.

- The main vaporizer support structure was changed from an open-spider to a hollow-cone configuration.

- Stiffening doublers were installed over cutouts in the main support structure, and gussets were provided to attach it to the system support flange.

b. Structural Integrity Test – The basic structural integrity of the SIT-5 system has been proven by a series of shock and vibration tests. This system satisfied design expectations with only minor exceptions that were corrected by straightforward component design modifications. The tested SIT-5 system shown in Fig. 5, included an electron-bombardment mercury ion thruster having a 5 cm anode diameter, a CIV subassembly, an NV subassembly, and a reservoir sub-assembly containing 6.2 kg of liquid mercury. The system was subjected to shock, sinusoidal, and random accelerations in each of the three mutually perpendicular axes defined in Fig. 5 in order to simulate the conditions encountered during booster launch. In the narrative which follows, the result of the tests and of inspections performed during and after completion of testing are discussed and appropriate design modifications are described.

(1) Test Procedure – For all tests, the SIT-5 system was mounted on an aluminum test flange which, in turn, was mounted on the exciter fixture as shown in Fig. 6. Table IV gives the test number, the type of test, and the primary axis of acceleration.

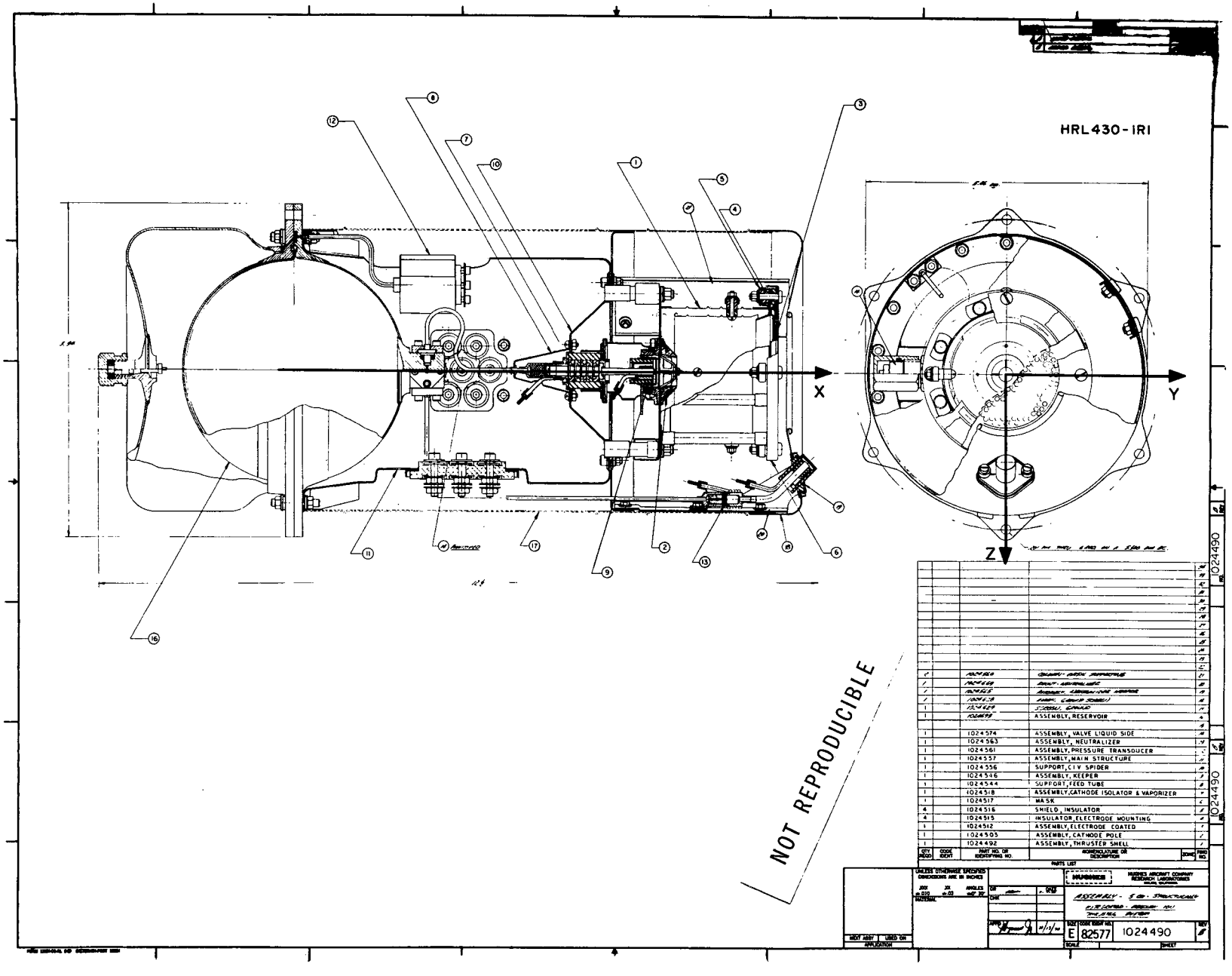

Fig. 5. Preshake Engineering Drawing of the SIT-5 System.

M 7655

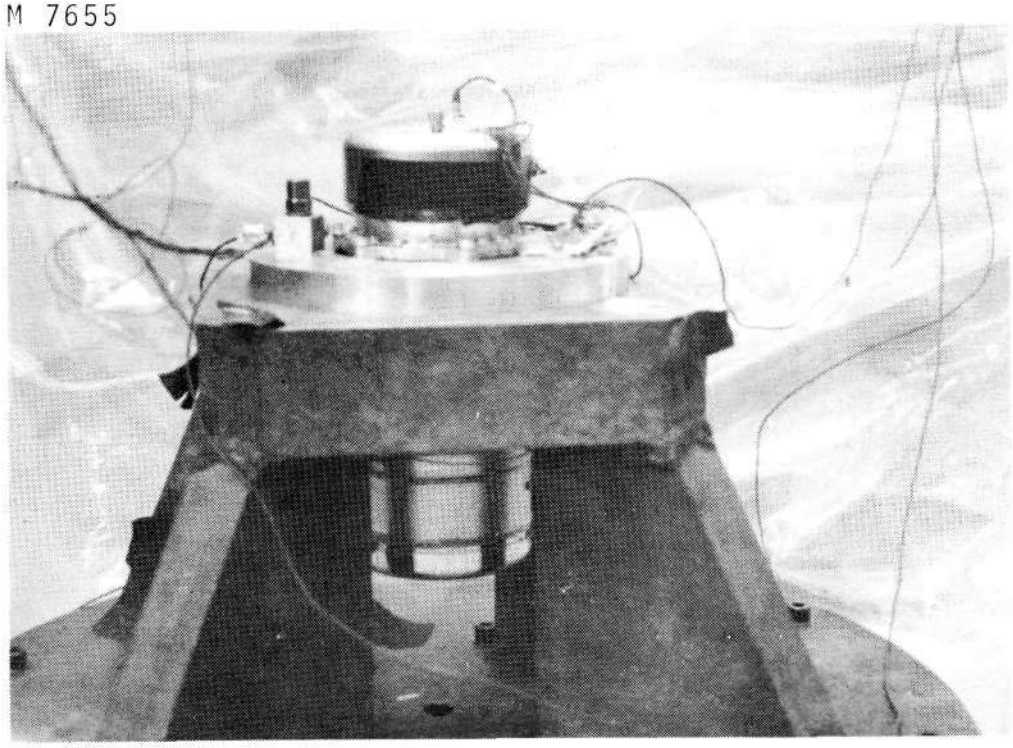

Fig. 6. Experimental Arrangement for Shock and Vibration Testing.

TABLE IV

Structural Integrity Test Definition

Test	Test Type	Primary Axis
1	Shock	X
2	Sine	X
3	Random	X
4	Random	Z
5	Sine	Z
6	Shock	Z
7	Shock	Y
8	Sine	Y
9	Random	Y

T278

(a) Shock Tests – In these tests, the SIT-5 system was subjected to three half-sine pulses in the positive and negative directions along each of the primary axis. The pulse amplitude was 30 G and the duration was 8 msec. The applied shock pulses were monitored by means of an accelerometer which had a resonant frequency of approximately 20 kHz*. The monitoring accelerometer signal and the signals

*The monitoring accelerometer for the shock tests was mounted approximately 3.5 in. from the SIT-5 mounting flange to facilitate the initial pulse-shaping tests which were performed without the SIT-5 system and its aluminum test flange. During the X-axis sine tests, the transmissibility gradient between this accelerometer location and an accelerometer located within one inch of the SIT-5 mounting flange was shown to be less than 10%. The transmissibility gradient between these two locations is even lower for the Y and Z axes, because of the extreme rigidity of the aluminum test flange along these axes.

from two cross-axis accelerometers were recorded simultaneously by means of a multibeam oscilloscope and a Polaroid camera. For most of the shock tests, the signal from the monitoring accelerometer was processed by a low-pass filter and recorded on a fourth trace. This permitted the determination of the acceleration pulse amplitude when ringing was present on the monitoring accelerometer trace.

(b) Sinusoidal Vibration Tests – The SIT-5 system was subjected to sinusoidal vibration along the three primary axes at levels defined in Table I. These tests were monitored with two primary-axis control accelerometers located 180° apart and two accelerometers positioned in the two cross-axis directions. All accelerometers were mounted on the aluminum test flange as close as possible (less than 1 in.) to the thruster system. Test data consisted of frequency amplitude plots of the control channel average, the individual control channel signals, and the signals from the cross-axis accelerometers. The vibration level was controlled by means of a feedback signal composed of the average of the signals from the two control accelerometers. In this way, the effects of test fixture resonances were eliminated for the primary axis of vibration.

(c) Random Vibration Tests – The SIT-5 system was subjected to random vibrations along each axis at levels defined in Table II. Prior to the qualification level tests, the vibration spectrum was constructed at a low power level in order to prevent excessive stressing of the SIT-5 system. Narrow band power-spectral-density plots of the control-channel average were then made at -3 dB from full level to verify the input specification. Similar plots were made during the first 20 sec and midway through the full-level run as a final verification of the input level. Spectral-density plots were also obtained for the output signals from the accelerometers in the two cross-axis directions.

(2) SIT-5 Measurements – Prior to, during, and after the completion of shock and vibration testing, various measurements were made to detect and record the development of failures and/or incipient failures of the SIT-5 system without the need for system disassembly. These are described below.

(a) Response Accelerometer Measurements – Ten uniaxis response accelerometers were mounted on the SIT-5 system in order to monitor local system responses. These accelerometers were positioned at locations where the accelerations were expected to be most severe on the basis of the preceding structural analysis. The locations and orientations of the response accelerators are indicated in Fig. 5.

(b) Critical Dimensions – A number of the geometrical dimensions were measured during the shock and vibration test program, which are considered to be critical to the operation of the SIT-5 thruster system. Table V lists the measured dimensions, the difference between measurements taken prior to and after completion of the shock and vibration tests, and the estimated measurement accuracy. Critical dimension sets Nos. 1 through 5 were measured only at the beginning and the end of testing; dimension sets Nos. 6 through 9 (excluding the off-axis X measurements for dimension set No. 6) were also measured after each shock and vibration test. In most cases, the difference between the initial and final value of a dimension is considered negligible. The shift of the ion extraction grid in the plane perpendicular to the thrust axis (set No. 6) is due to failure of the thruster mounting plate at the location of attachment of the insulating thruster support posts. This failure will be discussed in more detail later. The change in the Y position of the ground screen lip with respect to the

TABLE V

Critical Dimensions of the SIT-5 System

Critical Dimension	Difference Between Initial and Final Accuracy, in.	Estimated Measuring Accuracy, in.
1. Baffle position with respect to the cathode-cup pole piece		
X Dimension	0.000	±0.002
Y Dimension	0.000	±0.002
Z Dimension	0.000	±0.003
2. Axial distance between the main keeper and the cathode	0.000	±0.002
3. Axial distance between the main keeper and the thruster backplate	-0.001	±0.002
4. Main CIV position with respect to the SIT-5 mounting flange		
Y Dimension	0.003	±0.005
Z Dimension	-0.002	±0.005
5. Anode position with respect to the thruster shell		
X Dimension	0.003	±0.003
Y Dimension	-0.002	±0.010
Z Dimension	0.007	±0.010
6. Position of ion extraction grid with respect to the SIT-5 mounting flange		
X Dimension	0.000	±0.003*
Y Dimension	0.014	±0.002*
Z Dimension	-0.001	±0.002*
X Dimension at Y = +a†	0.002**	±0.005
X Dimension at Y = -a†	0.002**	±0.005
X Dimension at Z = +a†	-0.001**	±0.005
X Dimension at Z = -a†	0.001	±0.005
7. Innermost grid shadow-shield gap	0.000	-0.000 +0.005
8. Position of the ground screen lip with respect to the SIT-5 mounting flange		
X Dimension	0.000	±0.003*
Y Dimension	0.018	±0.005*
Z Dimension	0.002	±0.005*
9. Axial separation between the neutralizer cathode and the keeper	0.003	±0.002*

*Measurement accuracy was determined by the scatter in plotted data points which were obtained after each shock and vibration test.

†The quantity "a" is equal to the ion extraction grid radius.

**These data give the final variance from the condition in which the ion extraction grid is parallel to the plane of the mounting flange.

T279

SIT-5 mounting flange (set No. 8) is not considered to be important, because distortion of this small amount will not affect the SIT-5 operation.

(c) Electrical Continuity – The electrical continuity between five different SIT-5 electrode pairs which are normally not in electrical contact, was measured during each shock and vibration test. This was done in order to provide a remote indication of gross geometrical distortion and/or insulation failure without the necessity for system diassembly. Electrical continuity was detected as a current flow between electrodes. This provided a signal which was recorded by means of a Honeywell 1612 oscillograph having a rise time of 200 μsec. Table VI lists the electrode pairs for which data were obtained and indicates whether electrical contact was observed at any time during the shock and vibration test program.

TABLE VI

Electrical Continuity Measurements

Electrode Pairs	Electrical Contact Observed
Main cathode and keeper	No
Main cathode and ion extraction grid	Yes
Main cathode and anode	No
Main cathode and ground	Yes
Ground screen and neutralizer	No

T280

Electrical contacts observed between the main cathode and the ion extraction grid is believed to have been caused by small metal chips held by the magnetic field of the thruster between the grid mask and the outer edge of the screen pole piece. A number of such chips were discovered during the SIT-5 post-test disassembly; no permanent distortion was present which could otherwise account for the observed electrical contact. The contact between the main cathode and ground is believed to have been caused by the neutralizer vaporizer heater lead and/or the neutralizer ground lead, both of which were found to be disconnected during the final inspection. Either of these leads could have made electrical contact with the thruster shell during shock and vibration testing.

(d) Pressure Transducer Measurements — A pressure transducer is employed to monitor the nitrogen pressure in the SIT-5 gas-pressurized mercury reservoir. The output from this transducer was recorded by means of the Honeywell oscillograph during all tests in order to detect the development of any propellant or gas leaks. The pressure measured after each test did not vary during the testing program. Small fluctuations were observed in the transducer output during the last vibration test (Test 9).

(3) Direct Observation of Failures and Recommended Design Alterations — The measurements described thus far were directed mainly toward remote sensing and early detection of structural failures or incipient failures. The SIT-5 system was also inspected visually after each shock and vibration test. Because it was not desirable to disturb the system during the testing program, these observations only involved the system exterior and what could be seen of its interior through the semitransparent ground screen shroud. Following Test 4, visual observation indicated that the neutralizer vaporizer heater lead had become detached from the neutralizer heater terminal.

Following completion of all shock and vibration testing, the SIT-5 system was carefully disassembled and inspected for evidence of failures or incipient failures. When the neutralizer keeper was removed, the tantalum washer (see Fig. 7), which formed a heat shield and completed the enclosure of the neutralizer cathode, was found to be loose. Also considerable abrasion of the radiation shield by the neutralizer keeper insulator was evident as shown in Fig. 8. Although the problem of washer attachment can be solved entirely by an improved beam welded configuration, a more elaborate redesign shown in Fig. 9 was adopted which offered numerous advantages over the present design. In this design, keeper support is provided by a small bracket attached to the neutralizer subassembly mounting bracket at a point close to the stiffest region which occurs near the ground screen shield. A cathode-alignment collar welded directly to the keeper-support bracket insures parallel alignment between the cathode tube and the keeper structure. The tantalum radiation shield which surrounds the cathode heater is formed from one piece of tantalum in the shape of a cup with a flange at the lip and a hole through which the cathode tip is inserted. The radiation shield is restrained from motion, relative to the keeper structure, by sandwiching its lip-flange between the shoulder of the cathode alignment collar and the exposed end of the ceramic cylinder in the keeper structure. As necessary, shims can be included into the sandwich to adjust the interelectrode spacing between the keeper and the cathode tip. By virtue of the axial stiffness of the coaxial cylinders comprising this design, a high degree of structural integrity is anticipated from the new configuration.

M 7634

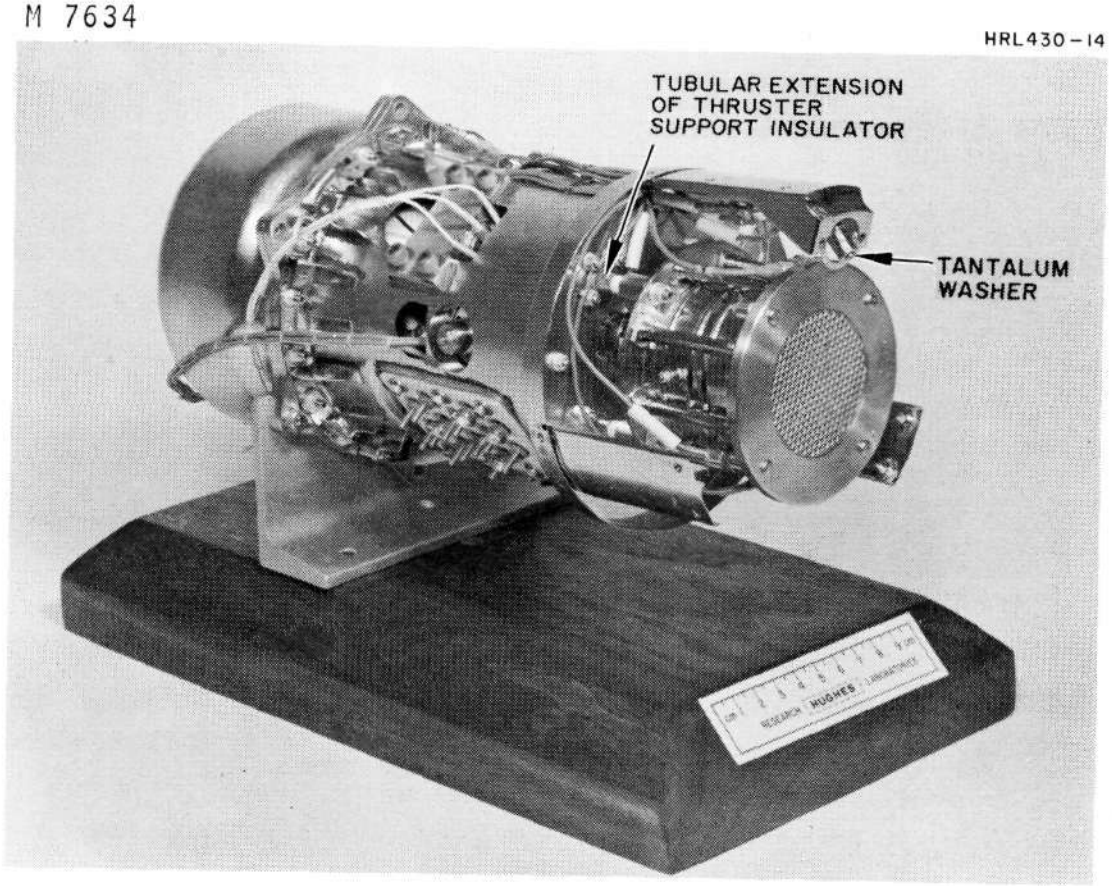

Fig. 7. The SIT-5 Thruster System Shown Attached to a Display Stand with Ground Screen Removed Prior to Structural Integrity Tests.

M 7731

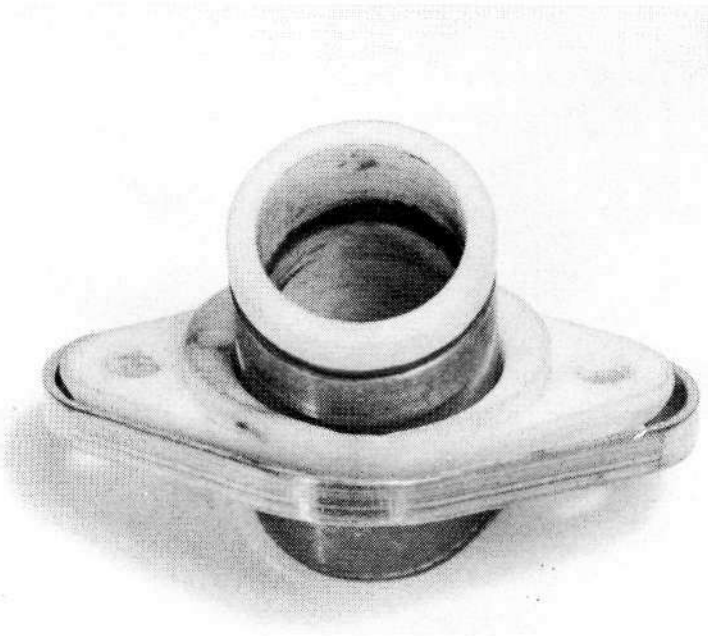

Fig. 8. View of the Inside Diameter of the Neutralizer Keeper Insulator Illustrating the Presence of Considerable Abrasion Between it and the Neutralizer-Cathode Heat Shield.

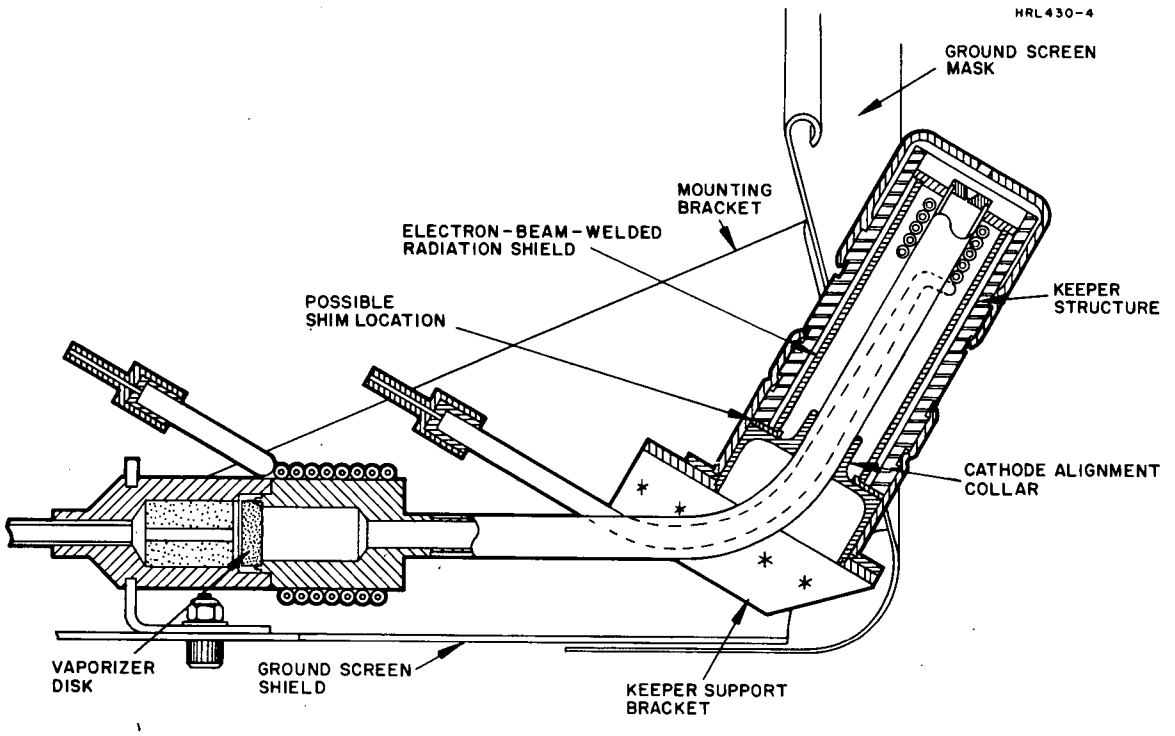

Fig. 9. Design Modification of the Neutralizer-Vaporizer-Keeper Support Structure.

Removal of the SIT-5 ground screen disclosed that several of the electrical leads were loose, in addition to those which were connected to the neutralizer vaporizer heater. These included the neutralizer ground lead, the main cathode vaporizer heater lead and the main vaporizer ground lead. In all cases, the connections were broken at the point where they were spot-welded to the associated thruster component. To avoid future failures of this type, it is recommended that a brazed or crimped connection be employed in the SIT-5 design.

Inspection of a region between the ion-extraction-grid mask and the outer edge of the screen pole piece indicated the presence of several small metal shards which were held in place by the magnetic field of the thruster. It is expected that this was the cause of the electrical shorting between the grid and the thruster which was observed during the shock and vibration tests. To avoid future occurrence, it is recommended that clean-room procedures be used in assembly of actual flight hardware.

Finally, close inspection of the thruster mounting plate indicated that it was cracked at the four attachment locations of the tubular extensions of the thruster support insulators (see Fig. 7). Figure 10 shows the upstream side of the mounting plate on which the locations of failure have been numbered. Figures 11 and 12 show closeup (10 x magnification) views of the cracks observed at location Nos. 2 and 4; similar cracks were observed at location Nos. 1 and 3. Figures 13 and 14 show cross-sectional views obtained at location No. 1 at 10 x and 40 x magnification respectively.

This failure is believed to have occurred for two reasons. First, the bending radius at the locations of failure was sufficiently small (0.010 to 0.020 in.) to cause severe local stressing. In addition, the thickness of the material at these locations was reduced by approximately 20% in the

M 7732

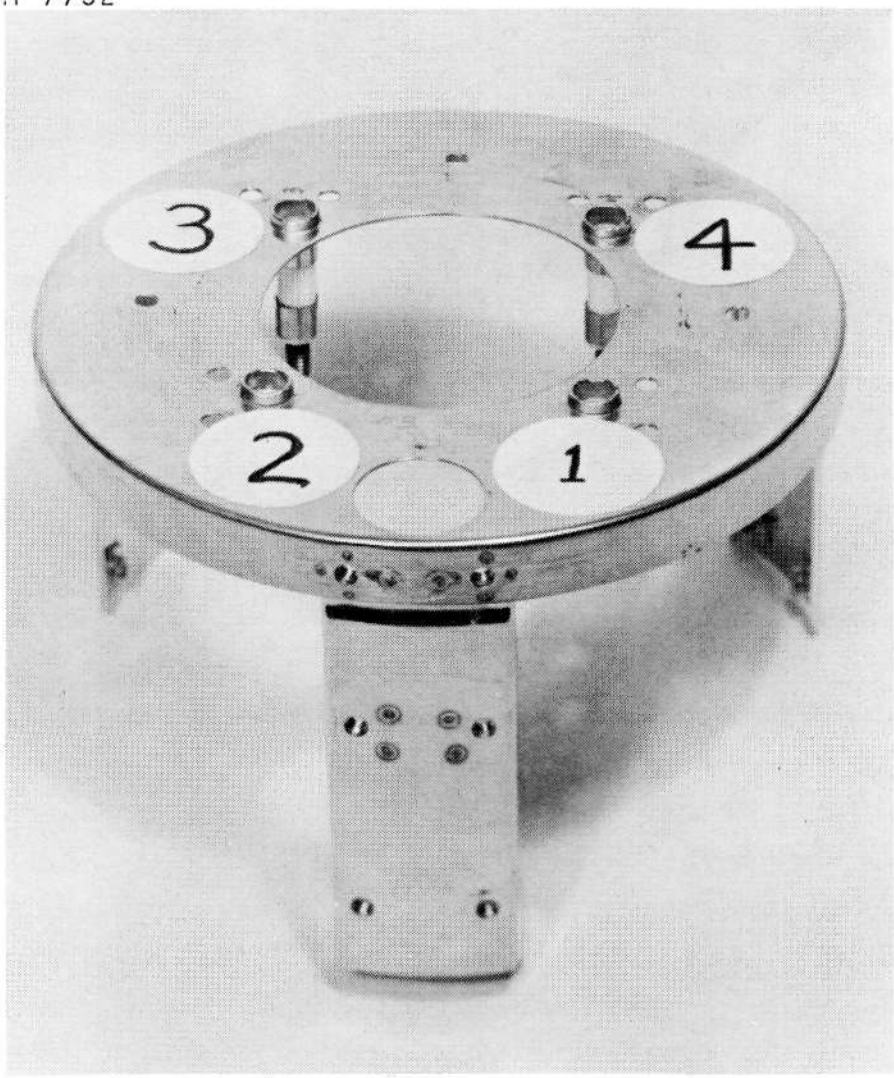

Fig. 10. The SIT-5 Thruster Mounting Plate Showing the Location (1 to 4) of Failure.

M 7662

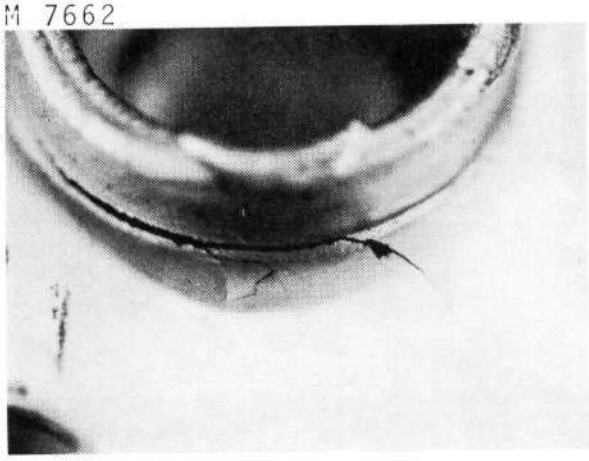

Fig. 11. Closeup View (10 x) at Location 2.

M 7661

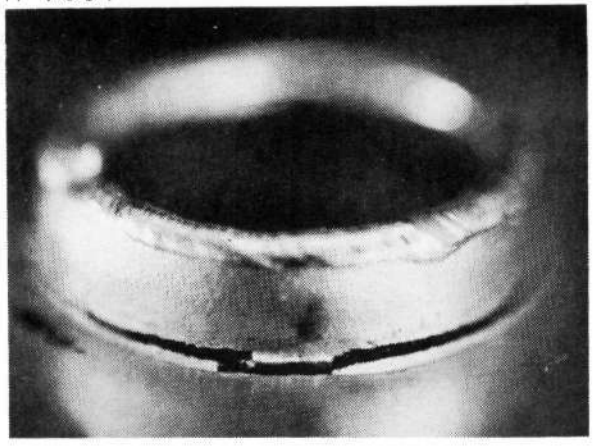

Fig. 12. Closeup View (10 x) at Location 4.

M 7659

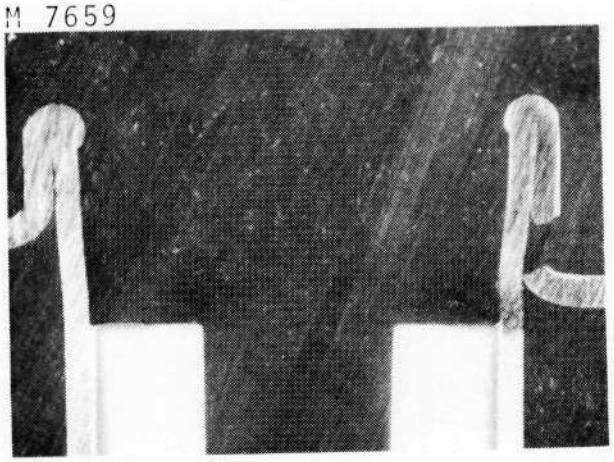

Fig. 13. Closeup (10 x Cross-Sectional View Taken at Location 1.

M 7660

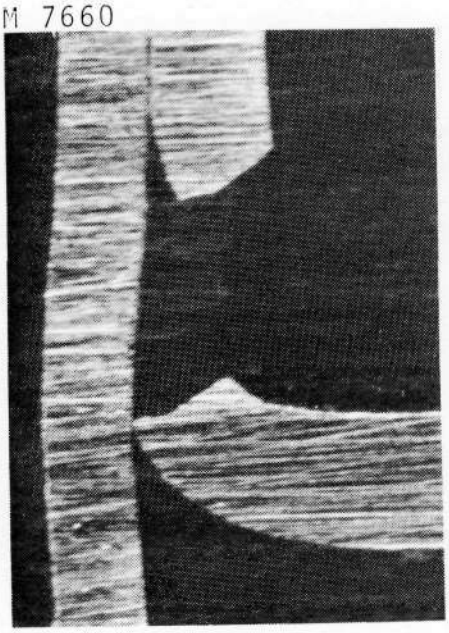

Fig. 14.
Closeup (40 x) Cross-Sectional View Taken at Location 1.

fabrication process as demonstrated in Figs. 13 and 14. Figure 15 illustrates the design modification which was adopted to prevent future filure in this mode. The increased bending radius combined with a braze fillet supply the desired structural integrity.

C. THRUSTER SUBASSEMBLY TESTS

Separate testing of various subassemblies prior to assembly of the integrated thruster system was carried out as a means of insuring against deficiencies in system operation which might otherwise delay program progress. By testing subassemblies separately from the thruster system, possible malfunctions or deficiencies in the operation of any component could be isolated and detected, a task which might have been more difficult after assembly of the thruster system.

1. Main Cathode Subassembly

Experimental tests were conducted to permit design evaluation of the main Cathode-Isolator-Vaporizer subassembly (CIV) which is employed in the SIT-5 thruster assembly.* The tested CIV incorporated a mercury fed 0.125 in. o.d. hollow cathode. A tightly fitting heater coil, enclosed by a single heat shield, was used to heat the cathode tip. A keeper

*To expedite acquisition of test data, a CIV was used in these tests that departed slightly from the final SIT-5 design. The minor nature of these departures, however, is thought to have had little or no effect on either the electrical or thermal operating characteristics of this subassembly. The length of the insulating section in the isolator of the tested CIV was 0.688 in. as opposed to a length of 0.529 in. for the SIT-5 design; the number of gridded isolation regions was the same, however. Also, the tested CIV employed a re-entrant vaporizer in which the vaporizer heater is almost completely enclosed within the isolator section, whereas only one turn of the vaporizer heater coil is enclosed in the SIT-5 design.

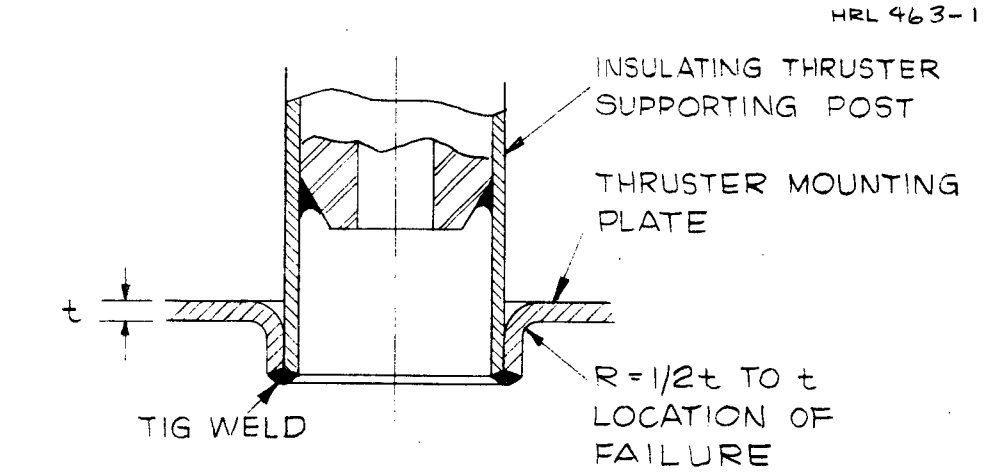

a. DESIGN FOR WHICH FAILURE WAS OBSERVED

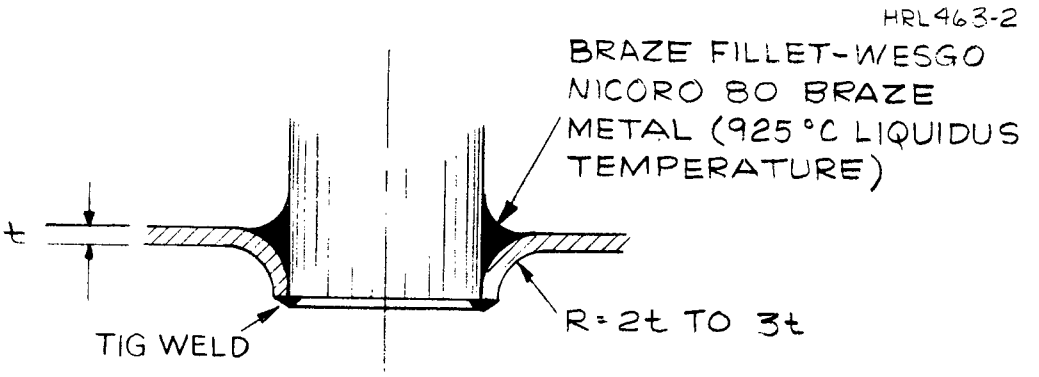

b. RECOMMENDED DESIGN ALTERATION

Fig. 15. Design Modification Adopted to Eliminate Failure of the Thruster Mounting Plate.

electrode having a 0.030 in. diameter central orifice enclosed this assembly. The upstream end of the cathode was connected to the alumina body of the isolator to facilitate operation of the cathode at an electrical potential different from that of the mercury reservoir. The porous tungsten vaporizer, which provides the separation between liquid and vapor mercury phases was connected to the upstream end of the isolator. The flow of mercury vapor was determined by the vaporizer temperature, which was controlled by means of a heater coil tightly clamped to the vaporizer structure.

The CIV subassembly was located in one arm of a 6 in. i.d., glass-cross vacuum system which utilizes an oil diffusion pump and a liquid nitrogen cold trap to maintain an ambient pressure of less than 10^{-5} Torr. A metal plate having a diameter of approximately 6 in. was bolted to the downstream end of the CIV in such a manner that plasma generated in the space between the cathode and collector was prevented from penetrating into the region surrounding the isolator. The collector was mounted on an axially movable rod which extended from the opposing arm of the glass cross. Mercury was supplied to the vaporizer from a cylindrical reservoir in which a piston is pressed against the mercury surface to provide the propellant driving force. The piston position is indicated by a dial indicator (calibrated to 0.0001 in.) which contacts the top of the piston shaft and permits accurate determination of the rate of mercury consumption. Three thermocouples were attached (equally spaced) along the length of the isolator. One was spot-welded to the metal flange at each end of the insulating section, and the third one was spot-welded to a wire which was tightly wrapped about the insulator midpoint. During operation, temperatures T_1, T_2, and T_3 were measured at the vaporizer flange, the midpoint, and the cathode flange, respectively.

All parameters of the test system satisfied the following contractual requirements:

- Environmental pressure: $P < 1 \times 10^{-5}$ Torr.
- Range of mercury flowrate equivalent: $I_{M,Hg}$ = 30 to 60 mA
- Voltage difference between the cathode and vaporizer end of isolator: V_{ISOL} = 1 kV
- Cathode-to-collector anode voltage: V_D = 35 to 50 V dc
- Collector current: I_D = 0.1 to 0.5 A
- Cathode-to-collector gap: ℓ (adjustable to maintain desired collector voltage and current)
- Cathode tip heater power: $P_{M,CH}$ = 0 to 5.3 W
- Cathode keeper current: $I_{M,K}$ = 0.2 to 0.5 A
- Cathode keeper voltage: $V_{M,K} < 20$ V dc
- Minimum isolator temperature: T_{ISOL} = 250 °C
- Isolator leakage current to ground: $I_{ISOL} < 5$ μA

a. Test Data and Discussion — Figure 16 illustrates, in graphical form, the dependence of the main-cathode keeper voltage $V_{M,K}$, collector current I_D, and the isolator leakage current I_{ISOL} on the cathode-to-collector voltage V_D for 0, 100, and 150% (approximately) of the rated cathode heater power (5.3 W). For these data, constant values were maintained for the mercury flow rate $I_{M,Hg} \sim 30$ mA, cathode keeper current $I_{M,K}$ = 0.35 A, and isolator voltage difference V_{ISOL} = 1 kV. Figure 17 shows similar plots where the cathode heater power is held constant ($P_{M,CH} = 0$), and the collector current is allowed to have three values, I_D = 0.1 A, 0.3 A, and 0.5 A. In Figure 18 the cathode heater power is

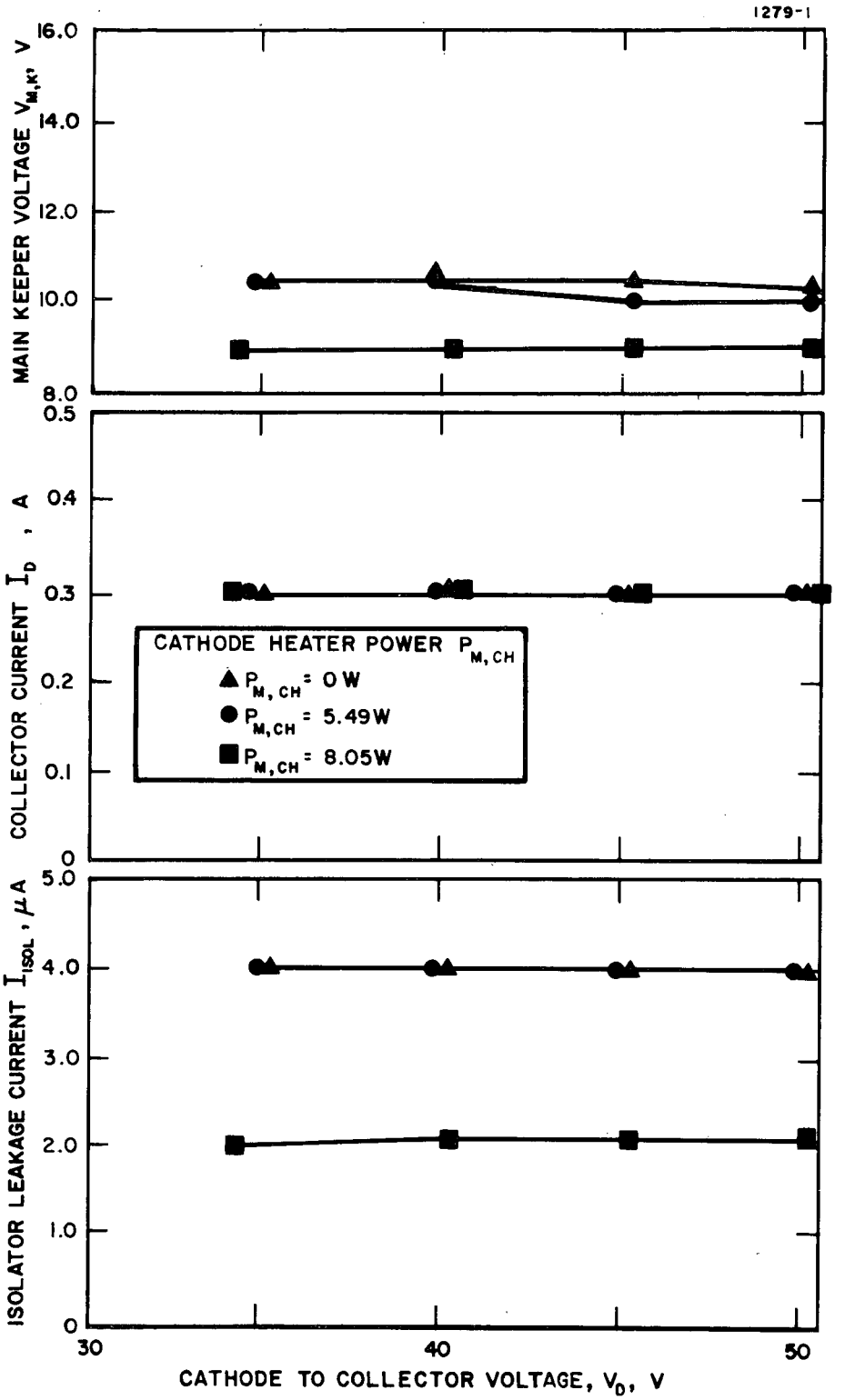

Fig. 16. Dependence of $V_{M,K}$, I_D, and I_{ISOL} on V_D for $I_{M,Hg} \simeq 30$ mA, $I_{M,K} = 0.35$ A, $I_D = 0.30$ A, and $V_{ISOL} = 1$ kV.

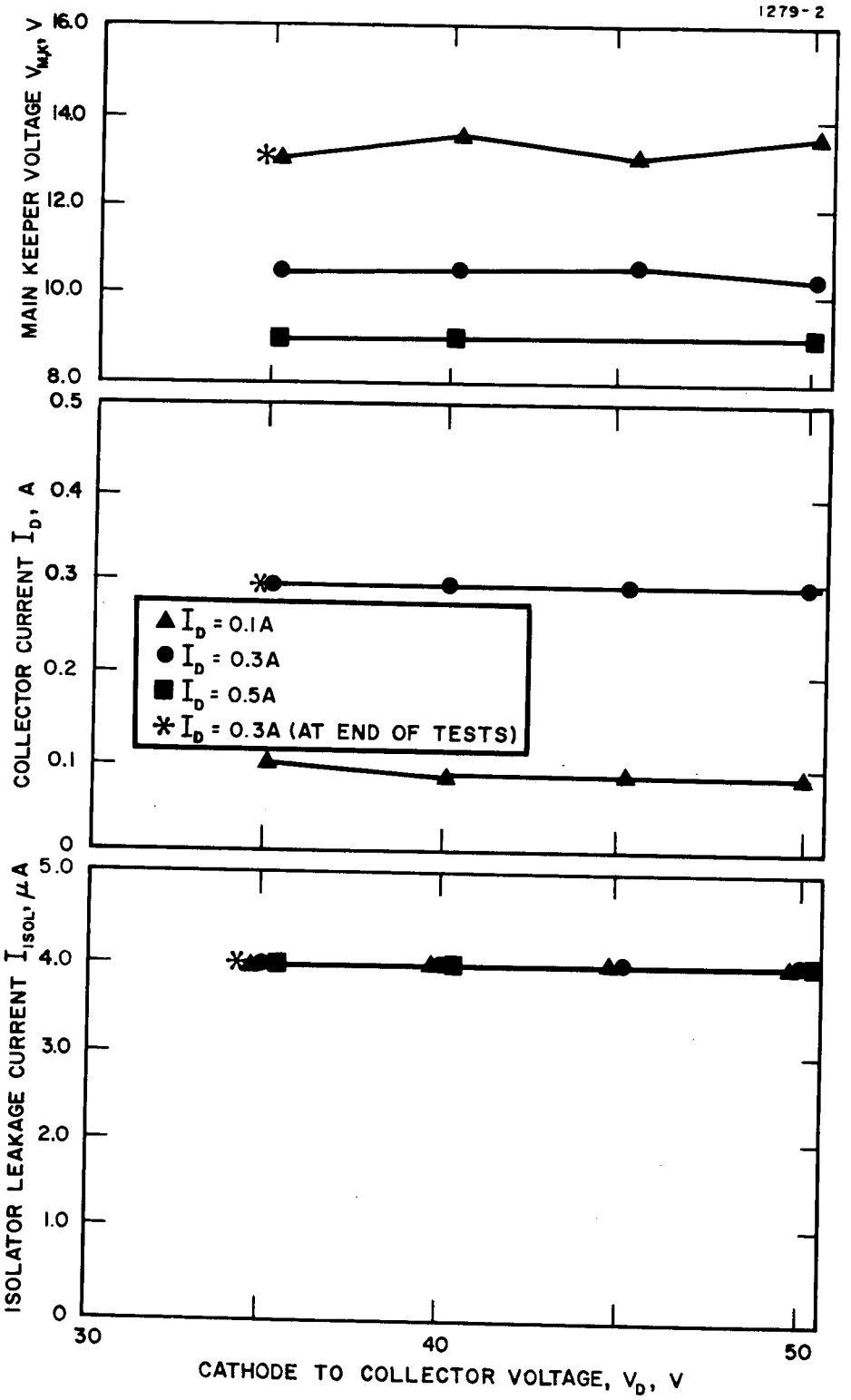

Fig. 17. Dependence of $V_{M,K}$, I_D, and I_{ISOL} on V_D for Three Values of I_D with $I_{M,Hg} \approx$ 30 mA, $P_{M,CH} = 0$, $I_{M,K} = 0.35$ A and $V_{ISOL} = 1$ kV.

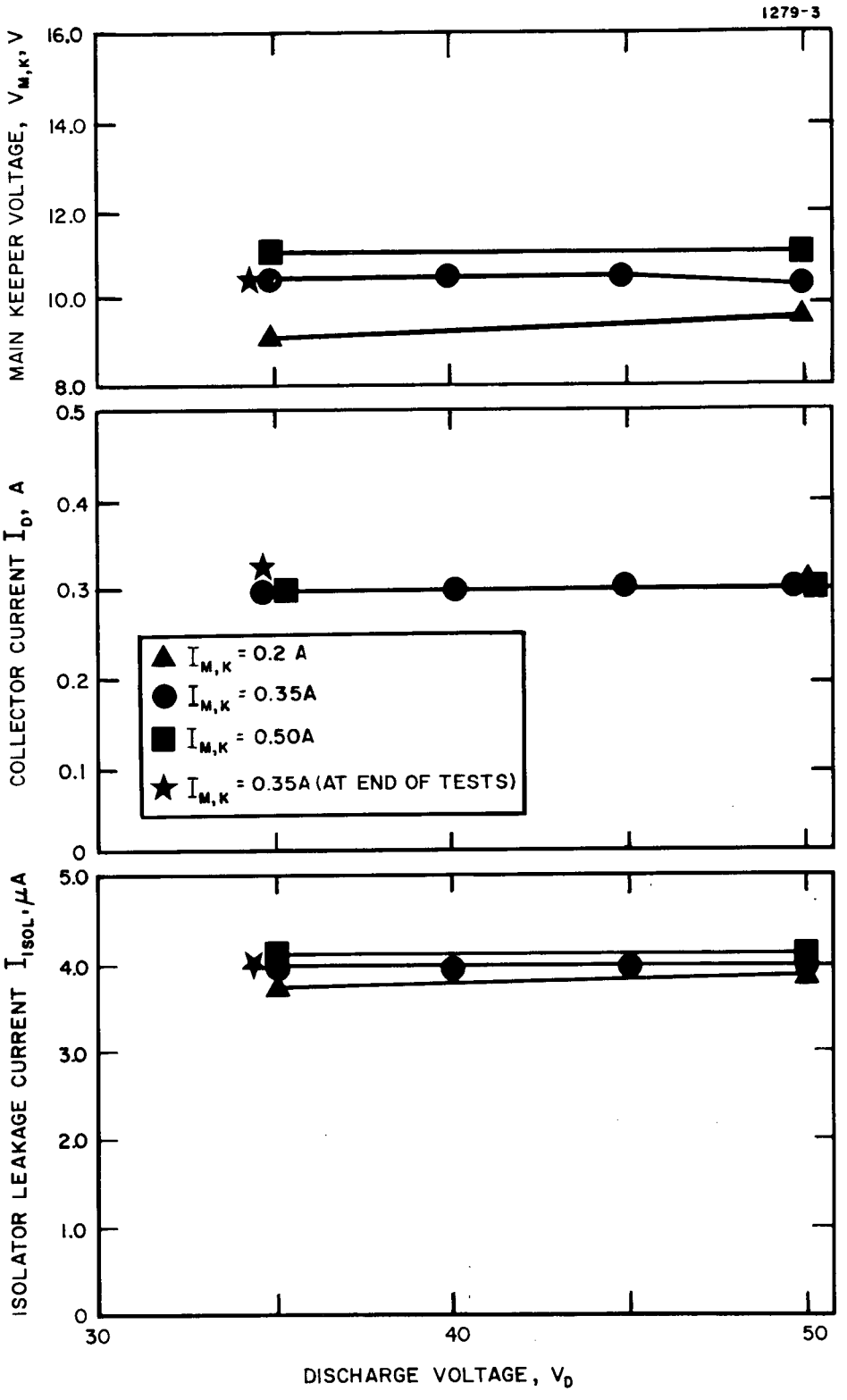

Fig. 18. Dependence of $V_{M,K}$, I_D and I_{ISOL} on V_D for Three Values of $I_{M,Hg} \simeq 30$ mA, $P_{M,CH}$ = 0.30 A, V_{ISOL} = 1 kV.

again held constant ($P_{M,CH} = 0$), and data are plotted for three values of the keeper current ($I_{M,K}$ = 0.2 A, 0.35 A, and 0.50 A) with the collector current held constant at I_D = 0.30 A. Figure 19 illustrates the dependence of the vaporizer temperature $T_{M,V}$ and the isolator temperatures T_1, T_2, and T_3 on cathode heater power level $P_{M,CH}$ for $P_{M,CH} \simeq 0$, 100, and 150% of the rated power. The neutral mercury flow rate for all data presented in Figs. 16 to 19 was maintained constant at approximately 30 mA. An indication of the high degree of reprodicibility and reliability of these data is exemplified by the starred (*) data points which were obtained at the end of a sequence of tests. It is seen that the agreement of these data points with comparable unstarred points taken near the beginning of the test sequence is very close.

Figures 20 through 23 illustrate a similar set of data plots which were obtained at a constant mercury flow rate of $I_{M,Hg} \sim 60$ mA. Oscillations in the cathode-to-collector voltage, collector current, and isolator leakage current were observed at the higher values of cathode-to-collector voltage.* Variation of the output impedance of the collector power supply over a wide range did not cause any noticeable alterations in the characteristics of these oscillations and they can, therefore, be presumed to be characteristic of the CIV and associated experimental arrangement alone.

Both the collector current and keeper voltage are nearly independent of the cathode-to-collector voltage. This results partly from the use of a constant current-collector power

*Values of the isolator leakage current were obtained which exceed 5 μA for small ranges of the cathode-to-collector voltage (see Figs. 20 and 21). These results are probably associated with the discharge oscillations observed at slightly higher cathode-to-collector voltages. It was correctly anticipated that this situation would be significantly altered for operation of the CIV with the 5-cm thruster and, therefore, no design changes are suggested at this point.

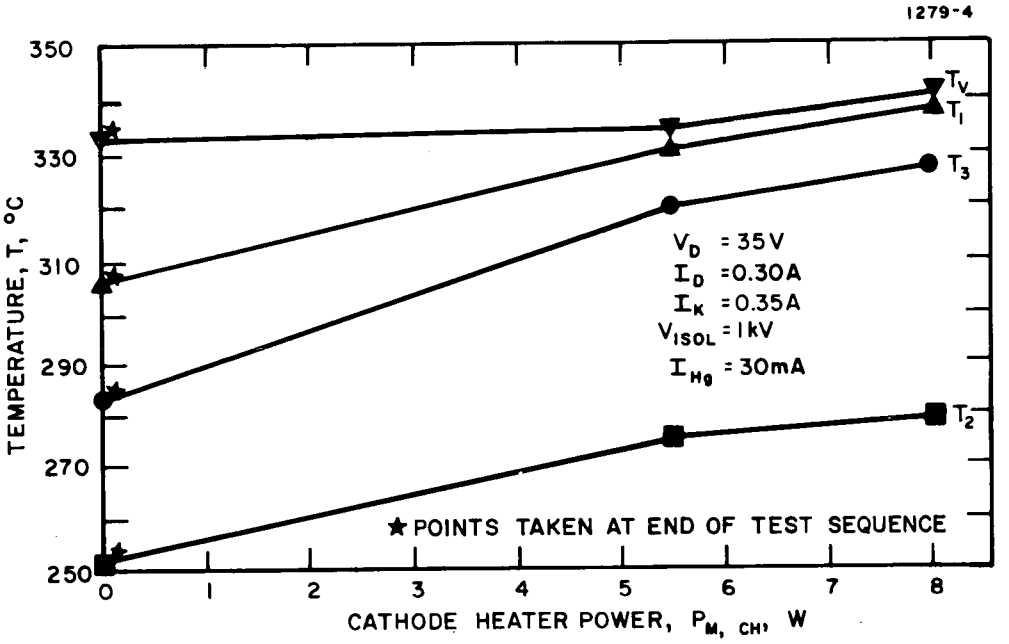

Fig. 19. Dependence of Isolator Temperatures T_1, T_2, T_3 and of Vaporizer Temperature $T_{M,V}$ on Cathode Heater Power $P_{M,CH}$ for a Constant (Approximately) Vaporizer Temperature $T_{M,V}$.

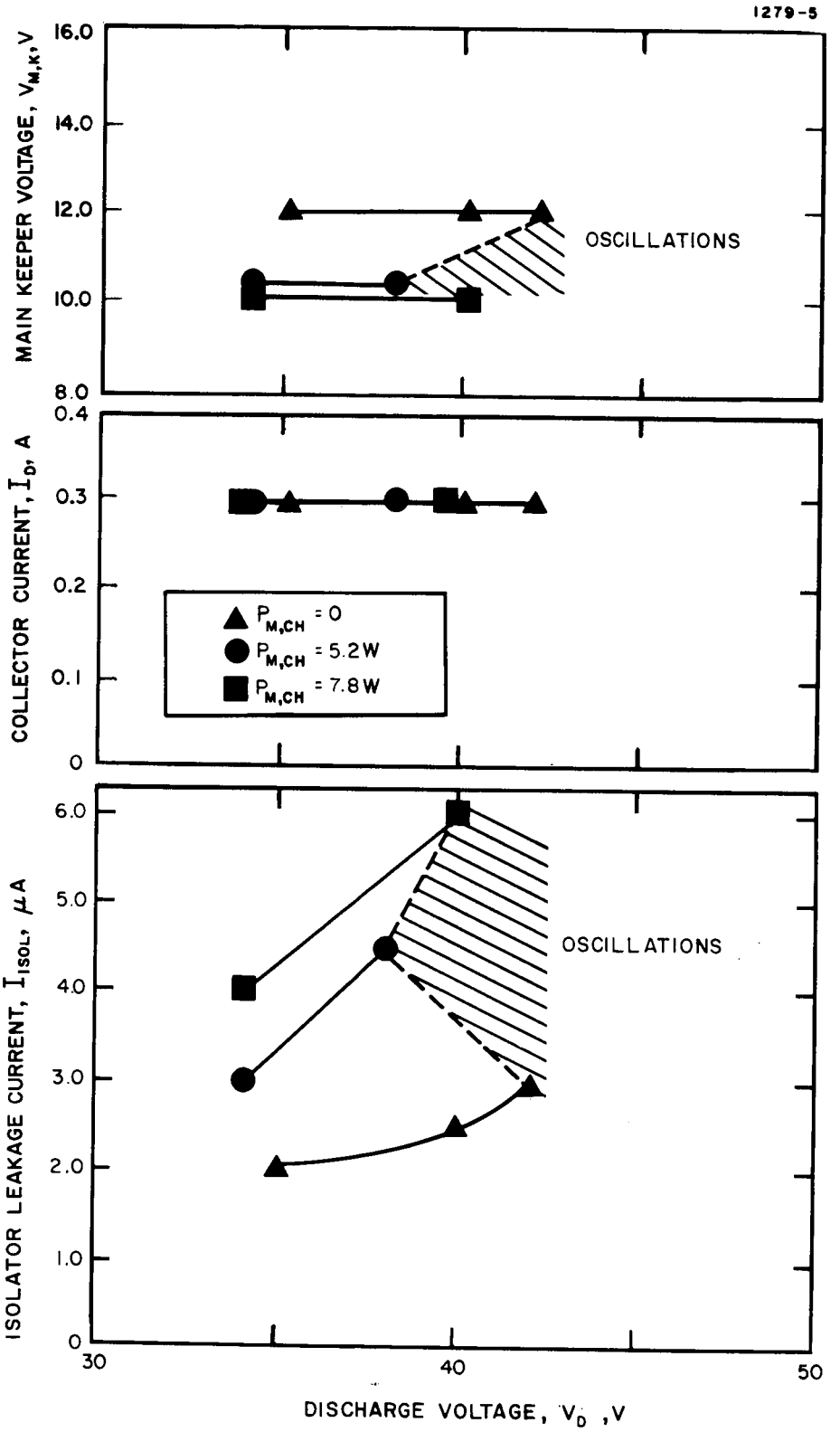

Fig. 20. Dependence of $V_{M,K}$, I_D, I_{ISOL} on V_D for Three Values of Cathode Heater Power $P_{M,CH}$ with $I_{M,Hg}$ = 61.5 mA, $I_{M,K}$ = 0.35 A, I_D = 0.30 A and V_{ISOL} = 1 kV.

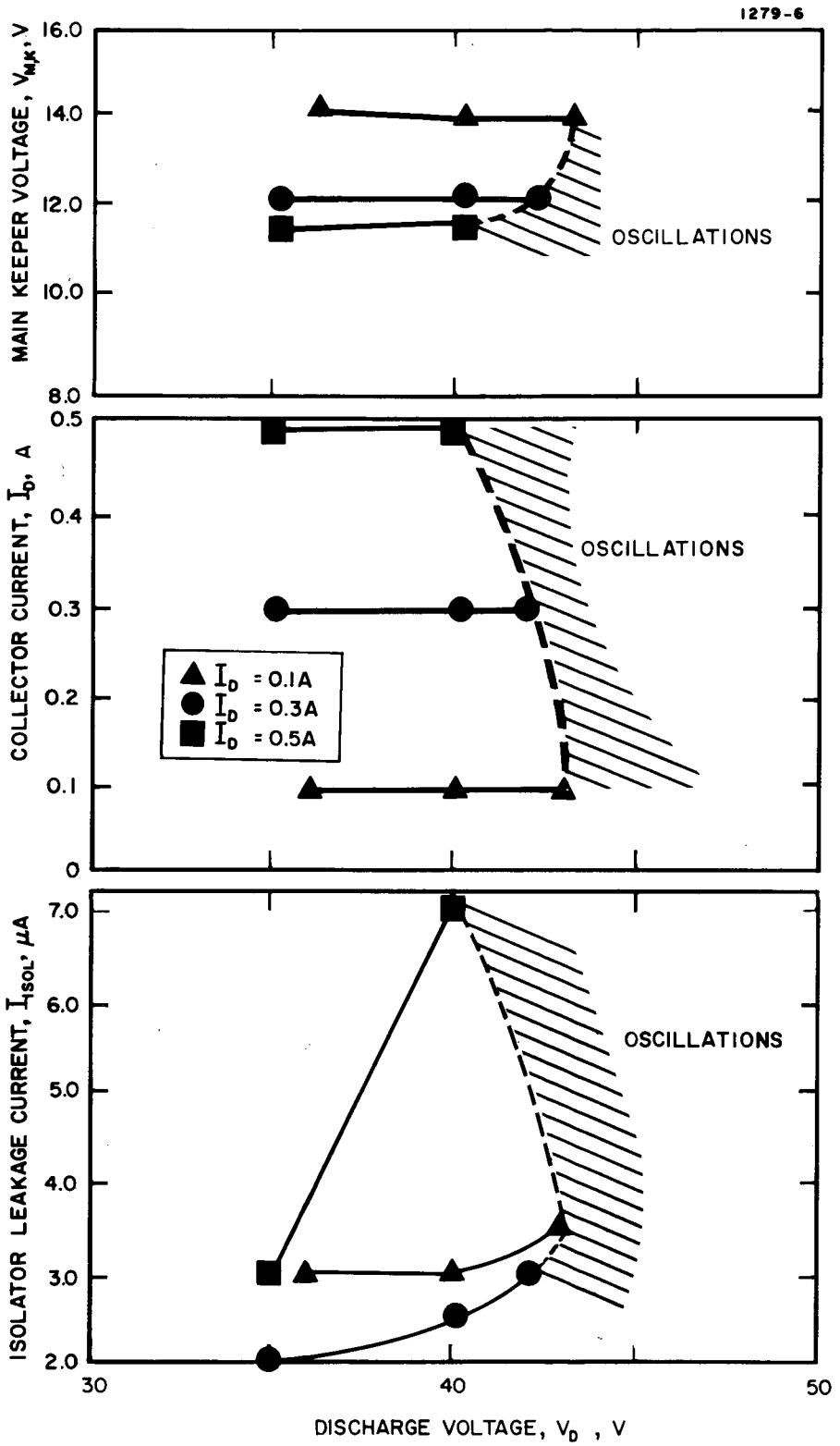

Fig. 21. Dependence of $V_{M,K}$, I_D, and I_{ISOL} on V_D for Three Values of Collector Current I_D with $I_{M,Hg}$ = 61.5 mA, $P_{M,CH}$ = 0, $I_{M,K}$ = 0.35 A and V_{ISOL} = 1 kV.

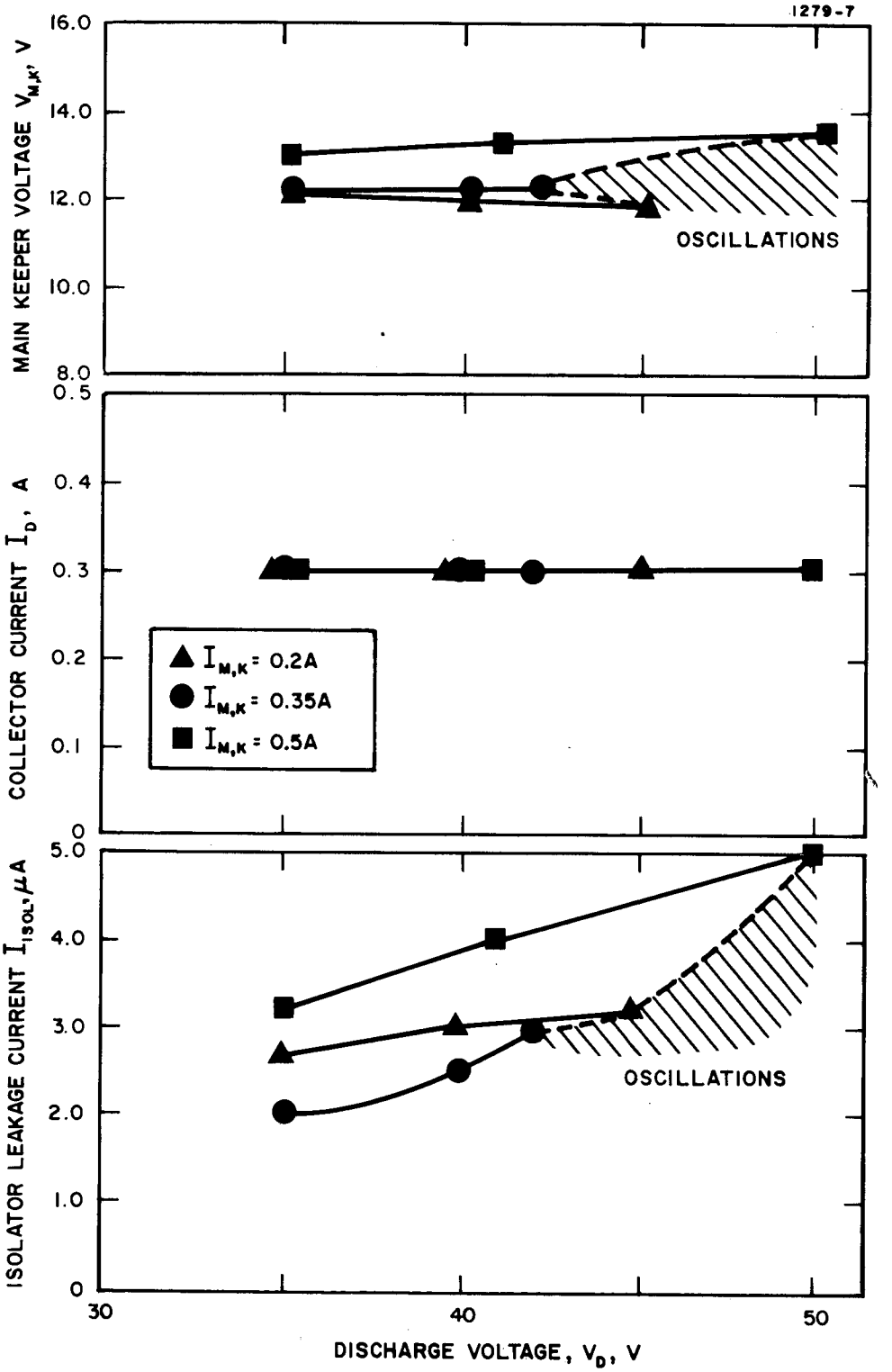

Fig. 22. Dependence of $V_{M,K}$, I_D and I_{ISOL} on V_D for Three Values of Keeper Current $I_{M,K}$, with $I_{M,Hg}$ = 61.5 mA, $P_{M,CH}$ = 0, I_D = 0.30 A and V_{ISOL} = 1 kV.

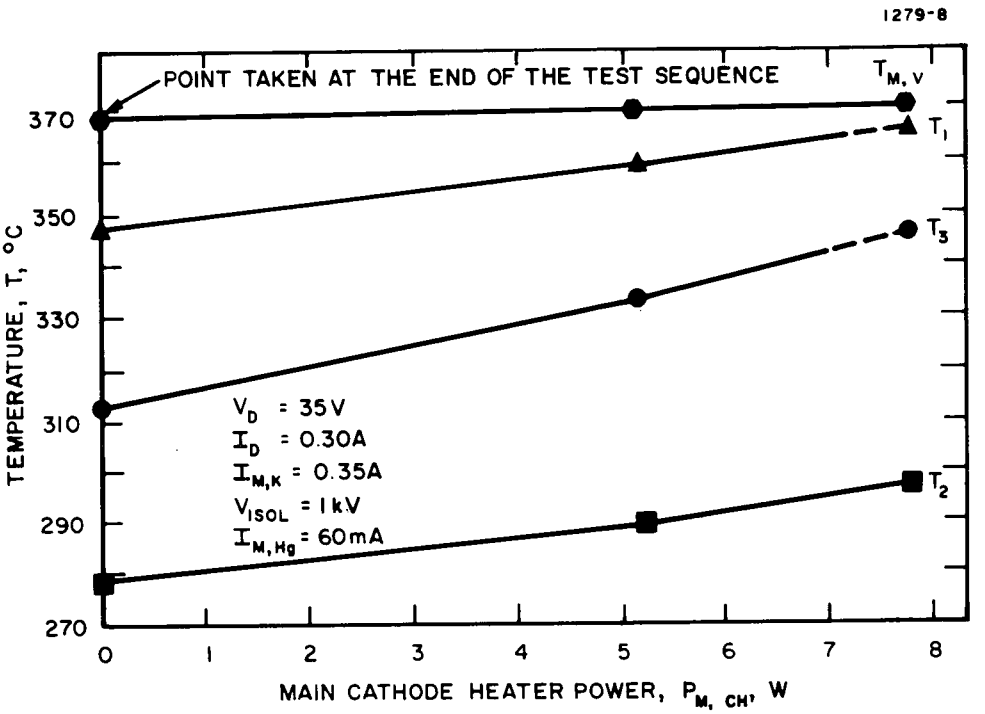

Fig. 23. Dependence of Isolator Temperatures T_1, T_2, T_3 on Main Cathode Heater Power $P_{M,CH}$ for a Constant Vaporizer Temperature $T_{M,V}$.

supply which was chosen in order to avoid introduction of apparent variables in the operation of the CIV and that would, in fact, be functions only of the power supply output characteristics.

On the basis of the experimental results described above, no design modifications have been recommended for the SIT-5 CIV design.

2. Neutralizer Vaporizer Subassembly

The neturalizer subassembly was tested to establish the vaporizer flow calibration and to determine the temperature distribution of the interconnecting tube from the vaporizer to the cathode (during steady state operation). To accomplish test objectives, the complete neutralizer subassembly (including heaters, keeper, etc.) was operated in vacuum with the vaporizer housing bracketed to a metal mounting disk to simulate attachment with the SIT-5 system.

Prior to evaluation under discharge conditions, the mercury propellant flowrate through the subassembly was determined as a function of vaporizer temperature while the cathode heater was powered alternately with 0, 5.3, and 8 W to simulate cathode operation at 0, 100, and 150% of rated power. The temperature at the midpoint of the vapor tube was monitored throughout this test.

a. Experimental Conditions — The neutralizer subassembly was located in one arm of a 6 in. i.d. glass-cross vacuum system which utilizes an oil diffusion pump and a liquid nitrogen cold trap to maintain an ambient pressure of $P < 10^{-5}$ Torr. The subassembly was attached to a metal plate (having a diameter of approximately 6 in.) in such a manner as to simulate the normal attachment of the keeper housing with the ground-screen mask of the SIT-5 system. A

collector (the collector was made of 50% transparent wire mesh to avoid gas trapping) was mounted on an axially movable rod which extended from the opposing arm of the glass cross. Mercury was supplied to the vaporizer from a 0.05 mm precision bore capillary burette calibrated in 0.001 cm^3 increments. Displacement of the mercury meniscus as a function of time permitted accurate determination of the mercury flowrate. Thermocouples were attached at the vaporizer location and at the midpoint of the vapor-feed tube leading from the vaporizer housing to the cathode tip.

All parameters of the test system satisfied the following contractual requirements.

- Environmental pressure: $P < 1 \times 10^{-5}$ Torr
- Range of mercury flowrate equivalent: $I_{N,Hg}$ = 1.5 to 3.5 mA
- Neutralizer heater power: $P_{N,CH}$ = 0 to 5.3 W
- Neutralizer keeper current: $I_{N,K}$ = 0.2 to 0.5 A
- Neutralizer keeper voltage: $V_{N,K}$ = 20 V dc
- Collector coupling current: I_C = 30 to 50 mA
- Collector coupling voltage with respect to cathode: $V_C < 40$ V (The movable anode was adjusted to obtain a current-voltage function as specified by the NASA Project Manager.)
- Minimum vapor tube temperature: T_t = 250°C

Test data were acquired to investigate the parametric dependences of:

- The mercury flowrate and the interconnecting-tube temperature as a function of vaporizer temperature for three levels of neutralizer heater power.

- The neutralizer keeper voltage and the collector voltage as a function of keeper current for 0, 100, and 150% of rated operating neutralizer heater power. These data were obtained for constant collector currents of 30 and 50 mA, both levels being run at neutralizer mercury flowrates of 1.5 and 3.5 mA of mercury flowrate equivalent.

b. Test Results and Discussion – Propellant flowrate $I_{N,Hg}$ through the neutralizer subassembly was calibrated prior to ignition of the first discharge (as required under the contract) in order to test for possible changes in calibration as a result of subsequent arc flashback to the vaporizer surface. No such effect was observed, however. As shown in Fig. 24, the propellant flowrate equivalent increased almost exponentially from a value of $I_{N,Hg}$ = 1 mA at a vaporizer temperature $T_{N,V}$ = 150°C to a value $I_{N,Hg}$ = 10 mA at $T_{N,V}$ = 224°C. The flow calibration, which was obtained prior to the initial cathode ignition, depended only on the vaporizer temperature and was unaffected by subsequent ignition of the neutralizer-cathode discharge.

At a keeper-discharge current $I_{N,K}$ = 300 mA, keeper-discharge voltage rose from a minimum value $V_{N,K}$ = 10 to 11 V for high values of vapor flowrate, to a maximum value $V_{N,K}$ = 22 V at a mercury flowrate equivalent $I_{N,Hg}$ = 1 mA, as shown in Fig. 25. Below this flowrate, the voltage rose steeply and the discharge extinguished. As shown in Fig. 26, the neutralizer subassembly and the nearby collector grid (simulating the ion beam) depended strongly on neutralizer-to-collector spacing, propellant flowrate, and keeper discharge current. Only slight temperature differences were indicated between a thermocouple mounted at the vaporizer location and another mounted at the midpoint of the vapor feed tube leading to the cathode tip. Because of its small magnitude, the exact value of this temperature difference is thought not to be significant at the level of thruster simulation provided by the neutralizer mounting disk.

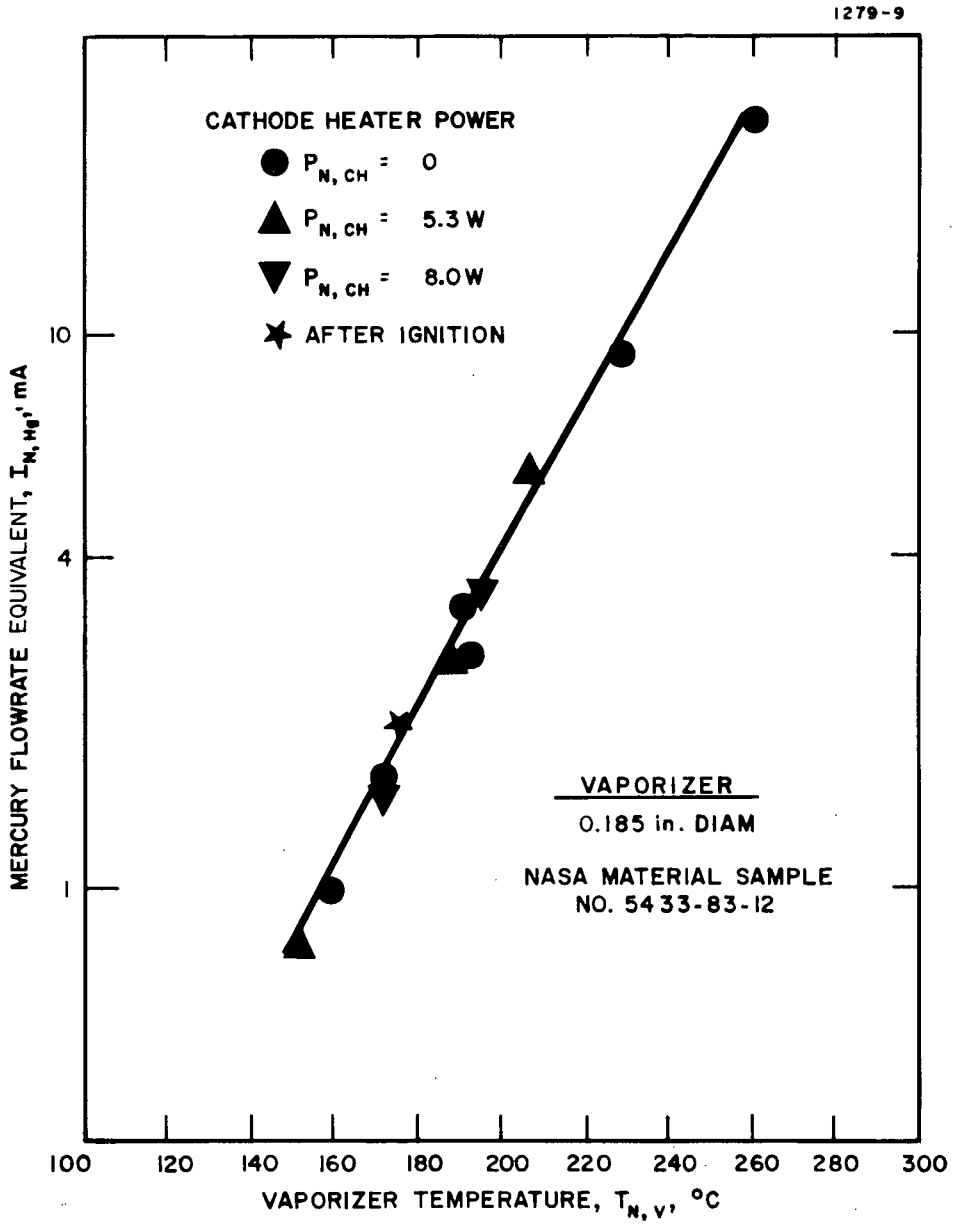

Fig. 24. Vaporizer Flow Characteristics of the Neutralizer Subassembly.

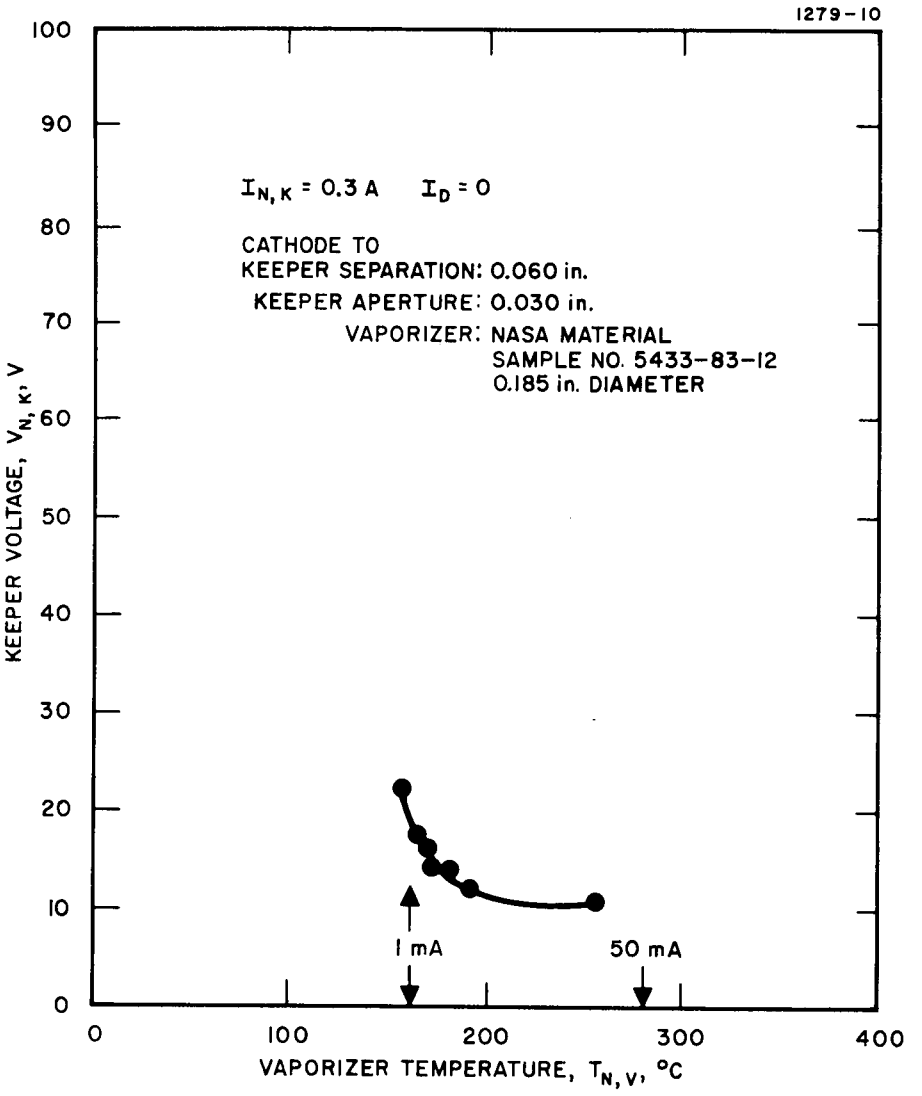

Fig. 25. Neutralizer Keeper-Discharge Characteristics.

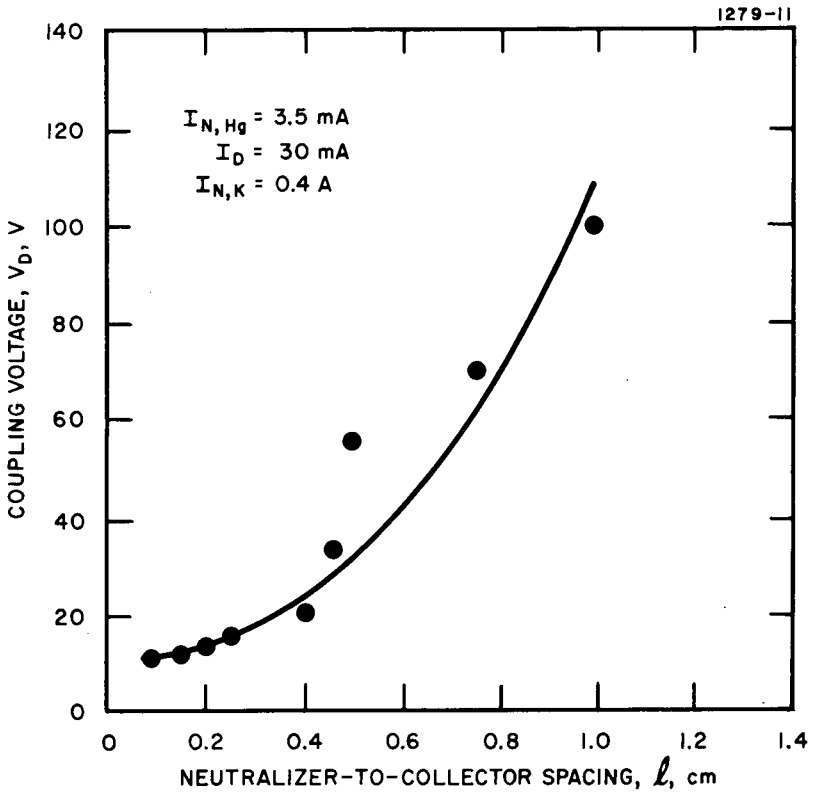

Fig. 26. Dependence of Coupling Voltage on Neutralizer-to-Collector Spacing.

Figures 27(a), (b), and (d) indicate the change in neutralizer-keeper voltage $V_{N,K}$ and collector-coupling voltage V_D as a function of keeper current $I_{N,K}$. Because of close thermal coupling and the high sensitivity of propellant flow-rate on neutralizer heater power, the vapor-tube temperature could not be maintained above $T_t = 250°C$, and operation of the neutralizer was confined to over-all power levels ranging from 3.7 to 5.1 W. No lack in performance resulted from this limitation, however. Figures 27(a), (b), (c), and (d) indicate the change in neutralizer keeper voltage $V_{N,K}$ and collector discharge voltage V_D as a function of keeper current $I_{N,K}$, with the keeper to collector distance $\ell = 1$ mm. Figures 27(a) and (b) describe operation at a neutral flow-rate equivalent $I_{N,Hg} = 3.5$ mA, while Figs. 27(c) and (d) relate to operation at $I_{N,Hg} = 1.5$ mA. Figures 27(a) and (c) describe operation at a coupling-discharge current $I_D = 30$ mA while Fig. 27(b) and (d) relate to operation at $I_D = 50$ mA. A common feature of all figures in this series is the keeper voltage which is relatively constant at a value $10 \text{ V} < V_{N,K} < 15 \text{ V}$ for low values of keeper current, but rises with higher values of $I_{N,K}$ particularly at the lower value of mercury flowrate equivalent $I_{N,K} = 1.5$ mA. In Fig. 27(d) the keeper voltage rises to the maximum value recorded of $V_{N,K} = 28$ V at $I_{N,K} = 0.5$ A. Collector coupling voltage V_D, on the other hand, is decreased by increasing keeper current $I_{N,K}$ and approaches a value $V_D \sim 10$ V for keeper current $I_{N,K} \gtrsim 0.4$ A, except in the case described by Fig. 27(b) where a higher value $I_{N,K} \gtrsim 0.8$ A was required.

The parametric variations of neutralizer operation covered in these tests spans the range required for satisfactory operation of the neutralizer with the SIT-5 thruster system. The curves demonstrate that low coupling-discharge voltages can be achieved between the beam and neutralizer

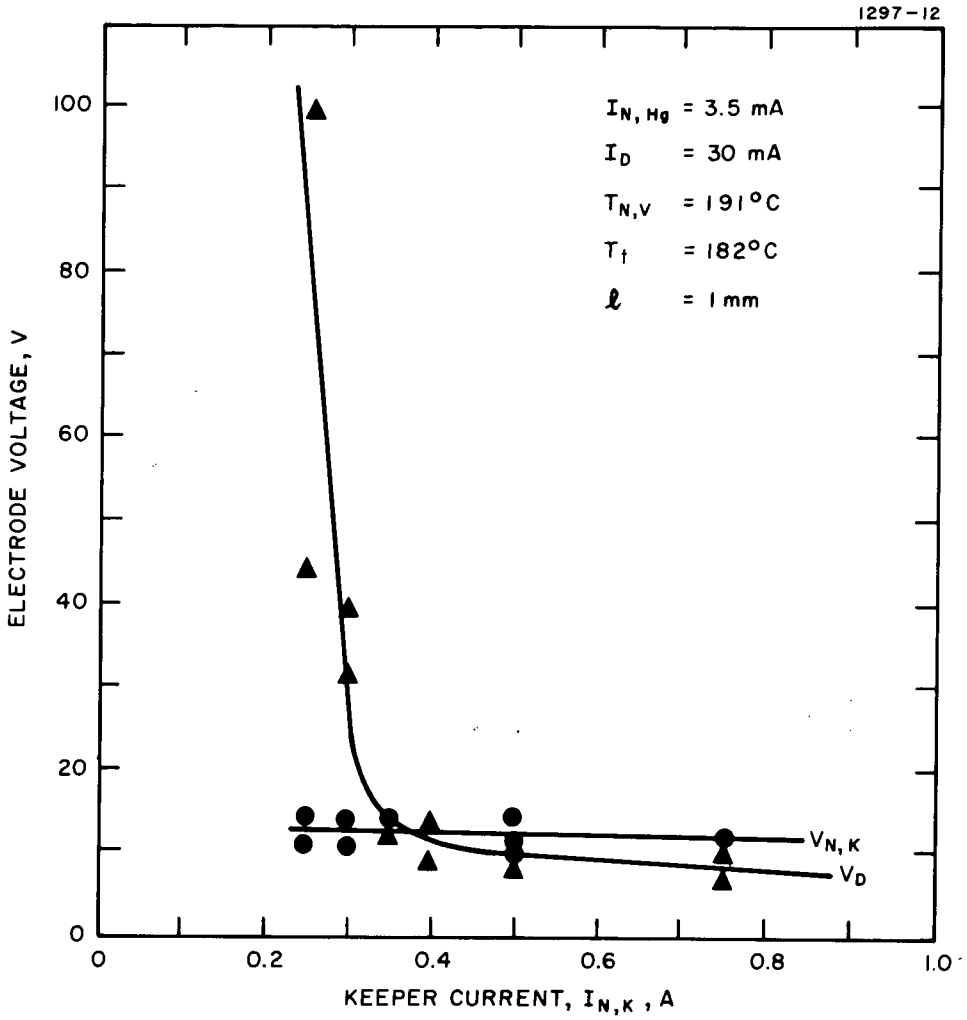

Fig. 27(a). Discharge and Keeper Voltage as a Function of Keeper Current.

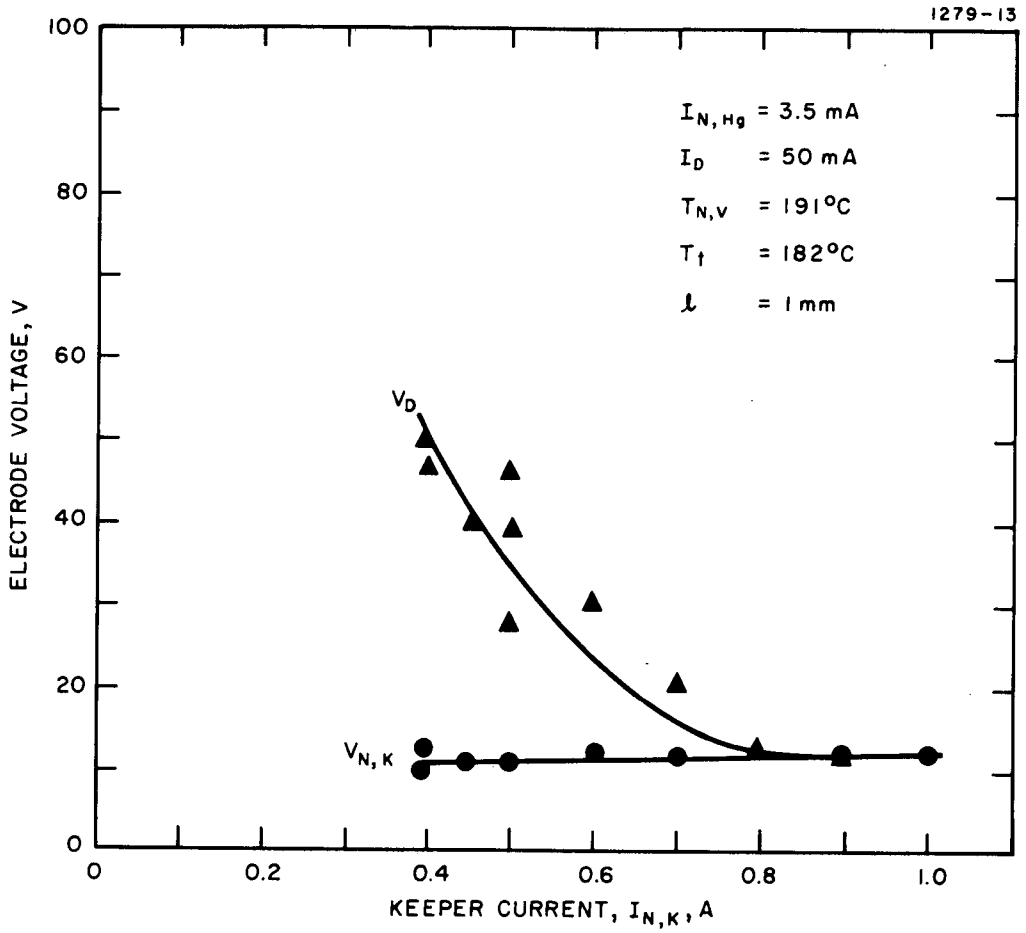

Fig. 27(b). Discharge and Keeper Voltage as a Function of Keeper Current.

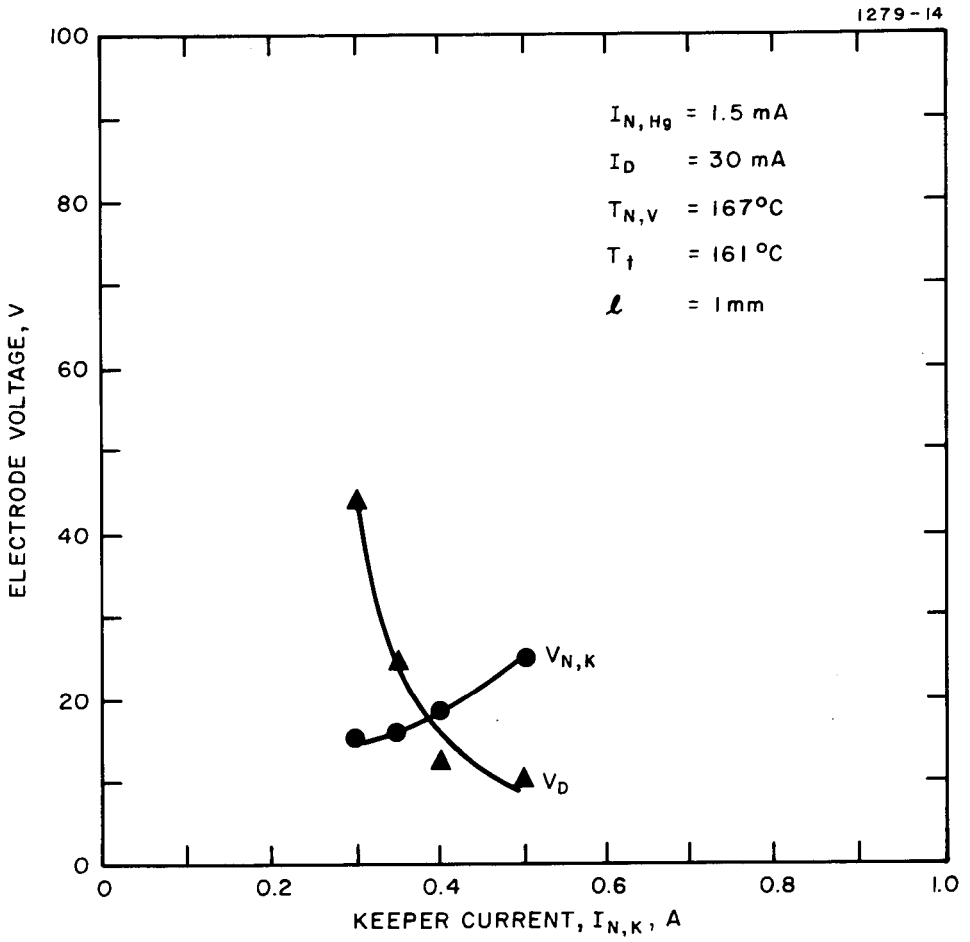

Fig. 27(c). Discharge and Keeper Voltage as a Function of Keeper Current.

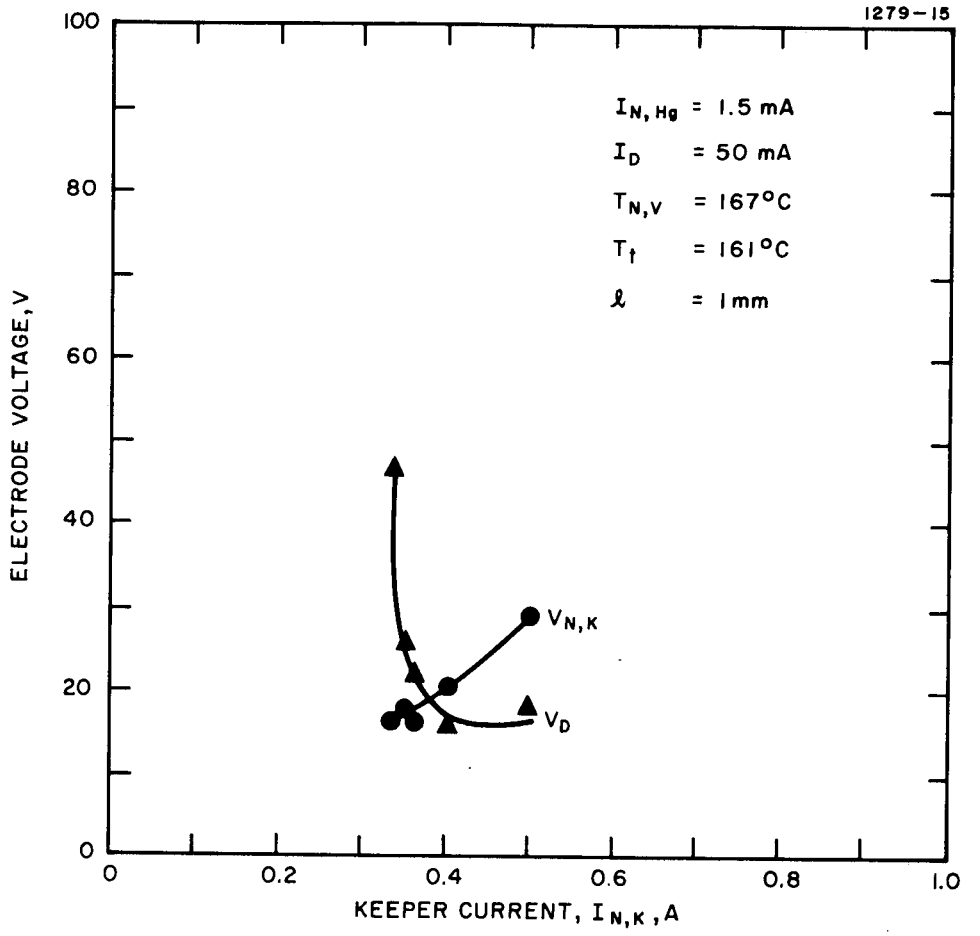

Fig. 27(d). Discharge and Keeper Voltage as a Function of Keeper Current.

plasma by proper balance of neutral mercury flowrate, keeper current, and neutralizer to beam spacing. The extreme dependence of coupling-discharge voltage V_D on neutralizer-to-collector spacing ℓ indicates the importance of careful placement of the neutralizer cathode with respect to the SIT-5 thruster. At neutralizer-to-collector spacing ℓ = 1 mm, both the keeper voltage $V_{N,K}$ and the coupling-discharge voltage V_D could be held below 20 V by setting the keeper current to a value in the range 0.3 A < $I_{N,K}$ < 0.7 A. On the basis of the experimental results discussed above, no design modifications were recommended for the SIT-5 neutralizer design.

3. Reservoir Feed System Subassembly

The reservoir feed system subassembly was tested to establish the pressure retention capability of the positive-expulsion propellant reservoir and to establish the long term capability for vaporizer phase separation under steady state and cyclic operation. The same (S/N 101) mercury propellant reservoir, feed line, and vaporizers were used in this test as had earlier been subjected to the dynamic environment imposed by the structural integrity tests.

After successful completion of the structural integrity tests, the S/N 101 assembly of the SIT-5 thruster system was mounted inside a vacuum chamber (fitted with a cold trap and operating at an environmental pressure of less than 10^{-5} Torr) for use in the reservoir feed system subassembly test. In the first part of this test, the neutralizer-vaporizer was held at a constant temperature to obtain a nominal mercury flowrate equivalent of $I_{N,Hg}$ = 2.5 mA. The main cathode vaporizer was heated cyclicly between $T_{N,V}$ = 100°C and a temperature required to obtain a nominal flowrate of $I_{M,Hg}$ = 50 mA. The cycling rate was a rapid as possible, consistent

with obtaining the required temperature excursion. The upper temperature limit was held for about 5 min for each cycle. At the conclusion of 50 hours of cyclic testing, a steady state test of 50 hours duration was conducted at a constant main-vaporizer temperature corresponding to a propellant flowrate equivalent of $I_{M,Hg}$ = 50 mA and neutralizer vaporizer temperature corresponding to $I_{N,Hg}$ = 2.5 mA. The system was weighed before and after both tests to determine the rate of propellant utilization.

a. Experimental Conditions – Throughout all testing, nitrogen pressure in the positive expulsion reservoir was monitored electrically by means of the Servonic pressure transducer, which was already attached at the time of the structural integrity test. This transducer was utilized in preference to external gauges to avoid the necessity of breaking the nitrogen system seal, thereby permitting the pressure retention capability of the positive expulsion system to be confirmed. Because no direct measure of mercury flowrate is provided with the SIT-5 system (except during testing where a burette feed system is used), vaporizer flow calibrations were inferred from the discharge characteristics of the main and neutralizer cathode subassemblies.

b. Vaporizer Flow Calibration – The temperature variation of a typical vaporizer flow characteristic has previously been shown in Fig. 24; this particular curve was generated during the neutralizer-vaporizer subassembly tests. In this curve, the propellant flowrate equivalent increases almost exponentially with a rate of one decade every 72°C from a value of $I_{N,Hg}$ = 1 mA at a vaporizer temperature $T_{N,V}$ = 152°C to a value $I_{N,Hg}$ = 10 mA at $T_{N,V}$ = 224°C. The slope of this curve with respect to temperature, however, is a function only of the vapor pressure of mercury and is virtually identical for all vaporizers, so that the curve is completely

specified if any point of the curve is known. With the S/N 101 assembly of the SIT-5 thruster, one specific value of neutral flowrate was inferred for each vaporizer by examining the discharge characteristic of the cathode fed by each vaporizer.

The discharge characteristics of the neutralizer subassembly described perviously were shown in Fig. 25. At a neutralizer-keeper discharge current $I_{N,K}$ = 300 mA, keeper discharge voltage rises from a minimum value $V_{N,K}$ = 10 to 11 V for high values of vapor flowrate to $V_{N,K}$ = 20 V at a mercury flowrate equivalent $I_{N,Hg}$ = 1 mA. Below this flowrate, the voltage rises steeply and the discharge extinguishes. Both the main and neutralizer cathodes of the S/N 101 system were thought to exhibit similar discharge characteristics with respect to their keepers, because the geometrical arrangement in both of its cathodes is almost identical to the one used to generate the data shown in Fig. 25. This characteristic was exploited, therefore, to generate intercept values for the flow characteristics of the two vaporizers associated with the reservoir-feed system subassembly.

Discharge characteristics for the main and neutralizer cathodes of the S/N 101 thruster assembly are shown in Figs. 28 and 29. Based on the data of Fig. 25, the vaporizer temperature at which the mercury flowrate equivalent reached a value of I_{Hg} = 1 mA was identified to occur where V_K = 20 V, which corresponds to a main cathode vaporizer temperature of $T_{N,V}$ = 180°C and a neutralizer-cathode vaporizer temperature of $T_{N,V}$ = 250°C. These values established the necessary intercept values which, with the temperature variation expected from Fig. 24, combine to generate the two vaporizer characteristics shown in Figs. 30 and 31. The two flow characteristics shown as solid curves provided the basis for determining the settings for the main and neutralizer vaporizer temperatures for the two 50 hour tests described below.

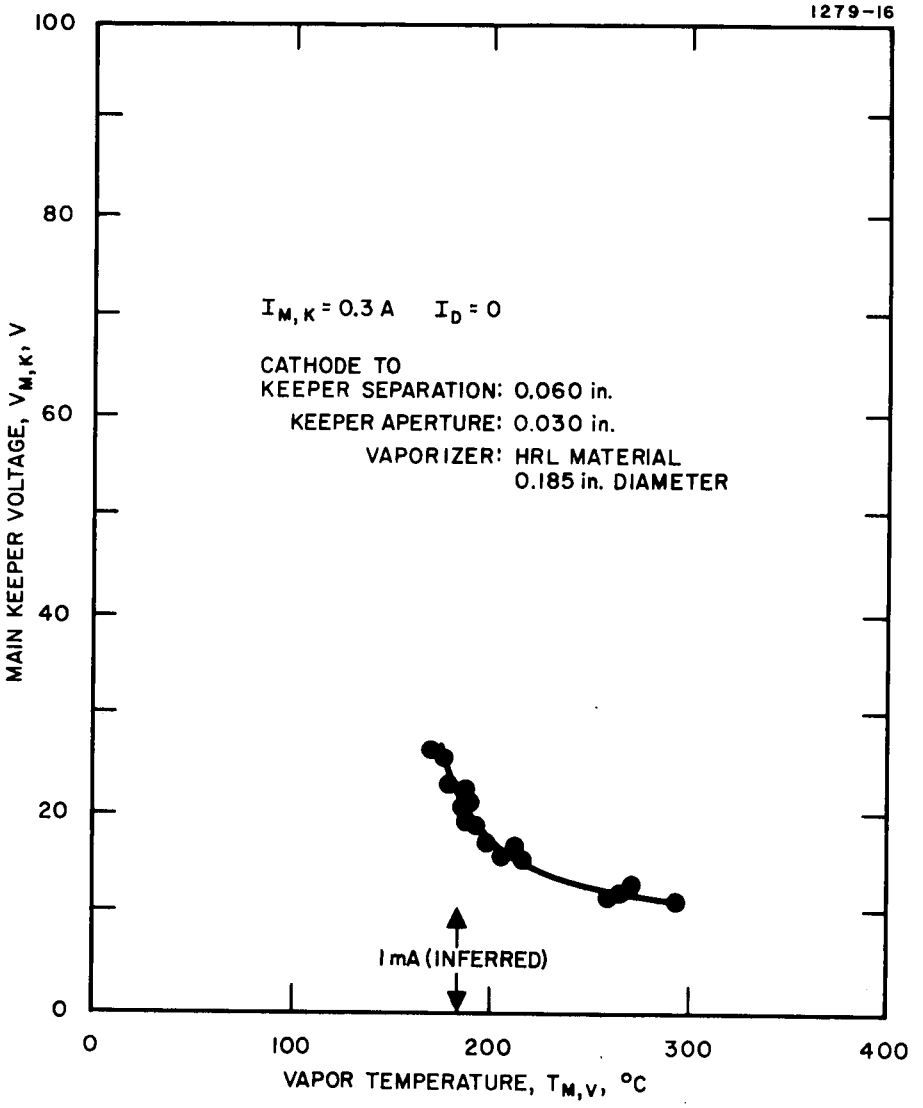

Fig. 28. Main Cathode Discharge Characteristics for the SIT-5 Thruster S/N 101.

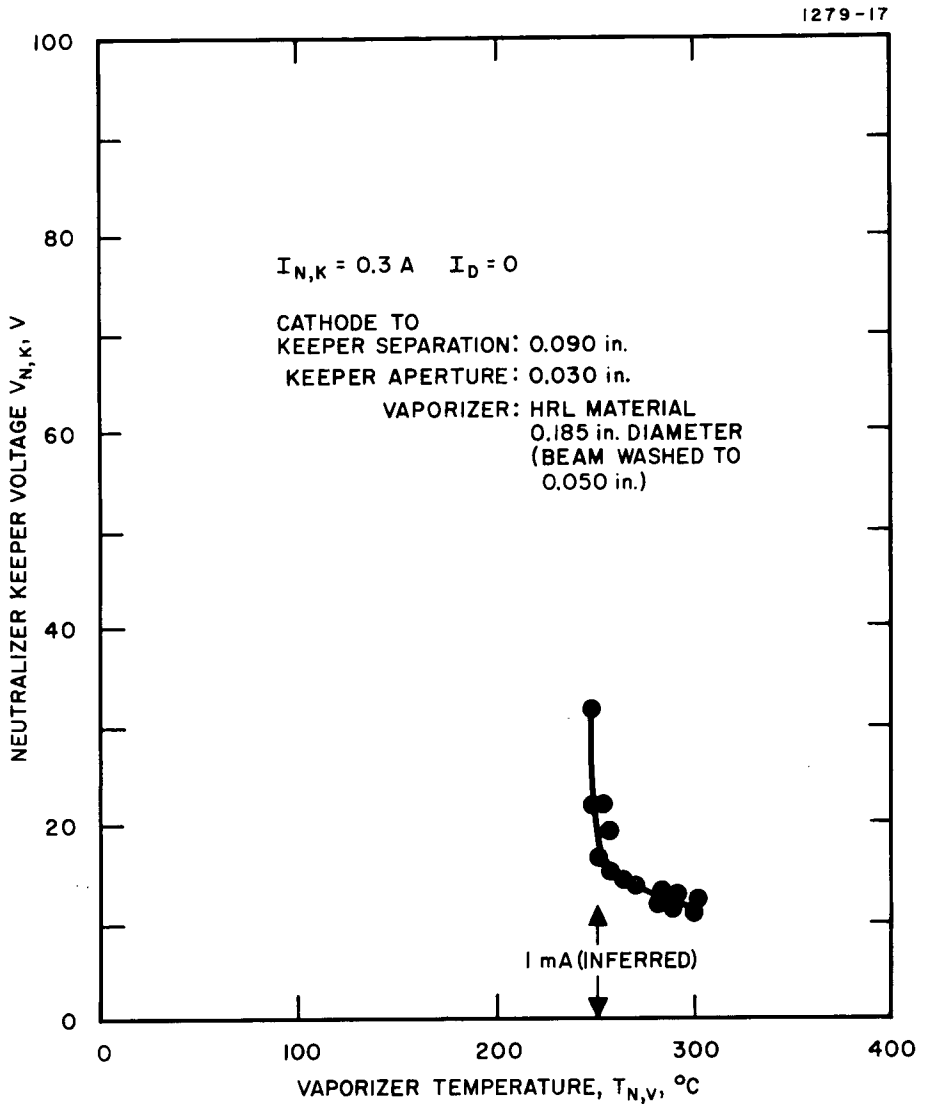

Fig. 29. Neutralizer-Cathode Discharge Characteristics for the SIT-5 Thruster S/N 101.

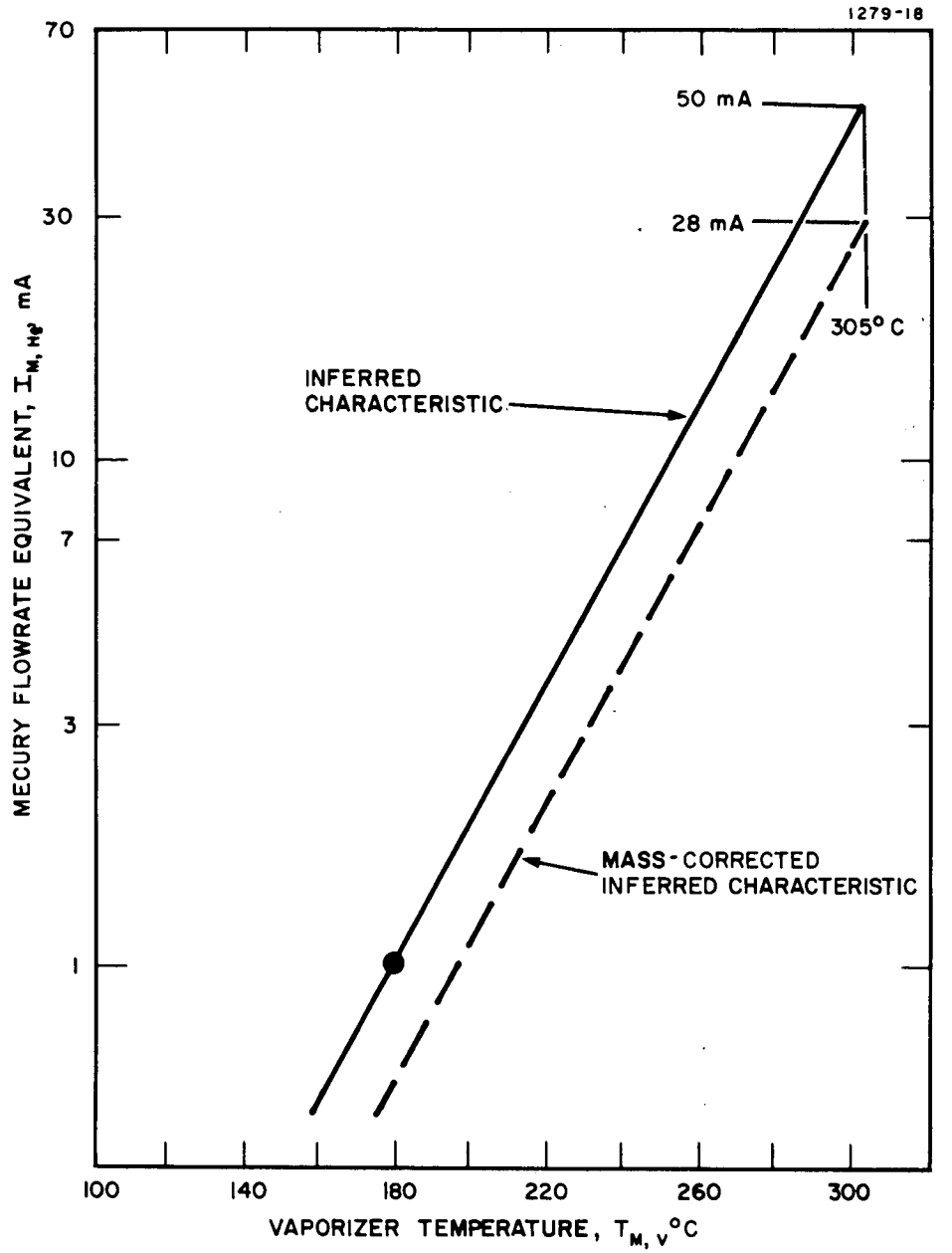

Fig. 30. Inferred Main Cathode Vaporizer Flow Characteristics for the SIT-5 Thruster S/N 101.

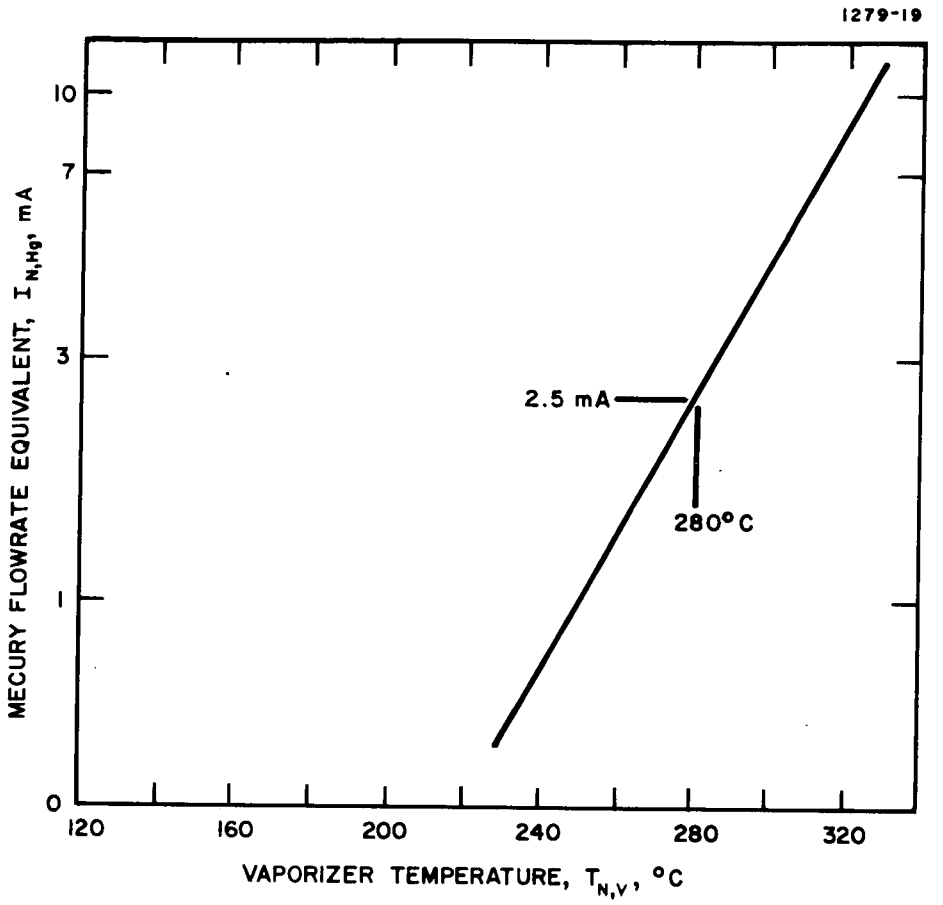

Fig. 31. Inferred Neutralizer-Cathode Vaporizer Flow Characteristics for the SIT-5 Thruster S/N 101.

c. Cyclic and Steady State Tests – A 50 hour cyclic test of the reservoir and feed system subassembly tests was conducted with the neutralizer vaporizer temperature set at $T_{N,V}$ = 280°C to establish a flowrate $I_{N,Hg}$ = 2.5 mA and with the main vaporizer temperature cycled between $T_{M,V}$ = 100°C and 305°C for a maximum flowrate $I_{M,Hg}$ = 50 mA. The cyclic test was followed directly by a 50 hour test conducted at full constant flow.

These tests established the pressure retention capability of the positive expulsion feed system and the long term capability for vapor phase separation under steady state and cyclic operation. Throughout the flow tests, nitrogen pressure was monitored electrically by means of the Servonic pressure transducer that is attached to the system. Before and after the completion of all testing, the system was weighed in order to calculate the average propellant flowrate. No variation in gas pressure was ascertained within the accuracy (±1%) of the transducer indication. Measurements of system mass before and after the 50 hour cyclic tests were identical at 8.284 kg. This was interpreted as an indication that the mercury vapor had recondensed in the vapor flow tubes and isolator. To prevent recondensation during the 50 hour constant flow test, both cathodes were heated with 4 W applied at the main cathode and 2 W at the neutralizer cathode. After the second 50 hour test, a total mass loss of 17 g was measured. This propellant mass corresponds to an integrated flow of F = 2300 mA hours of mercury flowrate equivalent, which is somewhat less than the value anticipated from the inferred vaporizer flowrate calibration presented in Figs. 30 and 31. On the basis of this mass measurement, a corrected value for the main vaporizer flow calibration was determined.

d. Mass Correction — A correction to the inferred main cathode vaporizer flow characteristics is shown as a dashed line in Fig. 30. This correction was derived in such a manner as to revise the original inferred flow characteristic to the extent that the integrated flowrate calculated from the mass-corrected characteristic would yield a total mass flow equal to the 17 g mass reduction actually measured. Because of the fact that only one mass measurement was available after operation of both the main and neutralizer-cathode vaporizer, there was no way of separating the mass flow due to one or the other. By assuming that the inferred calibration characteristic of the neutralizer-cathode vaporizer was correct, however, its relatively small contribution to the over-all flow could be substracted to permit separate evaluation of a mass-corrected value for the main cathode vaporizer flow characteristic.

Throughout the entire subassembly test, a time history was maintained of the temperature, and heater voltage and current of both vaporizers. This hisory is summarized in Table VII and used to calculate the inferred mass flowrate from both vaporizers on the basis of the solid curves of Fig. 30 and 31. The contribution during cyclic tests was evaluated from the total flow per cycle calculated from the temperature history of the main vaporizer during a typical cycle shown in Fig. 32. Using the solid curve of Fig. 30, the flow history of the main vaporizer during a single cycle was plotted. This curve, shown in Fig. 33 can be approximated closely by a trapezoid which rises linearly from zero to an inferred flowrate of $I_{M,Hg}$ = 48.5 mA in 0.45 hours, remains level at $I_{M,Hg}$ = 48.5 mA for 0.14 hours, and then falls linearly back to zero in 0.06 hours. The propellant flow integrated from this approximation is equal to F = 19.2 mA hour/cycle or $I_{M,Hg}$ = 19.2 mA hour/hour. On a similar basis,

TABLE VII

Summary of the Temperature History and Mercury Flow Calculated from the Solid Curves of Figs. 30 and 31

Test Description	Main Vaporizer		Neutralizer Vaporizer		Total Calculated Propellant Flow F', mA hour
	Temperature History	Calculated Flow, F, mA hour	Temperature History	Calculated Flow, F, mA hour	
Generating Figs 28 and 29	215°C for 4 hour 185°C for 4 hour 260°C for 1 hour 250°C for 1 hour	3.2 x 4 = 12.8 0.5 x 4 = 2.0 15 x 1 = 15.0 9.5 x 1 = 9.5	270°C for 7 hour 265°C for 6 hour	1.85 x 7 = 13.0 1.6 x 6 = 9.6	
Determining Cycle Time	100°C to 250°C for 7 hour (see Fig. 32)	3.7 x 7 = 26.0		0.0	
50 hour Cyclic Test	100°C to 305°C for 50 hour (see Fig. 32)	19.2 x 50 = 960.0	280°C for 50 hour	2.5 x 50 = 125.0	
50 hour Steady State Test	305°C for 50 hour	50 x 50 = 2500.0	280°C for 50 hour	2.5 x 50 = 125.0	
Subtotal		3525.3		272.6	3797.9

T281

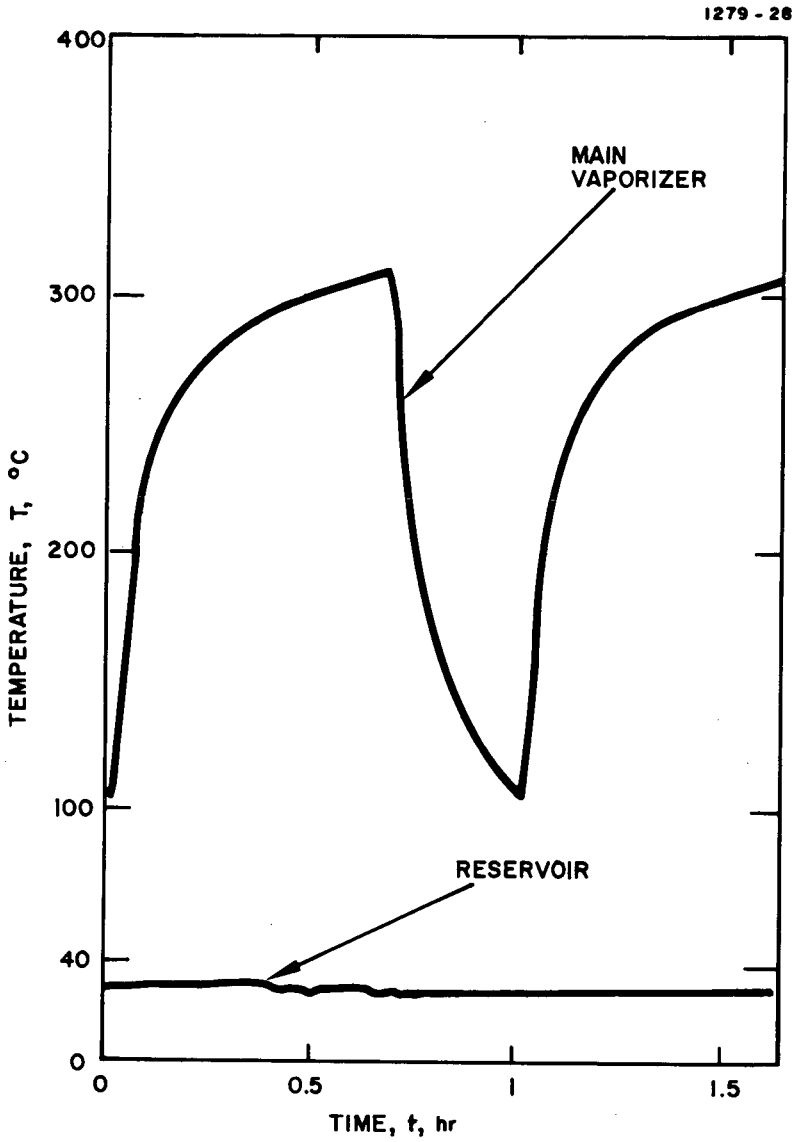

Fig. 32. Main Vaporizer and Reservoir Temperature Histories During the 50 Hour Cyclic Test.

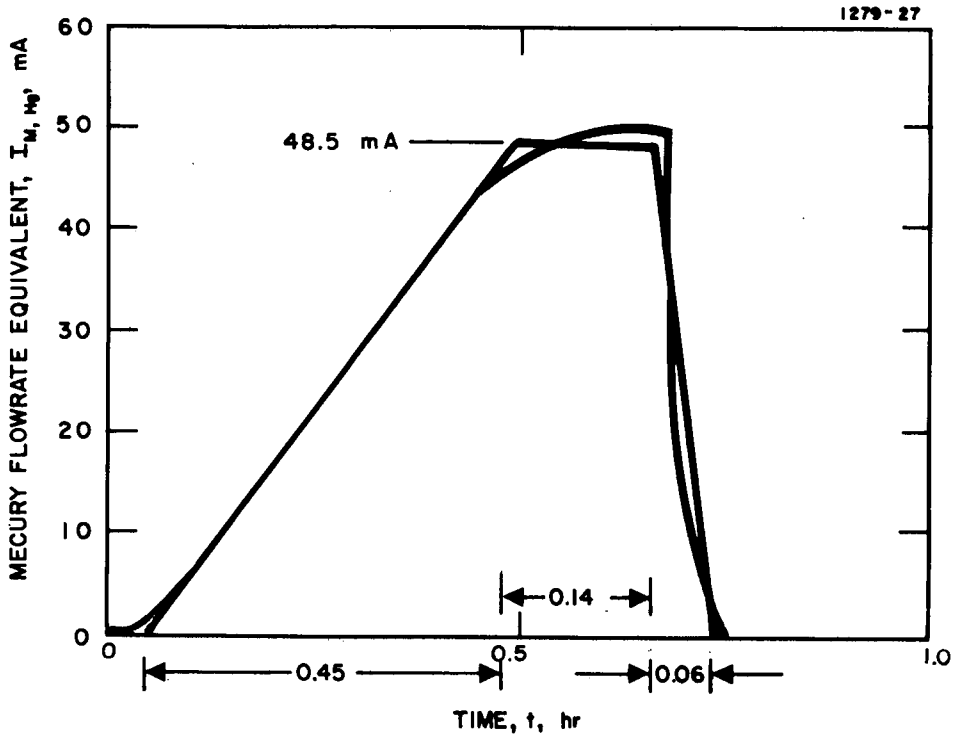

Fig. 33. Flow History of the Main Cathode Vaporizer During a Typical One-Hour Cycle From $T_{M,V}$ = 100°C to $T_{M,V}$ = 305°C.

cycles between $T_{M,V}$ = 100°C and $T_{M,V}$ = 250°C were shown to result in a propellant flow of $I_{M,Hg}$ = 3.7 mA hour/hour.

The total calculated integral flow of F' = 3797.9 mA hour, which is listed in Table VII, exceeds the value of propellant flow indicated by mass-loss measurements which was F' = 2300 mA hour. If the neutralizer flow calibration of Fig. 31 is assumed to be correct (merely as an expedient for evaluating mass-corrected value of the main vaporizer calibration) the total calculated value of the neutralizer propellant flow of F'_N = 272.6 mA hour can be subtracted from the total values yielding a mass-loss flow indication for the main cathode of F_M = 2028.4 mA hour and a calculated value of F_M = 3525.3 mA hour indicated from the uncorrected inferred flow calibration of Fig. 30. The ratio of these values F_M/F_M establishes the mass-corrected value of the inferred flow characteristic for the main vaporizer, which is shown as a dashed line in Fig. 30.

D. SYSTEM OPTIMIZATION AND PERFORMANCE

Two 50 hour and one 100 hour tests were conducted to document performance of the SIT-5 propulsion system. The initial 50 hour performance test established the thruster performance level both for steady state and cyclic operation after completion of discharge chamber optimization. For this test the flight-type propellant reservoir was replaced by a laboratory system to permit measurement of propellant flowrate. In the second 50 hour test, the entire thruster system was operated in its flight-type configuration to verify the efficacy of the over-all design. For both 50 hour tests, the system was operated with low specific impulse dielectric-coated grids as shown in Fig. 2. For the final 100 hour

test, the discharge chamber was coupled with a thrust-vectorable grid set developed under Contract NAS 3-14058 which is capable of two-dimensional high angle (±10°) beam deflection.

1. Optimization and Performance Test

The SIT-5 thruster system assembly was tested with its dielectric-coated ion extraction system to optimize and establish its performance characteristics. The test was divided into the following four parts:

(1) Short term tests for system optimization and to confirm the design and performance predictions.

(2) A 50 hour performance verification test using the best configuration determined from the short term tests.

(3) A cyclic test consisting of 10 cycles of thruster startup and shutdown.

(4) An eleventh cycle to full beam normal operation after startup from a standby condition.

A contractual goal for thruster operation with an over-all efficiency of η_T = 26.6% was approximated during over 50 hours of testing the SIT-5 thruster system. The best over-all performance was obtained with the electrical efficiency at η_E = 40% and the propellant utilization efficiency of η_m = 65%, including neutralizer losses which averaged about 9% of total propellant flow.

a. Experimental Plan

(1) Experimental Conditions – All tests were performed in an oil-diffusion-pumped vacuum system approximately 2 ft in diameter by 6 ft long; a liquid nitrogen cooled

cylindrical liner covered the sides of the chamber. Pressure did not exceed 1×10^{-6} Torr during the thruster operation. The thruster was mounted in front of a liquid nitrogen cooled circular disk so that all parts of the thruster were surrounded by liquid nitrogen cooled surfaces. The beam collector was a flat circular copper plate located at the end of the vacuum chamber. The thruster system was instrumented with thermocouples located at the following locations:

- Main vaporizer
- Isolator (inlet and outlet ends)
- Thruster endplate (at full and half anode radius)
- Thruster chamber outer surface (midpoint)
- Accelerator grid mount (at the outer edge)
- Neutralizer vaporizer
- Interconnecting tube between vaporizer and cathode
- Thruster system envelope (at the midpoint of thruster)

(2) Propellant Flow – Feed tubes from the main cathode and neutralizer cathode were connected to separate mercury reservoirs. For the main cathode, mercury was provided by the piston driven supply system described earlier. For the neutralizer cathode, the more sensitive flowmeter was employed which uses a capillary tube (open to atmosphere at the upstream end) to measure mercury consumption. Both feed systems were filled under vacuum in order to eliminate introduction of gas bubbles.

(3) Power Supply Calibration – Calibration and evaluation of all power supplies and data acquisition equipment conformed to approved reliability and quality assurance requirements. In addition to these requirements, evaluation of the equipment included but was not limited to:

- Voltmeter and ammeter calibration (zero to full scale in no less than five increments)
- Ripple content at 25, 50, 75, and 100% full load
- Transient response of voltage and current to load increases and decreases in step changes between zero and design operating conditions

Results of these calibrations are on file at HRL but are not included as part of this report.

(4) Data Acquisition – Data acquired for the tests described above included the following.

- Main vaporizer voltage and current ($V_{M,VH}$ and $I_{M,VH}$).
- Main cathode heater voltage and current ($V_{M,CH}$ and $I_{M,CH}$).
- Main keeper voltage and current ($V_{M,K}$ and $I_{M,K}$).
- Ion chamber discharge voltage and current (V_D and I_D).
- Net accelerating voltage ($V_B + |V_{Ac}|$).
- Ion beam current (I_B).
- Accelerator voltage (V_{Ac}).
- Accelerator drain current (I_{Ac}).
- Neutralizer vaporizer voltage and current ($V_{N,VH}$ and $I_{N,VH}$).
- Neutralizer keeper voltage and current ($V_{N,K}$ and $I_{N,K}$).

- Neutralizer coupling current, (I_C).
- Neutralizer coupling voltage, (V_C).
- Neutralizer heater voltage and current ($V_{N,CH}$, $I_{N,CH}$).
- Propellant flow rates ($I_{M,Hg}$ and $I_{N,Hg}$).
- Ion chamber energy per beam ion (V_{Disch}).
- Electrical efficiency (η_E).
- Propellant utilization efficiency, (η_m).
- Over-all efficiency, (η_T).

b. Short-Term Optimization Tests — Optimization of the SIT-5 thruster performance began even before completion of the first module by utilization of another 5 cm thruster which had been constructed under a Hughes IR&D program (IR&D-5). Because the thruster was not identical to the SIT-5, no attempt was made to optimize discharge chamber performance, instead the thruster was used to study the dependence of neutralizer coupling voltage on the neutralizer position and on the neutral mercury flowrate. A hollow cathode with an enclosed keeper (0.076 cm diameter keeper aperture) was placed close to the original SIT-5 design position (see Fig. 5) at a 45° angle with the beam axis and with the aperture located 3.18 cm downstream and 1.27 cm radially outward from the knee of the screen pole piece. With a neutralizer keeper current $I_{N,K}$ = 400 mA, the neutral mercury flowrate was reduced while thruster operating conditions were held constant at a beam current I_B = 38 mA and a mass utilization efficiency η_m = 65%. As shown in Fig. 34, the coupling voltage rose from V_C = 20 V at a neutral flowrate equivalent $I_{N,Hg}$ = 7 mA to a maximum value of 40 V at

the minimum flowrate tested ($I_{N,Hg}$ = 5 mA). Because of the similarity of the tested configuration to the SIT-5 design, it became clear that design modifications would be required under the optimization program to reduce the coupling voltage in order to achieve the contract goal of $V_C \leq 40$ V at $I_{N,Hg} \simeq 2$ mA.

In a subsequent test, the position of the neutralizer-keeper aperture was moved upstream and radially inward each by 0.63 cm from the original design position of the SIT-5 thruster, and the angle of intersection between the neutralizer and thruster axis was increased from 45 to 60°. Neutralizer to ion beam coupling voltages of less than 15 V were measured in operation of the IR&D-5 thruster at a neutralizer flowrate $I_{N,Hg}$ = 2 mA (see triangular data point in Fig. 34). At this flowrate, the neutralizer operated stably with a keeper discharge voltage $V_{N,K}$ = 17 V at $I_{N,K}$ = 300 mA of discharge current. Reduction in neutral flowrate below this level had little effect on coupling properties, but did result in a precipitous rise in cathode to keeper discharge voltage and in frequent (once every half hour) extinctions of the neutralizer discharge. As a result of these optimization tests, the design of the neutralizer mounting structure was modified (see Fig. 9) to conform to the second configuration, which resulted in adequate coupling characteristics with the reduced ($I_{N,Hg} \simeq 2$ mA) neutral flowrate.

Optimization of the SIT-5 discharge chamber itself was initiated with a thruster in which electromagnets had been incorporated to provide a variable magnetic field intensity. Enlargement of the main keeper orifice from 0.076 cm to 0.127 cm was the only modification from the design configuration required to achieve acceptable performance. In that configuration, the SIT-5 thruster has been operated at a

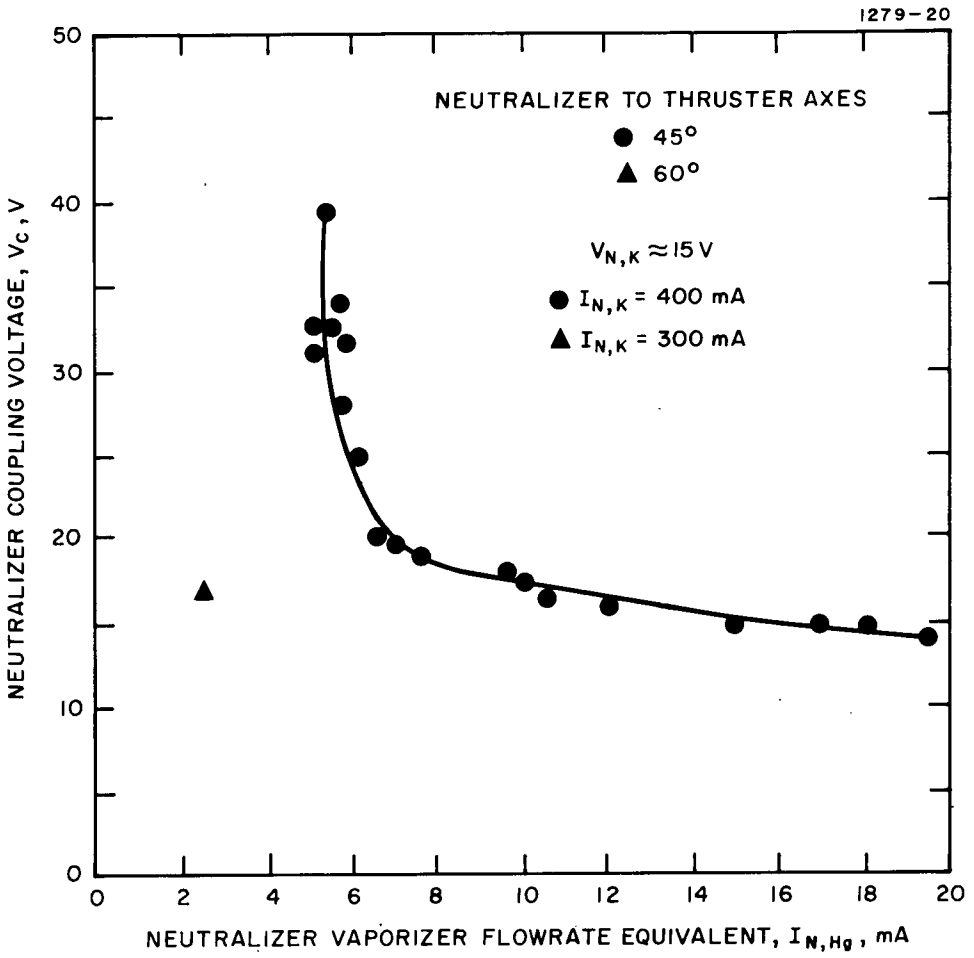

Fig. 34. Neutralizer-to-Beam Coupling Characteristics.

thrust level of 0.41 mlb (beam current I_B = 35 mA, and beam voltage V_B = 650 V) with a discharge energy per ion of 352 eV/ion and a discharge chamber mass utilization efficiency η_m' = 78.5%.*

Subsequently, similar performance was achieved with the eight 0.450 cm diameter permanent magnets indicated in the original design by a single modification, which involved doubling the axial length of the collar pole piece from the original design value of 0.476 to 0.952 cm. The magnetic field pattern for that geometry, shown in Fig. 35, was not discernibly different from that used in the short term optimization tests. In this configuration, a discharge chamber mass-utilization efficiency as high as $\eta_m' > 75\%$ was achieved with a discharge chamber energy $V_{disch} \leq 400$ eV/ion. Based on these results, and with anticipation of successful operation of the redesigned neutralizer cathode subassembly, thruster assembly S/N 102 was prepared for operation in the 50 hour test.

c. Performance Test (50 hours) – After the short term tests were completed, a 50 hour verification test was conducted with the S/N 102 module of the SIT-5 system. The purpose of the test was to verify the short term operational parameters over a longer period of time.

---

*Throughout this report, mass utilization efficiency and beam power have been calculated using beam currents equal to the coupling currents. This is a conservative calculation since it considers only the ions that leave the thruster. Neutral mercury atoms (created by charge exchange) also leave the thruster at the same velocity as the ions. The newly created ions from the charge exchange are attracted to the accel electrode where they add to the drain current.

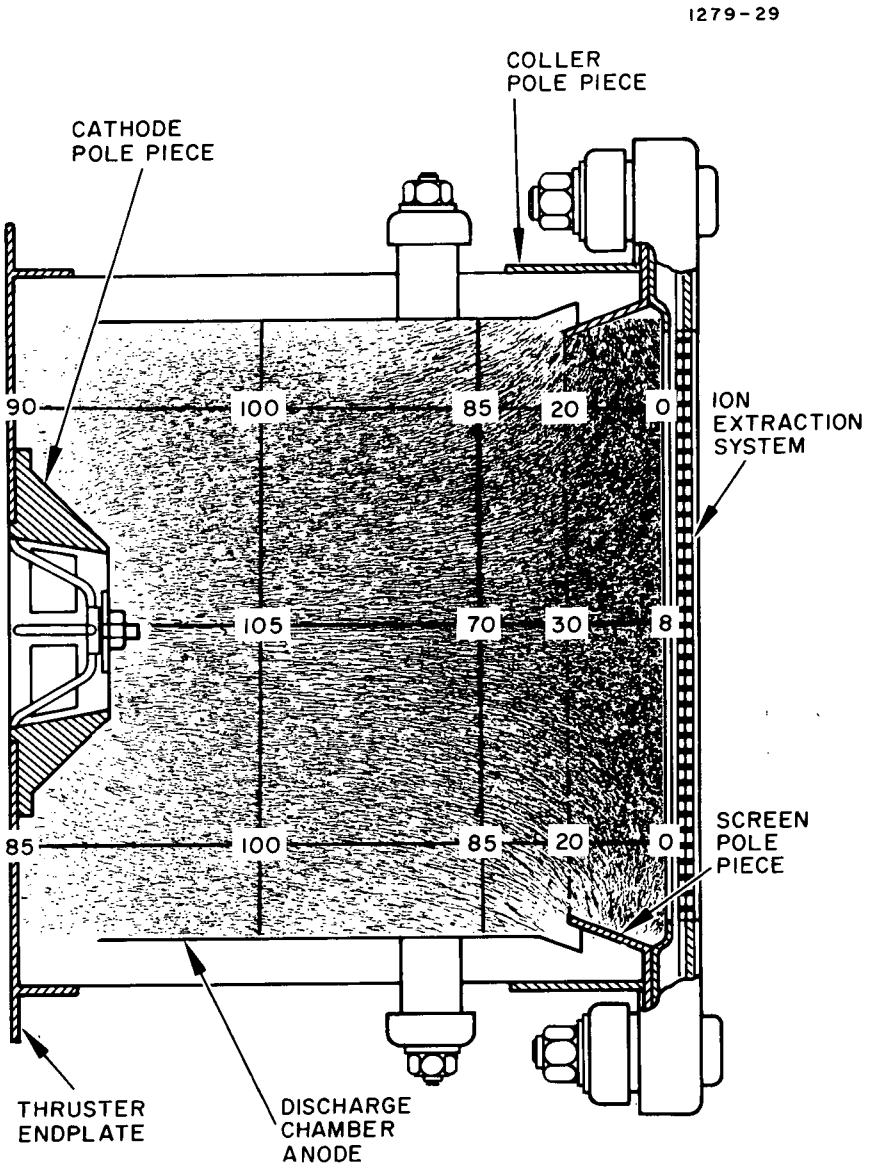

Fig. 35. Magnetic Field Pattern in the SIT-5 Discharge Chamber. (Indicated Magnetic Field Intensity is Measured in Gauss.)

Prior to the start of the 50 hour test, the neutralizer was moved slightly from the position shown in Fig. 9. Its new location was 1.5 cm downstream and 0.456 cm radially outward from the outermost beam aperture of the ion-extraction system. In this configuration, the aperture of the neutralizer keeper lay on a line extending at 17° to the thruster axis from the outermost beam aperture. In order to hold thruster operation at a constant set point, power to the main cathode vaporizer was regulated to maintain a constant temperature at the vaporizer. Later in the test (after approximately 20 hours), the control loop of the main vaporizer power was changed from the vaporizer temperature to the beam current. This method appeared to be more satisfactory because the main vaporizer power remained nearly constant. The results of this test can best be shown by reproducing typical data points taken during the test. These data are shown in Table VIII and are those recorded at two hour intervals. The change of control loops is also indicated in Table VIII; at the bottom of the table, sets of average values are shown. These sets are:

- Data taken with the vaporizer temperature controlling the main vaporizer power (21 hours 34 min)
- Data taken with the beam current controlling the main vaporizer power (28 hours 27 min)
- Data averaged over the entire period

The calculated results are listed in Table IX. The efficiencies were virtually the same in all cases with the electrical being over η_E = 40%, the mass (including the neutralizer) η_m = 65.2%, and the total over η_T = 26%.

TABLE VIII

Summary of the 50 Hour Test Data

TIME INTERVALS	TIME	FLOW		┌1.09 x 10^5→		BEAM				ISOL	DISCHARGE			COUPLING		KEEPER				CATHODE HEATER				VAPORIZER								VAC
	t (min)	MAIN Hg (CC)	NEUT. Hg (CC)	M Hg cc/min	N Hg cc/min	M I_{Hg} (mA)	N I_{Hg} (mA)	V_B (V)	I_B (mA)	V_{Ac} (V)	I_{Ac} (mA)	I_I (μA)	V_D (V)	I_D (mA)	I_M (A)	V_C (V)	I_C (mA)	M V_K (V)	M I_K (mA)	N V_K (V)	N I_K (mA)	M V_{CH} (V)	M I_{CH} (A)	N V_{CH} (V)	N I_{CH} (A)	M V_V (V)	M I_V (A)	N V_V (V)	N I_V (A)	M T_V (mV)/2	N T_V (mV)/2	M T_V (°C)	N T_V (°C)	P (Torr)
	5/3/71																																	
	1556							650	36	250	0.8	—	37	295	—	12	33	10	100	10	500	0	0	0	0	3.9	1.7	3.2	1.4					
	1800					46.4	7.26	650	34.3	250	2.2	—	42	300	—	35	32	10	100	10	700	0	0	0	0	4.0	1.75	2.8	1.2	4.25	5.82	230	307	$2(x10)^{-7}$
	2000					41.8	4.0	650	33	250	2.1	—	43	220	—	35	30	10	100	10	850	0	0	0	0	AUTO		2.6	1.1	4.22	5.73	229	302	2^{-7}
	2200					43.0	5.8	650	34	250	2.4	—	42	250	—	16	32	9	100	10	900	0	0	0	0	AUTO		2.5	1.1	4.2	5.80	228	306	1.5^{-7}
	5/4/71																																	
①	0000					47.5	3.3	650	35	250	2.5	—	41	250	—	23	33	9	100	10	500	0	0	0	0	AUTO		2.6	1.15	4.22	5.78	229	305	
	0200					50.0	5.8	650	35.5	250	2.7	—	41	262	—	23	33.5	9	100	11	400	0	0	0	0	AUTO		2.65	1.17	4.21	5.73	228	302	
	0400					46.4	5.5	650	35	250	2.8	—	42	252	—	33	32	9	100	11	460	0	0	0	0	4.8/3.6	21/1.55	2.7	1.18	4.2	5.7	228	301	
	0600					47.5	3.3	650	34.5	250	2.85	—	42.5	250	—	28	32	9	100	11	480	0	0	0	0	AUTO		2.65	1.17	4.19	5.69	227	300	1^{-7}
	0800					46.4	3.3	650	35	250	2.2	—	41.5	257	—	19	33	9	100	9	500	0	0	0	0	4.75/3.55	2.05/1.55	2.85	1.22	4.20	5.93	228	312	
	1000					42.6	4.85	650	34	250	2.3	—	43	370	—	17	32	8	100	9	600	0	0	0	0	AUTO		2.75	1.20	4.15	5.90	225	311	
	1200					47.6	5.80	650	34	250	2.5	—	42	370	—	28	32	8	100	10	600	0	0	0	0	AUTO		2.65	1.15	4.15	5.78	225	305	1^{-7}
	1330					48.7	4.0	650	34	250	2.6	—	43	360	—	28	32	8	100	10	500	0	0	0	0	AUTO		2.60	1.11	4.15	5.72	225	302	1^{-7}
	1330+					● MAIN VAPORIZER POWER CONTROL CHANGED FROM MAIN VAPORIZER TEMPERATURE TO BEAM																													
	1503							650	35	250	2.2	—	42	250	—	34	33	10	100	10	500	0	0	0	0			2.3	1.11	4.02	5.76	219	305	1^{-7}
	1700					40.7	4.0	650	35	250	2.8	—	42	250	—	22	32.5	10	100	10	500	0	0	0	0	4.3	1.85	2.65	1.15	4.19	5.78	227	305	6.2^{-8}
	1901					45.2	2.9	650	34	250	2.8	—	43	250	—	20	30.5	10	100	10	500	0	0	0	0	4.21	1.81	2.7	1.17	4.17	5.79	226	305	6^{-8}
	2103					45.3	4.72	650	34	250	2.8	—	42	245	—	28	32	9	100	9	500	0	0	0	0	3.75	1.62	2.8	1.2	4.06	5.8	221	306	5.8^{-8}
	2300					46.4	4.36	650	34	250	2.9	—	42	245	—	27	31	9	100	9	500	0	0	0	0	3.75	1.62	2.8	1.2	4.05	5.79	220	305	5.8^{-8}
	5/5/71																																	
	0100					46.4	5.1	650	34	250	2.95	—	42	245	—	27.5	31	9	100	9	500	0	0	0	0	4.30	1.87	2.85	1.23	4.22	5.80	229	306	6^{-8}
	0300					44.1	4.7	650	34	250	3.0	—	42	242	—	22.5	31	9	100	9	500	0	0	0	0	4.38	1.89	2.82	1.23	4.22	5.80	229	306	5.5^{-8}
②	0500					44.1	4.7	650	34	250	3.0	—	42	250	—	22	31	9	100	9	500	0	0	0	0	4.3	1.85	2.85	1.23	4.22	5.81	229	307	5.5^{-8}
	0700					44.1	4.0	650	34	250	3.0	—	42	245	—	22.5	31	9	100	9	500	0	0	0	0	4.38	1.88	2.83	1.22	4.22	5.80	229	306	6^{-8}
	0900					42.9	4.0	650	34	250	3.0	—	42	245	—	26	31.5	9	100	9	500	0	0	0	0	4.32	1.86	2.80	1.21	4.20	5.78	228	305	
	1135					46.7	4.27	650	34	250	2.8	—	42	250	—	28	31	9	100	9	500	0	0	0	0	3.70	1.6	2.85	1.22	4.05	5.80	220	306	5^{-8}
	1300					61.5	4.4	650	34	250	2.9	—	42	260	—	30	31	9	100	9	500	0	0	0	0	4.35	1.87	2.85	1.22	4.25	5.8	230	306	5^{-8}
	1500					41.7	3.6	650	34	250	3.0	—	42	250	—	26	31	9	100	9	500	0	0	0	0	3.70	1.61	2.85	1.22	4.05	5.8	220	306	5^{-8}
	1700							650	32	250	2.9	—	42	240	—	22	30	10	100	9	500	0	0	0	0	3.65	1.59	2.85	1.22	4.00	5.88	218	310	5^{-8}
	1900					45.2	4.7	650	34	250	3.0	—	42	245	—	23.5	31.0	9.5	100	9.5	500	0	0	0	0	3.68	1.60	2.85	1.22	4.00	5.8	218	306	4.7^{-8}
	2100					44.1	4.36	650	34.1	250	3.0	—	42	255	—	24	31.5	9.5	100	9.5	500	0	0	0	0	3.70	1.59	2.80	1.22	4.00	5.8	218	306	4.7^{-8}
																AVERAGE DATA SET																		
																					POWER					POWER		POWER					
①	21 hr 34 min					45.5	4.37	650	34.7	250	2.38	—	41.7	279.1	—	27.7	32.5	9.1	100	5.9 W		0	0	0	0	7.0 W		3.13 W						
②	28 hr 27 min					43.6	4.25	650	34.07	250	2.98	—	42.05	247.4	—	24.8	31.2	9.3	100	4.5 W		0	0	0	0	7.06 W		3.4 W						
①+②	50 hr 1 min					44.4	4.30	650	34.34	250	2.68	—	41.90	261.3	—	26	31.7	9.17	100	5.1 W		0	0	0	0	7.04 W		3.29 W						

TABLE IX

Summary of 50 Hour Test Evaluation

	Time Periods		Total Time Average
	1	2	
P_B	21.2 W	20.3 W	20.6 W
P_{Ac}	2.1 W	2.7 W	2.4 W
P_C	0.9 W	0.8 W	0.8 W
P_D	11.6 W	10.4 W	11.0 W
$P_{M,CH}$	0.0 W	0.0 W	0.0 W
$P_{M,VH}$	7.0 W	7.1 W	7.1 W
$P_{M,K}$	0.9 W	0.9 W	0.9 W
$P_{N,CH}$	0.0 W	0.0 W	0.0 W
$P_{N,VH}$	3.1 W	3.4 W	3.3 W
$P_{N,K}$	5.9 W	4.5 W	5.1 W
P_{Total}	52.6 W	50.1 W	51.2 W
η_E	40.1%	40.5%	40.3%
η_m' (beam)	69.3%	71.6%	71.4%
η_m (beam + neutralizer)	65.2%	65.2%	65.2%
η_T	26.1%	26.4%	26.3%

T283

The test encountered no significant difficulties. The main keeper discharge and/or neutralizer keeper discharge went off unintentionally only five times during the test. They could be re-ignited within a minute in all cases. Generally speaking, the loss of both discharges occurred at the same time and seemed to be the result of an arc within the thruster. The observed reduction in discharge chamber mass utilization efficiency (from $\eta_m' = 75\%$ during the optimization phase to a value $\eta_m' = 71\%$ during the 50 hour test) is attributed to the use of different CIV subassemblies for the two tests. Although both subassemblies were fabricated to the same nominal specifications, undetected differences in their actual configuration are thought to have resulted in a significant performance variations. A more pronounced example of such a variation is discussed with regard to the Design Verification Test in Section D-2.

d. Cyclic Test – The thruster system performance test was concluded with a cylic test consisting of ten cycles of thruster startup and shutdown. The objective of the cyclic test was to provide performance data for the SIT-5 thruster to go from a low level standby condition to a state of full power and return to the low level condition. The low level condition, with a standby power of 10.3 W and total mercury flowrate equivalent of $I_{T,Hg} = 3.8$ mA, was consistent with low power and low propellant consumption while maintaining the main cathode-to-keeper and neutralizer cathode-to-keeper discharges. Both keeper discharges operated without a single extinction during the 19 hours standby operation prior to the start of the cyclic test and the 9 hours required for the cyclic test.

(1) Determination of Parameters – In preparation for the cyclic test, the sequencing schedule and power requirements for cyclic operation were determined by thruster operation. This operation followed the 50 hour test of the S/N 102 thruster which remained undisturbed in the vacuum chamber between the two tests.

(2) Standby Power Requirement – The power requirements were determined for operation of the main-cathode and neutralizer-cathode vaporizers in the standby condition. The ground rule for this determination was to maintain the keeper discharge currents at I_K = 100 mA and keeper voltages at approximately V_K = 20 V. Because the discharges in the main cathode and neutralizer cathode were ignited, no power was required for cathode heaters. During the initial test, beam voltage (V_B = 650 V) and accel voltage (V_{Ac} = -250 V) were left on. Data were obtained with the thruster in vacuum with the thruster surrounded by surfaces cooled to liquid nitrogen temperature. The power to both vaporizers was lowered until the predetermined keeper voltages and currents were reached. The choice for the main vaporizer heater voltage was $V_{M,VH}$ = 2.8 V and for neutralizer vaporizer heater voltage $V_{N,VH}$ = 2.5 V. With voltages set, the thruster was placed in the standby condition for over 16 hours to obtain a propellant flowrate. These data are shown in Table X.

(3) Full Power Vaporizer Requirements – For start-up from the standby condition, approximate heater voltages of $V_{M,VH}$ = 5.7 V for the main vaporizer and $V_{N,VH}$ = 4.0 V for the neutralizer vaporizer were used. Typical results for $V_{M,VH}$ = 5.6 V and $V_{N,VH}$ = 4.0 V are shown in Fig. 36. Because the initial power settings were higher than the normally required steady state value, these settings resulted in attaining normal operating temperatures within

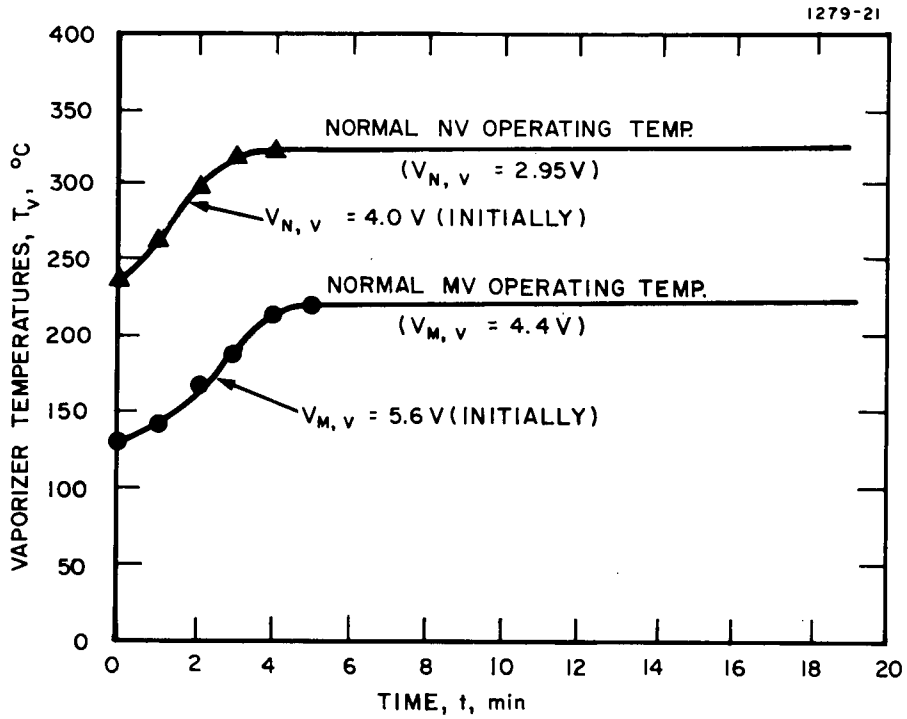

Fig. 36. Vaporizer Temperatures as a Function of Time After Startup from Standby Conditions.

three or four minutes and were used at the start of each cycle of the 10 cycle test. When the operating temperatures were reached, the normal steady state power settings were decreased to those for normal full power operation. These were $V_{M,VH}$ = 4.4 V and $V_{N,VH}$ = 2.95 V for a main cathode vaporizer temperature $T_{M,V}$ = 218°C and neutralizer vaporizer temperature $T_{N,V}$ = 306°C, respectively. A considerably longer time is required to attain normal operating temperature when only normal steady state power settings are used.

TABLE X

Standby Operating Values for SIT-5 Thruster S/N 102

	Main	Neutralizer
Keeper Voltage, V_K, V	24.0	16.0
Keeper Current, I_K, mA	100.0	100.0
Keeper Power, P_K, W	2.4	1.6
Vaporizer Heater Voltage, V_{VH}, V	2.8	2.5
Vaporizer Heater Current, I_{VH}, A	1.25	1.1
Vaporizer Power, P_V, W	3.5	2.75
Vaporizer Temperature, T_V, °C	139.0	248.0
Mercury Flowrate Equivalent, I_{Hg}, mA	2.42	1.42
Total Power, P_T, W	5.9	4.35

T284

(4) Full Power Discharge Sequence — The sequence of settings leading to the full power condition were determined next. The initial neutralizer vaporizer power (going from standby to full power) was purposely chosen so that the neutralizer vaporizer operating temperature was reached before the main vaporizer reached its normal operating temperature. Once the proper neutralizer vaporizer temperature was reached, the neutralizer keeper power was increased so that the keeper current would rise from the standby current of $I_{N,K}$ = 100 mA to $I_{N,K}$ = 500 mA. At this point the power to the neutralizer-vaporizer heater was lowered to its normal full power steady state setting. No difficulty was encountered with the neutralizer discharge even though beam and accel voltages were on.

Shortly after the neutralizer keeper current had reached its predetermined level, the main vaporizer temperature reached its full power operating temperature, and the main vaporizer power was lowered to its normal value. Tests showed that the main keeper current should be increased to $I_{M,K}$ = 500 mA from its standby of 100 mA prior to starting the chamber discharge. This minimized the loss of one or both keeper discharges from the arcing that occurred when the chamber discharge started. In order to avoid excessive beam current from the residual mercury in the discharge chamber, it was found that the chamber discharge current should be set initially at I_D = 100 mA; then, as the beam current drops, it can be increased to the normal discharge chamber current (from the 50 hour test) of I_D = 250 mA. Occasionally, this startup procedure would result in arcing and one or both of the keeper discharges would be lost. Because of this, it was decided that the beam and accel voltages should be off during the standby condition and turned on after the chamber discharge was on. This procedure also made it easier to

start the chamber discharge. Once the chamber discharge current was at I_D = 100 mA, the beam and accel voltages were increased from zero to their nominal values of V_B = 650 V and V_{Ac} = -250 V, respectively. When the beam decreased, as the excess propellant was used up, it was found that the chamber discharge could be raised to I_D = 250 mA and the thruster was then in a steady state condition. After operating for more than 5 min, the main keeper current could be lowered to $I_{M,K}$ = 400 mA and then to $I_{M,K}$ = 300 mA in another 5 min. Lowering the main keeper current below 300 mA in such a short time would occasionally cause the loss of the chamber and keeper discharges. The thruster was allowed to operate at a keeper current of 300 mA for about 1/2 hour before it was lowered to 100 mA. For the cyclic test, a steady state full power operation of 15 min with the main keeper current at 300 mA was chosen. To demonstrate that the keeper current could be lowered to 100 mA after a 1/2 hour operation at 300 mA, an eleventh cycle of longer duration was added to the cyclic test.

(5) Standby Sequence – To go from full power condition to the standby state, the chamber discharge was turned off, and the main vaporizer heater and neutralizer vaporizer heater voltages were lowered to the standby voltage setting determined at the beginning of cyclic studies. At first, this was done with the beam and accel voltages on. As mentioned earlier, however, it was later changed so that these voltages were turned off after the chamber discharge was off. To prevent the loss of the keeper discharges when the chamber discharge was extinguished, the main keeper current had to be increased to $I_{M,K}$ = 500 mA. Once the chamber discharge was extinguished and beam and accel voltages were off, the main keeper and neutralizer

keeper currents were lowered to the standby state of I_K = 100 mA. The rate of temperature drop of the two vaporizers with the low power settings is shown by the solid lines in Fig. 37. Temperature was decreased from the operating to the standby level by turning off the vaporizer power until the standby temperatures were reached. The rate of temperature decrease under these conditions is shown in Fig. 37. When the standby temperatures were reached, power was put into the heaters to keep the temperatures nearly constant. By using this two-stage method, standby temperatures were reached in a few minutes instead of an hour.

(6) Cyclic Test Results – The result of the prior studies were incorporated into a plan for the ten cycle test that was submitted to the NASA Program Manager for approval. The sequence schedule recommended in this plan is shown in Table XI with the approximate times given for each step. These times were followed as closely as possible for ten cycles. The ten cycle test began after the thruster was left for a period of 19 hours in the standby conditions with the surrounding sink temperature of -320°F to simulate a full shadow. During this standby, mercury flowrate and power measurements were obtained and the results were shown earlier in Table X (i.e., $I_{T,Hg}$ = 3.8 mA and P_T = 10.7 W). While Table XI shows the expected sequence and value for each cycle, the actual values for the first cycle are shown in Table XII. This sequence was repeated until the ten cycle test was complete. The average time per cycle was 47 min, and it took approximately ten minutes to go from the standby condition to a full beam.

A temperature profile was taken during the sixth cycle of the test and is shown in Fig. 38. As expected, the neutralizer vaporizer, neutralizer cathode, main vaporizer and

TABLE XI

Sequence of Operations for Startup and Shutdown or the SIT-5 Thruster System

TIME	CYCLE			BEAM				ISOL	DISCHARGE			COUPLING		KEEPER				CATHODE HEATER				VAPORIZER						STANDBY TOT	
t (min)	SEQUENCE OF OPERATIONS	M I_{Hg} (mA)	N I_{Hg} (mA)	V_B (V)	I_B (mA)	V_{Ac} (V)	I_{Ac} (mA)	I_I (μA)	V_D (V)	I_D (mA)	I_M (A)	V_C (V)	I_C (mA)	M V_K (V)	M I_K (mA)	N V_K (V)	N I_K (mA)	M V_{CH} (V)	M I_{CH} (A)	N V_{CH} (V)	N I_{CH} (A)	M V_V (V)	M I_V (A)	N V_V (V)	N I_V (A)	M T_V (°C)	N T_V (°C)	POWER (W)	FLOW (mA)
0	STANDBY	2.28	1.35	0	0	0	0	—	0	0	—	—	—	25	100	20	100	0	0	0	0	2.8	1.22	2.5	1.1	132	243	10.7	3.63
0+	HEAT VAPORIZERS																					5.7		4.0					
2	REDUCE $V_{N,V}$																							3.2			325		
1	INCREASE $I_{N,K}$																500												
4	REDUCE $V_{M,V}$																					4.5				228			
	INCREASE $I_{M,K}$														500														
	START DISCHARGE																												
4.5	INCREASE V_B, V_{Ac}			650		250																							
5	INCREASE I_D								40	250																			
10	BEAM IS STEADY			650	33	250																							
1	DECREASE $I_{M,K}$														400														
15	DECREASE $I_{M,K}$														300														
30	BEGIN SHUTDOWN			650	34	250	1	—	40	250	—	12	33	10	300	10	500	0	0	0	0	4.5	2.0	3.2	1.4	228	325		
	INCREASE $I_{M,K}$														500														
	REDUCE DISCHARGE				0				0	0																			
	TURN OFF V_B, V_{Ac}			0	0	0																							
	TURN OFF VAPORIZERS																					0		0					
	LOWER KEEPERS														100		100												
33	RAISE $V_{N,V}$																							2.5			232		
36	RAISE $V_{M,V}$																					2.7				150			
36-45	HOLD IN STANDBY																											10.7	3.63
45+	BEGIN STARTUP																												
	REPEAT FOR 10 CYCLES																												

TABLE XII

Parameter Values for the First Cycle of Cyclic Test

TIME	CYCLE			BEAM				ISOL	DISCHARGE			COUPLING		KEEPER				CATHODE HEATER				VAPORIZER						STANDBY TOT.	
t (min)	SEQUENCE OF OPERATIONS	M I_{Hg} (mA)	N I_{Hg} (mA)	V_B (V)	I_B (mA)	V_{Ac} (V)	I_{Ac} (mA)	I_I (μA)	V_D (V)	I_D (mA)	I_M (A)	V_C (V)	I_C (mA)	M V_K (V)	M I_K (mA)	N V_K (V)	N I_K (mA)	M V_{CH} (V)	M I_{CH} (A)	N V_{CH} (V)	N I_{CH} (A)	M V_V (V)	M I_V (A)	N V_V (V)	N I_V (A)	M T_V (°C)	N T_V (°C)	POWER (W)	FLOW (mA)
-10	STANDBY	2.42	1.42	0	0	0	0	—	0	0	—	0	0	24	100	16	100	0	0	0	0	2.8	1.25	2.5	1.1	138	248	10.3	3.8
0	HEAT VAPORIZERS			0	0	0	0	—	0	0	—	0	0	24	100	16	100	0	0	0	0	5.7		4.0		138	248		
2 1/2	REDUCE $V_{N,V}$			0	0	0	0	—	0	0	—	0	0					0	0	0	0	5.7		3.2			325		
	INCREASE $I_{N,K}$			0	0	0	0	—	0	0	—	0	0			10	500	0	0	0	0	5.7		3.2			325		
4 1/4	REDUCE $V_{M,V}$			0	0	0	0	—	0	0	—	0	0			10	500	0	0	0	0	4.7		3.2		218	325		
	INCREASE $I_{M,K}$			0	0	0	0	—	0	0	—	0	0	10	500	10	500	0	0	0	0	4.7		3.2		218	325		
	START DISCHARGE			0	0	0	0	—		100	—			10	500	10	500	0	0	0	0	4.7		3.2		218	325		
	INCREASE V_B, V_{Ac}			650		250		—			—			10	500	10	500	0	0	0	0	4.7		3.2		218	325		
7	INCREASE I_D			650		250		—		250	—			10	500	10	500	0	0	0	0	4.7		3.2		218	325		
10	BEAM IS STEADY			650	38	250	0.8	—	34	250	—			10	500	10	500	0	0	0	0	4.3	1.85	3.2	1.4	218	320		
15				650		250		—	40	250	—			10	500	10	500	0	0	0	0	4.8	2.0	3.3	1.4	216	330		
15+	REDUCE $I_{M,K}$			650		250		—			—			10	400	10	500	0	0	0	0								
17				650	35			—	37	270	—	12	34	10	400	10	500	0	0	0	0	5.0	2.1	3.3	1.4	214	330		
20	REDUCE $I_{M,K}$			650				—			—			10	300			0	0	0	0								
21				650	36	250	1.1	—	33	270	—		35	10	300	10	500	0	0	0	0	4.3	1.9	3.3	1.4	211	330		
25				650	34	250	1.1	—	34	250	—	12	33	10	300	10	500	0	0	0	0	4.4	1.9	3.3	1.4	209	330		
30				650	36	250	1.2	—	34	255	—	12	35	10	300	10	500	0	0	0	0	4.2	1.8	3.25	1.4	204	332		
30+	GO TO STANDBY			650		250		—			—							0	0	0	0	4.2	1.8	3.25	1.4	204	332		
	INCREASE $I_{M,K}$			650		250		—			—			10	500	10	500	0	0	0	0	4.2	1.8	3.25	1.4	204	332		
	REDUCE DISCHARGE			650	0	250		—	0	0	—	0	0					0	0	0	0	4.2	1.8	3.25	1.4	204	332		
	TURN OFF V_B, V_{Ac}			0	0	0	0	—	0	0	—	0	0					0	0	0	0	4.2	1.8	3.25	1.4	204	332		
	TURN OFF VAPORIZERS			0	0	0	0	—	0	0	—	0	0					0	0	0	0	0	0	0	0	204	332		
	LOWER KEEPERS			0	0	0	0	—	0	0	—	0	0	16	100	14	100	0	0	0	0	0	0	0					
33	RAISE $V_{N,V}$			0	0	0	0	—	0	0	—	0	0		100		100	0	0	0	0	0	0	2.5					
34	RAISE V_{MV}			0	0	0	0	—	0	0	—	0	0		100		100	0	0	0	0	2.8		2.5					
34+	HOLD IN STANDBY			0	0	0	0	—	0	0	—	0	0		100		100	0	0	0	0	2.8		2.5					
40	END STANDBY			0	0	0	0	—	0	0	—	0	0		100		100	0	0	0	0	2.8		2.5		150	248		
40+	START 2ND CYCLE																												

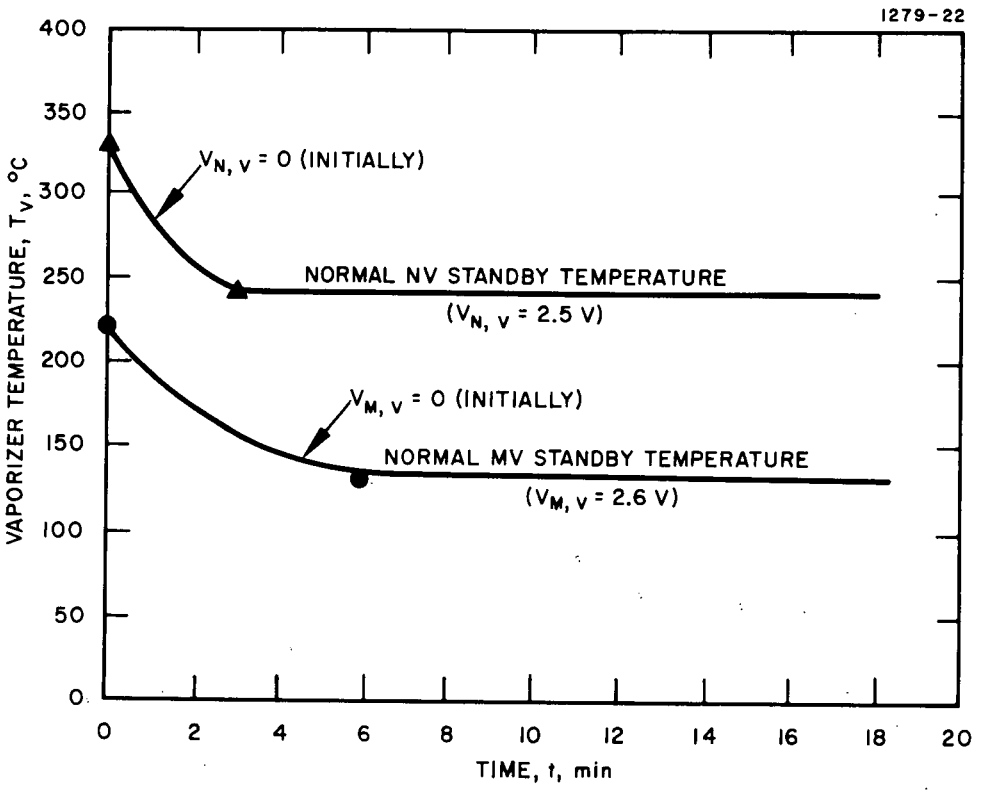

Fig. 37. Vaporizer Temperatures as a Function of Time After Shutdown from Normal Operation.

downstream isolator temperatures increase as the full power condition is approached. There is only a slight temperature rise on the endplate, shell, accel, and ground screen, while the feed line and reservoir temperatures are virtually constant throughout the cycle. The paradoxical temperature profile of the isolator at its upstream end was explained by post-test inspection which showed that this thermocouple had broken loose, making the measurement invalid.

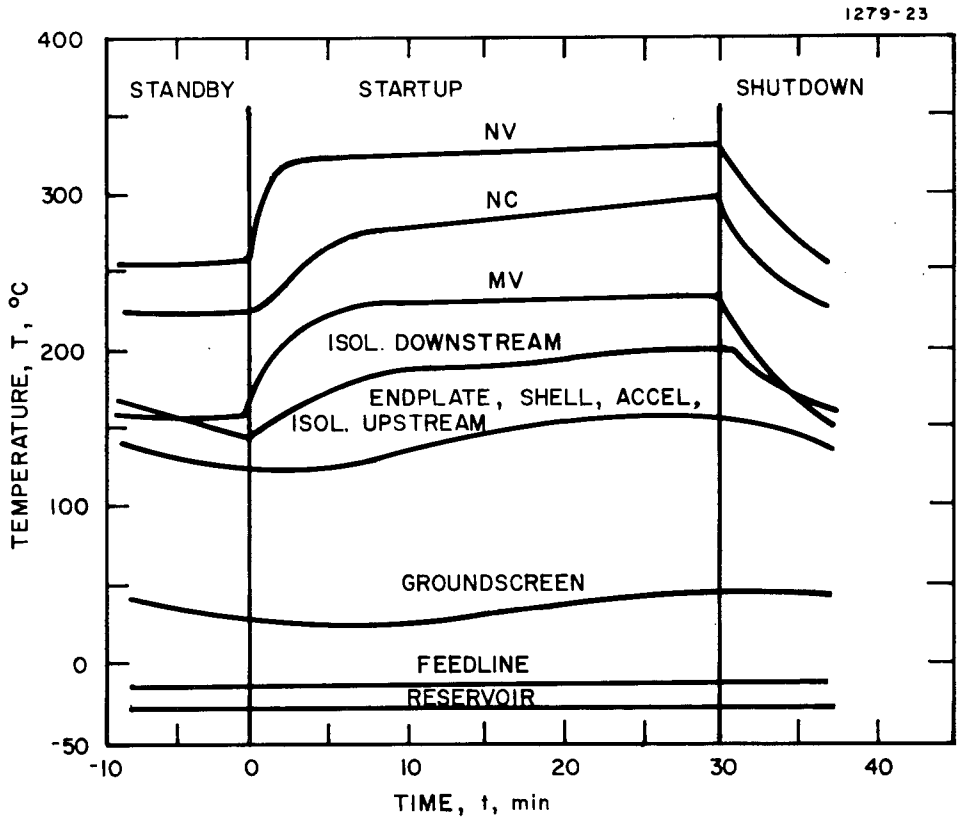

Fig. 38. SIT-5 Temperature History During Cycle No. 6.

An eleventh cycle was initiated in the same manner as the others. The purpose of the eleventh cycle was to show that given enough operation time, the main keeper current could be lowered to $I_{M,K}$ = 100 mA. This was accomplished after 1/2 hour of full operation by reducing the main keeper current to 100 mA in steps. After operating the thruster at full power with the main keeper current at 100 mA, the test was terminated. The results of cycle 11 are shown in Table XIII. The data point at 70 min is representative of the normal power requirements and is shown in Table XIV. The test was concluded; both keepers having been on for a period of 28 hours and 11 cycles with no loss of keeper discharge power.*

2. Design Verification Test

The complete SIT-5 thruster assembly (in its optimized configuration) was tested with its dielectric-coated ion extraction system to verify operation in conformance with design criteria. Conformance with electrical performance criteria was obtained from a 50 hour test of the S/N 101 thruster system with an electrical efficiency η_E = 38%. Anomalous behavior of the main cathode vaporizer subassembly, however, prevented meaningful measurement of the mass-utilization efficiency. After completion of the 50 hour test, an optimal startup procedure was established for the SIT-5 system.

*When cathode-to-keeper discharges are extinguished, re-ignition is insured by utilization of a keeper discharge power supply with an open circuit voltage of 460 V. Starting from an extinguished condition with the vaporizer temperature at T_V = 100°C, ignition of the main cathode is acquired after eight minutes with a main cathode heater power of 32 W, and of the neutralizer after six minutes with a neutralizer-cathode heater power of 28.5 W.

TABLE XIII

Parameter Values for the Eleventh Cycle of the Cyclic Test

TIME	CYCLE		BEAM				ISOL	DISCHARGE			COUPLING		KEEPER				CATHODE HEATER				VAPORIZER					
t (min)	SEQUENCE OF OPERATIONS		V_B (V)	I_B (mA)	V_{Ac} (V)	I_{Ac} (mA)	I_I (μA)	V_D (V)	I_D (mA)	I_M (A)	V_C (V)	I_C (mA)	M V_K (V)	M I_K (mA)	N V_K (V)	N I_K (mA)	M V_{CH} (V)	M I_{CH} (A)	N V_{CH} (V)	N I_{CH} (A)	M V_V (V)	M I_V (A)	N V_V (V)	N I_V (A)	M T_V (°C)	N T_V (°C)
-1	STANDBY		0	0	0	0	—			—	0	0	21	100	16	100	0	0	0	0					150	248
0	HEAT VAPORIZERS		0	0	0	0	—			—	0	0	21	100	16	100	0	0	0	0	5.8	2.5	4.0	1.8	150	248
2 3/4	REDUCE $V_{N,V}$		0	0	0	0	—			—	0	0					0	0	0	0	5.8		3.1			320
	INCREASE $I_{N,K}$		0	0	0	0	—			—	0	0				500	0	0	0	0	4.3					
3	REDUCE $V_{M,V}$		0	0	0	0	—			—	0	0					0	0	0	0					223	
	INCREASE $I_{M,K}$		0	0	0	0	—			—	0	0		500			0	0	0	0						
	START DISCHARGE		0	0	0	0	—		100	—	0	0					0	0	0	0						
	INCREASE V_B, V_{Ac}		650		250		—		100	—							0	0	0	0						
4			650	26	250		—		100	—							0	0	0	0						
4+	INCREASE I_D		650	40	250		—		250	—							0	0	0	0						
9	BEAM DROP		650	20	250		—		250	—							0	0	0	0						
10	BEAM STEADY		650	36	250	2.1	—		250	—	12	34	10	500	10	500	0	0	0	0	4.3	1.84	3.15	1.39	223	325
15			650	33	250	2.1	—		250	—	12	31	10	500	10	500	0	0	0	0	4.5	1.90	3.15	1.39	223	330
15+	REDUCE $I_{M,K}$		650		250		—		250	—			10	400	10	500	0	0	0	0						
20			650	35	250	2.2	—		250	—	12	33	10	400	10	500	0	0	0	0	4.4	1.85	3.20	1.39	226	332
20+	REDUCE $I_{M,K}$		650		250		—		250	—			10	300	10	500	0	0	0	0						
21			650	34	250		—		250	—	12	32	10	300	10	500	0	0	0	0	4.45	1.89	3.10	1.34	228	330
25			650	35	250	2.4	—		250	—	12	33	10	300	10	500	0	0	0	0	4.45	1.89	3.10	1.33	228	327
30			650	35	250	2.4	—		250	—	11.7	33	10	300	10	500	0	0	0	0	4.4	1.88	3.10	1.33	228	330
35			650	35.5	250		—	34	250	—	11.8	33	10	300	10	500	0	0	0	0	4.4	1.88	3.05	1.31	225	329
35+	REDUCE $I_{M,K}$		650		250		—			—			10	200	10	500	0	0	0	0						
36			650	36	250	2.5	—	38	250	—	11.9	34	10	200	10	500	0	0	0	0	4.45	1.89	3.05	1.31	228	327
40			650	35.5	250	2.6	—	39	250	—	11.9	33	10	200	10	500	0	0	0	0	4.4	1.85	3.04	1.31	228	327
40+	REDUCE $I_{M,K}$		650		250		—			—			10	100	10	500	0	0	0	0						
41			650	35	250	2.7	—	40	250	—	11.8	32.5	10	100	10	500	0	0	0	0	4.40	1.85	3.05	1.31	228	329
55			650	35	250	2.7	—	40	250	—	11.8	32.5	9	100	10	500	0	0	0	0	4.40	1.86	3.03	1.30	228	327
60			650	35	250	2.7	—	40	250	—	11.8	32	9	100	10	500	0	0	0	0	4.40	1.86	3.03	1.30	228	327
65			650	35	250	2.7	—	40	250	—	11.8	32	9	100	10	500	0	0	0	0	4.40	1.86	3.03	1.30	228	328
65+	SHUT DOWN																									

TABLE XIV

Performance Profile at the End of the Cyclic Test

P_B	=	20.8 W
P_{Ac}	=	2.4 W
P_D	=	10.0 W
P_C	=	0.4 W
$P_{M,K}$	=	0.9 W
$P_{M,VH}$	=	8.2 W
$P_{N,K}$	=	5.0 W
$P_{N,VH}$	=	3.9 W
P_T		51.6 W
$\eta_E = P_B/P_T$	=	40.4%

T288

a. Description of the Experiment

(1) Experimental Conditions — Verification testing of the SIT-5 system was conducted in an oil-diffusion-pumped vacuum system approximately 2 ft in diameter by 6 ft long. A cylindircal liquid-nitrogen cooled liner was located in the chamber, and the thruster was located near the axis of the liner. The thruster system was mounted on a circular plate that was attached directly to one end of the chamber. The beam collector was a flat circular copper plate located at the opposite end of the chamber. Pressure did not rise above $P = 1 \times 10^{-6}$ Torr throughout the testing.

The S/N 101 thruster system was complete with a self-contained feed system that uses a rubber bladder for positive expulsion of the liquid mercury. This system was the same

one that had earlier undergone vibration testing, and the mercury in the feed system was the same as that originally present during the vibration test. The neutralizer assembly was changed to the new design prior to the test by substitution of a new neutralizer subassembly S/N 106. To avoid depressurizing the feed system, the physical exchange was accomplished with the feed line to the neutralizer frozen. The thruster system was instrumented with thermocouples located at the neutralizer vaporizer, the main vaporizer, and at the reservoir. Power supplies and data acquisition equipment were identical with those described earlier for test of a SIT-5 system with a laboratory-type burette feed system. Calibration and evaluation of all power supplies and data acquisition equipment conformed to the previously mentioned reliability and quality assurance requirements.

(2) Data Acquisition – Data acquired for this test included the following.

- Main vaporizer voltage and current, ($V_{M,VH}$, $I_{M,VH}$).
- Cathode heater voltage and current, ($V_{M,CH}$, $I_{M,CH}$).
- Cathode keeper voltage and current, ($V_{M,K}$, $I_{M,K}$).
- Ion chamber discharge voltage and current, (V_D, I_D).
- Net accelerating voltage ($V_B + |V_{Ac}|$).
- Ion beam current, (I_B).
- Accelerator voltage, (V_{Ac}).
- Accelerator drain current, (I_{Ac}).
- Neutralizer vaporizer voltage and current, ($V_{N,VH}$, $I_{N,VH}$).

- Neutralizer keeper voltage and current, ($V_{N,K}$, $I_{N,K}$).
- Neutralizer coupling current, (I_C).
- Neutralizer coupling voltage, (V_C).
- Neutralizer heater voltage and current ($V_{N,CH}$, $I_{N,CH}$).
- Ion chamber energy per beam ion, ($V_{Disch.}$).
- Electrical efficiency, (η_E).
- Propellant utilization efficiency, (η_m).
- Over-all efficiency, (η_T).

b. Test Results and Discussion – Data obtained in the design verification tests have been presented in the Final Data Submittal on 2 July 1971. To aid in the discussion of these tests, the data are summarized in Table XV.

(1) 50 Hour Test – Discharge-chamber performance with this thruster was essentially the same as that reported for the S/N 102 thruster in the thruster system performance tests. All values remained fairly constant throughout the 50 hour test period as evidenced by the performance values shown in Table XV. Data are presented for the thruster at the 12.5, 25, 37.5, and 50 hour data points. As in the results presented for the 50 hour Performance Test, the coupling current is taken to be the true beam current when calculating the electrical efficiency. No reservoir power was included in Table XV, because the heater was turned off one hour after start of the test. The reservoir remained above 40°C after the reservoir heater was turned off. This heater may not be required when the thruster is operating in space at full beam power. Neutralization of the ion beam was accomplished throughout most of the test with a coupling voltage ranging from 15 to 18 V.

TABLE XV

Typical Performance Values During the 50 Hour Test of SIT-5 S/N 101

Date Time $\Delta t \sim$ hour	6/7/71 21:30 12.5 hours	6/8/71 10:00 25 hours	6/8/71 23:00 37.5 hours	6/9/71 11:18 50 hours
P_B, W	21.1	21.1	20.8	20.8
P_{Ac}, W	0.7	0.7	0.8	0.8
P_C, W	0.5	0.5	0.5	0.5
P_D, W	10.8	10.6	10.5	10.4
$P_{M,CH}$, W	0.0	0.0	0.0	0.0
$P_{M,VH}$, W	10.8	10.3	10.2	10.1
$P_{M,K}$, W	1.0	1.0	1.0	1.0
$P_{N,CH}$, W	0.0	0.0	0.0	0.0
$P_{N,VH}$, W	1.4	1.4	1.3	1.3
$P_{N,K}$, W	9.2	9.1	9.2	9.2
P_T, W	55.5	54.7	54.3	54.1
η_E	38%	38.6%	38.3%	38.5%

T289

Propellant flowrate was not directly measurable during the test because the flight-type propellant reservoir was used rather than the laboratory-type burette feed system. However, direct weighing of the system was done before and after completion of all testing which included determination of operational values, the 50 hour Design Verification Test, and determination of startup procedure from a standby condition. Mass consumption during these tests was 85.6 g, an amount far greater than normally required for the thruster operation.

This anomalous result has prompted the following analysis of propellant losses. Because neutralizer and main vaporizer temperatures were monitored throughout the tests between weighings, the amount of propellant consumed can be estimated from previously determined flow characteristics. In the case of the main cathode, mercury flowrate versus vaporizer temperature is known from the earlier reservoir-feed subassembly tests. The dashed line in Fig. 30 was obtained from a mass measurement and is considered to be more accurate than the solid line that was obtained by an inference from a keeper discharge voltage characteristic.

A similar flowrate versus temperature curve for the neutralizer feed does not exist because the neutralizer was a replacement unit. A flow calibration was obtained by inference from the discharge characteristics from an identical nuetralizer used in the earlier thruster performance test. As with the other neutralizer, it was assumed that a flowrate of $I_{N,Hg} \simeq 1$ mA occurred when the keeper discharge voltage was $V_{N,K} = 20$ V. Once this point and temperature is determined, the flow calibration curve can be generated by using the slope that is common to all vaporizers. The resultant curve is shown in Fig. 39, along with the calibration curve of the first neutralizer used on this system. Using the

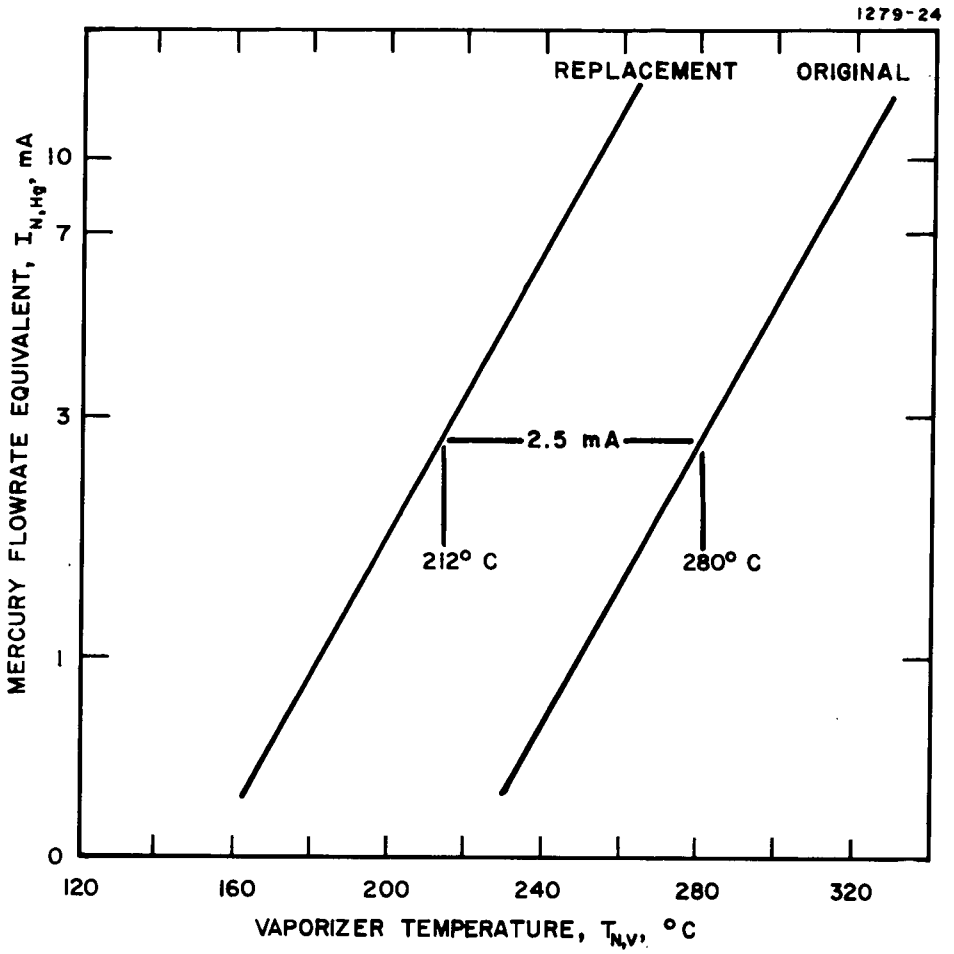

Fig. 39. Inferred Neutralizer-Cathode Vaporizer Flow Characteristic for the SIT-5 Thruster S/N 101.

flow data mentioned above and integrating over the period of time involved for the testing, mass values were obtained as indicated in Table XVI.

TABLE XVI

Calculated Mercury Flow

Period of Measurement	Calculated Flow
Determination of operation points	7.56 g
50 hour test	28.29 g
Determination of startup procedure	0.03 g
TOTAL	35.88 g

T290

The calculated flow accounts for only 42% of the 85.6 g of mercury consumed and leads to the conclusion that the flow of the propellant to the main vaporizer has changed from its earlier calibration. The only plausible explanation is that a leak has developed in the main feed line and that it has continued to enlarge from test to test. It is not possible, therefore, to determine that part of the total mercury flow which actually passes into the discharge chamber and meaningful measurement of mass utilization efficiency is not possible.

The likelihood that a crack might develop in the vaporizer subassembly has been indicated by several cracks which have been detected in other CIV's at an electron beam weld located between the stainless steel liquid housing of the vaporizer and the tantalum porous-plug receptical. A small opening at this location is highly disruptive, because it can prevent the intrusion of liquid mercury (because of

surface tension forces) while passing copious quantities of mercury vapor when the vaporizer is heated. The cause of these cracks is attributed to the difficulty in achieving a satisfactory weld between stainless steel and tantalum at this location and will be avoided by utilizing an all-tantalum construction with future CIV subassemblies.

(2) Startup Procedure – After completion of the 50 hour test, both the main and neutralizer cathode discharges were extinguished, and re-ignited several times to establish a typical startup procedure for the SIT-5 system. Startup was defined from a condition with all discharges off and the main vaporizer and neutralizer vaporizer temperature set at 100°C. The beam voltage and accel voltage was also off at this time. A satisfactory startup procedure is described by the following sequence.

(1) To initiate startup, the main keeper and neutralizer keeper voltages are set at 460 V.

(2) The neutralizer vaporizer heater voltage is set at 5 V and the neutralizer cathode heater current is held at 4 A. The main vaporizer heater voltage is also set at 5 V and the main cathode heater current at 4 A.

(3) After 4 min, the neutralizer temperature reaches a value of 225° at which time the neutralizer-cathode heater current is increased to 5 A and held constant.

(4) After 6 min the neutralizer keeper discharge ignites after which the neutralizer-vaporizer heater voltage is decreased to 2.5 V. Ignition occurs with a cathode heater current of 5 A and voltage of 5.7 V. At this time, the main cathode heater current is increased to 5.5 A.

(5) The main keeper discharge ignites after 8 min elapsed time after which the main vaporizer heater voltage is decreased to its normal operating value of 4.9 V. Ignition occurs with a main cathode current of 5.5 A and 5.8 V.

Immediately after ignition of each cathode, the respective cathode heater is turned off completely, because sufficient heat is generated by the keeper discharge (even with discharge currents as low as 100 mA) to sustain cathode operation. At the conclusion of the tests to determine a suitable startup procedure, the SIT-5 thruster was shipped to the Lewis Research Center.

3. Durability and Thrust Vectoring Test

The 13 month development of the SIT-5 thruster system was culminated with completion of the final 100 hour Durability Test. This operation served to evaluate the level of system performance (including its thrust vectoring capability) when paired with the beam deflection device developed at HRL under Contract NAS 3-14058. In this configuration, the system was operated at an electrical efficiency η_E = 46.8% with a propellant utilization efficiency η_m = 64% (including neutralizer losses).

To accurately evaluate steady state design point operation of the thruster system in its nonvectoring mode, the thruster itself was operated in the configuration with its propellant feed lines connected to flow metering devices rather than being attached to the flight-type propellant reservoir as required for design verification testing. After completion of the performance test described earlier, the S/N 102 thruster was modified to mate with an electrostatic beam deflection system (Dual Grid System II-1-A). The detailed structure of this system has been described earlier[3] under Contract NAS 3-14058. It is designed to operate at a beam voltage V_B = 1.2 kV and an accel voltage V_{Ac} = -1.2 kV.

These voltages were used with the SIT-5 system to ensure proper operation; no problems were detected as a result of the added potential drop being applied across the high voltage isolator.

a. Experimental Plan

(1) Experimental Conditions – All performance tests were conducted in a vacuum environment in which the ambient pressure did not exceed 1×10^{-6} Torr during normal thruster operation. The thruster was mounted directly from the end bell of a 5 ft diameter by 15 ft long vacuum chamber. All power conditioning equipment was identical with that used in earlier tests of the SIT-5 system (with dielectric-coated extraction system) with the exception of a higher voltage beam supply, and a specially constructed accel beam deflection supply. The accel supply consisted of four supplies (built to HRL specifications) ganged in pairs to provide positive and negative voltages in each of the X and Y directions.

Techniques for evaluating the thrust vectoring capability of 5 cm thrusters were established earlier at HRL under Contract NAS 3-14058. All facilities developed under that effort were made available for the testing described below. The beam-deflection data-acquisition system employs a specially designed beam probe to monitor beam current density. The 65 cm long probe, contains 35 individual Faraday cups behind 0.16 cm diameter apertures. To reduce data collection time in the subject test, only 13 cups were used. The probe carrier runs on two tracks that allow it to be positioned in the Z (axial) and X (horizontal) directions by two pulse driven stepper motors actuated from outside the tank. Thus, the beam intensity may be sampled within the volume downstream of the thruster ranging from X = ±33.34 cm, Y = ±30.5 cm, and Z = 3.2 to 64.8 cm from the accelerator electrode.

Circuitry is provided to automatically step the probe carrier in the X and Z directions. A data recording system is used to measure magnitude of the beam current samples collected in the probe cups and automatically records this information on punched tape, which can be then fed directly into the computer for analysis. In operation, a typical scan consists of setting the probe carriage at the desired Z distance and then scanning each of 13 Faraday cups at 13 preselected equally spaced positions in the X direction. Such a scan takes approximately 6-1/2 min to perform.

Data were analyzed with the aid of a computer, which was used to fit a three-dimensional surface to the beam intensity measurements taken in a particular plane. The computer calculates the position of the centroid of the volume defined by this surface, the magnitude of the total current represented by the surface, and the location of the curves of equal current intensity over the surface. These contours can be plotted automatically by the computer using a Calcomp plotter. This automated data collection and processing system has proved to be of considerable value in completing the performance mapping of the various deflection systems.

(2) Test Schedule – Performance tests of system design point operation included:

- Short term tests (less than 8 hours) to demonstrate conformance to design and performance requirements. Modifications to the assembly were made as necessary to obtain a configuration capable of achieving the required performance.

- A 100 hour durability test using the best configuration as determined from short term tests. This test established reliability of performance and durability under steady state operation at optimum conditions.

(3) Data Acquisition – The durability test was conducted for a period of 100 hours of steady state operation design conditions. During this operation vectored beam data were obtained on a nominal basis of twice daily. Thruster operating data acquired during all tests were similar to those obtained in the thruster system performance test. Ion beam profile data showing current density distribution, beam envelope, and thrust vector angle obtained for the 100 hour test only. For one set of measurements, the current density distribution was plotted as a contour map of constant density values. As a check of system accuracy, the current density integrated over the beam envelope area was compared with the metered ion beam current. Thrust vector angle was obtained for a range of vectoring conditions.

Calibration and evaluation for all power supplies and data acquisition equipment conformed to the previously approved reliability and quality assurance requirements.

Thruster performance data acquired from the durability test included the following.

(1) Main vaporizer heater voltage and current ($V_{M,VH}$, $I_{M,VH}$).

(2) Cathode tip heater voltage and current ($V_{M,CH}$, $I_{M,CH}$).

(3) Cathode keeper voltage and current ($V_{M,K}$, $I_{M,K}$).

(4) Ion chamber discharge voltage and current (V_D, I_D).

(5) Net accelerating voltage ($V_B + |V_{Ac}|$).

(6) Ion beam current (I_B).

(7) Accelerator voltage (V_{Ac}).

(8) Accelerator drain current (I_{Ac}).

(9) Neutralizer vaporizer heater voltage and current ($V_{N,VH}$, $I_{N,VH}$).

(10) Neutralizer keeper voltage and current ($V_{N,K}$, $I_{N,K}$).

(11) Neutralizer coupling current (I_C).

(12) Neutralizer coupling voltage (V_C).

(13) Neutralizer tip heater voltage and current ($V_{N,CH}$, $I_{N,CH}$).

(14) Propellant flowrates ($I_{M,Hg}$, $I_{N,Hg}$).

(15) Ion chamber energy per beam ion (V_{Disch}).

(16) Magnetic field strength (B).

(17) Electrical efficiency (η_E).

(18) Propellant utilization efficiency (η_M).

(19) Over-all efficiency (η_T).

Feed tubes from the main cathode and neutralizer cathode were connected to separate mercury reservoirs. For the main cathode, the cylindrical reservoir was used; for the neutralizer cathode, the more sensitive capillary tube was employed to measure mercury consumption. Both feed systems were filled under vacuum conditions in order to eliminate gas bubbles in the mercury.

b. Short Term Optimization Tests – The SIT-5 thruster system, with its thrust-vectorable ion-extraction system, was optimized by a series of eight separate discharge chamber modifications. As a result of this optimization, the maximum discharge chamber mass utilization efficiency was raised from an initial value $\eta_m' = 50\%$ to a value $\eta_m' = 65\%$. The modifications included the following variations:

- Size and position of the electron-flow baffle.
- Transmission and baffling of propellant diversion ports in the cathode cup pole piece.
- Mode of operation of the neutralizer cathode.
- Length of the collar pole-piece.
- Diameter of the main keeper aperture.
- Level of main keeper discharge current.
- Potentials applied to the accel and screen electrodes.

While each of the variations resulted in measurable performance deviations no abrupt aberrations of discharge chamber performance were detected and only relatively minor configuration changes were required (from the single grid model) to optimize thruster performance to the level described above. These changes are listed below.

- The outer layer of perforated screen was removed from the cathode cup pole piece.
- The main keeper aperture was enlarged from 0.127 to 0.254 cm.
- The electron diversion baffle was enlarged from 0.635 to 0.950 cm and located in a plane 0.159 cm downstream of the lip of the cathode cup piece.

An abrupt change was observed, however, in the value of neutralizer coupling voltage V_C as a function of neutral mercury flowrate to the neutralizer cathode. Whereas, earlier thruster measurements seemed to indicate a monotonically increasing value of coupling voltage with decreasing neutral flowrate. Experience gained in these tests indicated a precipitous drop in the coupling voltage which occurs

after the neutral flowrate equivalent is reduced below the level ($I_{N,Hg} \simeq 1$ mA) at which the keeper discharge voltage begins to rise above its nominal minimum value of $V_{N,K}$ = 10 V to 12 V. This phenomena was exploited also in design verification testing of the single grid SIT-5 system S/N 101, which occurred later.

For the thrust vectorable configuration, a neutralizer-keeper discharge voltage of $V_{N,K} \geq 22$ V was required to maintain a coupling voltage of $V_C < 40$ V as set by the contract goal. During the first 17 hours of the 100 hour durability test, the neutralizer was operated in a high temperature mode in which the coupling voltage was held at $V_C \simeq 22$ V with a neutralizer-keeper discharge current of $I_{N,K} = 900$ mA. In this mode, the neutralizer keeper is heated sufficiently by discharge power that it operates with a dull red glow. While operation in the mode was entirely stable, acquisition of this mode of operation is not straightforward but requires the temporary use of the cathode heater to raise keeper and cathode temperature to a level where stable operation in the high temperature mode is obtained.

Because of the difficulty in mode acquisition and the high level of power required for operation in the high temperature mode, an attempt was made to further optimize neutralizer performance after the 17th hour of the 100 hour test. It was found that if the neutralizer-keeper discharge current was reduced below $I_{N,K} \simeq 900$ mA, the high temperature mode was lost with an attendant drop in keeper discharge voltage. The elevated keeper voltage was restored, however, by lowering the quantity of neutral mercury flow through the neutralizer cathode. A set point for neutralizer operation was identified at $V_{N,K} \simeq 22$ V, $I_{N,K} = 640$ mA where the keeper voltage and current were both sufficiently high to ensure adequate coupling $V_C \lesssim 40$ V while stable with respect to excursions into the earlier mode and operating at somewhat reduced neutralizer-keeper power. The neutral flowrate

equivalent was also reduced at this set point to a value of $I_{N,Hg} \sim 1$ mA. Operation at this set point was held for the duration of the 100 hour test.

c. 100 Hour Test Performance – The SIT-5 system was operated with open-loop power-conditioning circuitry throughout the duration of the 100 hour test. During most of the operation, manual adjustment of power to the main and neutralizer vaporizers was required once or twice each hour. Otherwise, the test proceeded without incident, other than that imposed by a loss of discharge once or twice per day and the temporary loss of the beam deflection accel power supply after the first full day of operation. Thruster performance was recorded every half hour and thrust vector data were recorded on a nominal basis of twice daily, once in the morning and once in the afternoon, for each day of operation.

(1) Design Point Operation – The beam current was held near a nominal value $I_B = 33$ mA by manual adjustment of the main vaporizer power supply. Measurements of performance data were submitted to the NASA Project Manager in the Final Data Submittal of 2 July 1971, but are summarized below. Table XVII lists values of parameters for periods of time (typically several hours), over which they remained essentially constant. The last line of this table includes average values of the propellant flowrate equivalent measured at the main and neutralizer cathode. During the longest period of essentially constant performance (20 hours recorded on 6/17/71), the average propellant utilization efficiency was equal to the average value of $\eta_m' = 64\%$ for the entire test. The associated parametric set of thruster operating values provides a complete and consistent set for development of thruster performance parameters.

TABLE XVII

100 Hour Test Data

TIME	FLOW			3480 → 1.09 x 10⁵ →				BEAM				ISOL	DISCHARGE			COUPLING		KEEPER				CATHODE HEATER				VAPORIZER								VAC	PAGE ____ TEST ____		
t (min)	MAIN Hg mil	NEUT. Hg (CC)	M Hg mil/min	N Hg cc/min	M I_{Hg} (mA)	N I_{Hg} (mA)	V_B (V)	I_B (mA)	V_{Ac} (V)	I_{Ac} (mA)	I_I (μA)	V_D (V)	I_D (mA)	I_M (A)	V_C (V)	I_C (mA)	M V_K (V)	M I_K (mA)	N V_K (V)	N I_K (mA)	M V_{CH} (V)	M I_{CH} (A)	N V_{CH} (V)	N I_{CH} (A)	M V_V (V)	M I_V (A)	N V_V (V)	N I_V (A)	M T_V (mV)/2	N T_V (mV)/2	M T_V (°C)	N T_V (°C)	P (Torr)	eV/ion	TOTAL η_m	η_T
6/14/71																																				
19:45	105.21	—	X	X	—	—	1200	34	1150	0.16	—	40	400	—	>50	34	8	50	20	600	0	0	0	0	4.4	1.9	3.4	1.4	5.0	5.0	267	267	$4(10)^{-6}$			
23:00	102.03	0740	3.18/225	X	49.2	—	1200	34	1150	0.18	—	43	400	—	22	34	7	50	24	900	0	0	0	0	4.3	1.8	2.4	1.04	4.79	5.2	257	282	6^{-7}	505	6.9	
6/15/71																																				
02:30	98.55	0785	3.48/210	.0095/210	58	2.35	1200	35	1160	0.20	—	41	409	—	22.5	35	8	50	25	900	0	0	0	0	4.35	1.82	2.40	1.04	4.97	5.2	266	282	5^{-7}	480	58	
06:00	95.25	0820	3.30/210	.00335/210	54.8	1.8	1200	34	1160	0.19	—	43	400	—	22	34	7.5	50	25	900	0	0	0	0	4.13	1.78	2.38	1.04	4.70	5.2	253	282	4^{-7}	508	60	
12:30	89.49	.0844	5.86/390	.0026/390	52.2	0.67	1200	34.5	1150	0.19	—	43	410	—	23	34	8	50	24	900	0	0	0	0	4.5	1.9	2.4	1.05	5.0	5.2	267	282	4^{-7}	510	65	
						● CHANGE FROM HIGH TEMPERATURE MODE OF NEUTRALIZER OPERATION																																	
14:30	87.79	.0855	1.70/120	.0011/120	49.4	1.0	1200	33	1150	0.16	—	45	400	—	37	33	0	0	23	640	0	0	0	0	4.5	1.8	2.4	1.02	4.82	4.8	2.58	257	4^{-7}	562	66	
14:33	87.76	.0462	X	X		● RESET CAPILLARY FLOWMETER-ACCEL METER OUT																																	
17:00	85.62	.0465	2.14/147	.0003/147	50.8	0.2	1200	33.5	1170	(0.16)	—	44	405	—	38	33	0	0	23.5	640	0	0	0	0	4.4	1.83	2.35	1.02	4.79	4.79	257	257	4^{-7}	542	66	
20:00	79.20	.0625	6.42/420	.0160/420	52.1	4.15	1200	34	1180	(0.16)	—	43	400	—	38	34	0	0	24	640	0	0	0	0	4.38	1.82	2.35	1.02	4.77	4.80	256	257	2^{-7}	532	61	
6/16/71																																				
09:32	70.88	.0663	8.32/572	.0038/572	50.5	0.72	1200	34	1180	(0.16)	—	43	400	—	38	34	0	0	25	640	0	0	0	0	4.4	1.8	2.35	1.02	4.75	4.8	255	257	4^{-7}	505	66.5	
						● BEAM OFF TO REPAIR ACCEL SUPPLY																																	
10:15	70.07	.0678	X	X	—	—	1200	33	1180	0.2	—	44	400	—	>50	34	0	0	50	500	0	0	0	0	4.4	1.8	—	—	4.8	4.7	257	253	4^{-7}	530	—	
10:32	69.82	.0678	0.25/17	0/17	51	0	1200	33	1180	0.17	—	44	400	—	40	33	0	0	30	620	0	0	0	0	4.4	1.8	2.35	1.05	4.79	4.8	257	257	4^{-7}	530	65	
20:00	61.65	.0714	8.17/568	.0036/568	50	0.72	1200	33.5	1160	0.18	—	43	402	—	40	33.5	0	0	22	640	0	0	0	0	4.26	1.8	3.45	1.46	4.73	5.0	254	267	2^{-7}	518	65	
24:00	57.93	.0746	3.72/240	.0032/240	54	1.45	1200	33	1160	0.18	—	44	395	—	37	33	0	0	22.5	640	0	0	0	0	4.2	1.8	2.4	1.45	4.71	5.0	253	267	2^{-7}	530	60	
6/17/71																																				
20:00	40.21	.0852	17.72/1200	.0106/1200	51.2	0.97	1200	33.5	1180	0.17	—	42	400	—	38	33.5	0	0	24	640	0	0	0	0	4.25	1.78	3.35	1.40	4.66	5.0	250	267	2^{-7}	500	64	29.8
6/18/71																																				
00:30	36.18	.0879	4.03/270	.0028/270	52	1.0	1200	33.5	1180	0.17	—	42.5	405	—	36	33.5	0	0	24	640	0	0	0	0	4.23	1.75	3.32	1.40	4.63	5.0	249	267	2^{-7}	513	63	
04:00	33.20	.0900	2.98/210	.0021/210	49.5	1.1	1198	33.5	1200	0.2	—	42	410	—	48	34.2	0	0	22	650	0	0	0	0	4.40	1.77	3.60	1.55	4.70	5.03	253	269	2^{-7}	512	66.4	
						● BEAM OFF (BLOWN FUSES)-RESET CAPILLARY FLOWMETER																																	
07:30	30.20	.0518	X	X	—	—	1200	34	1200	0.2	—	42	400	—	47	34	0	0	33	600	0	0	0	0	4.35	1.80	3.39	1.44	4.72	5.01	253	267	3^{-7}	495	—	
15:34	22.89	.0566	7.31/484	.0068/484	52.6	1.08	1200	33.7	1180	0.17	—	43.6	394	—	31.5	33.7	0	0	24	650	0	0	0	0	4.20	1.76	3.80	1.60	4.62	5.20	249	277	2^{-7}	510	63	
24:00	15.62	.0613	7.27/506	.0047/506	50	1.01	1200	33	1180	0.17	—	44	385	—	31	33	0	0	22.5	650	0	0	0	0	4.2	1.75	3.57	1.52	4.63	5.18	249	276	2^{-7}	513	65	
6/19/71																																				
04:15	12.10	.0630	3.52/255	.0017/255	48.2	0.73	1200	34	1190	0.2	—	42.2	405	—	33.0	34	0	0	22.8	645	0	0	0	0	4.2	1.75	3.53	1.47	4.60	5.01	248	267	2^{-7}	502	70	
TYPICAL DATA SET					<51.5	1.2>	1200	33.5	1180	0.17	—	42	400	—	38	33.5	0	0	24	640	0	0	0	0	4.25	1.78	3.35	1.40	4.66	5.0	250	267	2^{-7}	500	<64>	29.8

The profile of thruster performance given earlier in Table III shows an electrical efficiency η_E = 46.8% which results in an over-all thruster efficiency η_T = 29.8%.

(2) Beam Deflection Measurements – The extent of beam deflection was measured using the data acquisition system described earlier. All scans were obtained with the beam probe positioned 37.25 in. downstream of the vacuum chamber endplate which placed the Faraday cup probes at a distance 16.25 in. downstream of the beam deflection system of the SIT-5 thruster. The multicup probe was indexed in thirteen 2 in. steps from left to right (looking downstream) across the vacuum chamber. At each step, ion currents to thirteen cups were sampled and recorded automatically on teletype and tape punch displays.

Data were analyzed with the aid of the Hughes GE-600 computer with calculated, among other things, the X and Y component positions for the centroid of ion beam current density, the integral over the current density, and the location of the curves of equal current intensity over the surface.

Data analysis indicated that beam deflection characteristics of the SIT-5 system were essentially identical to those reported for the same deflection system with the LeRC GFE thruster in the final report under Contract NAS 3-14058 with respect to the shape of the equal-density contours and their displacement with deflection voltage. With zero deflection voltage, the beam centroid fell near the center of the measurement matrix. When deflection voltage was applied, the position of the centroid was displaced. The curves plotted in Fig. 40 describe the angular deflection of the beam centroid with respect to the center of the ion extraction system. The deflection sensitivity averaged over

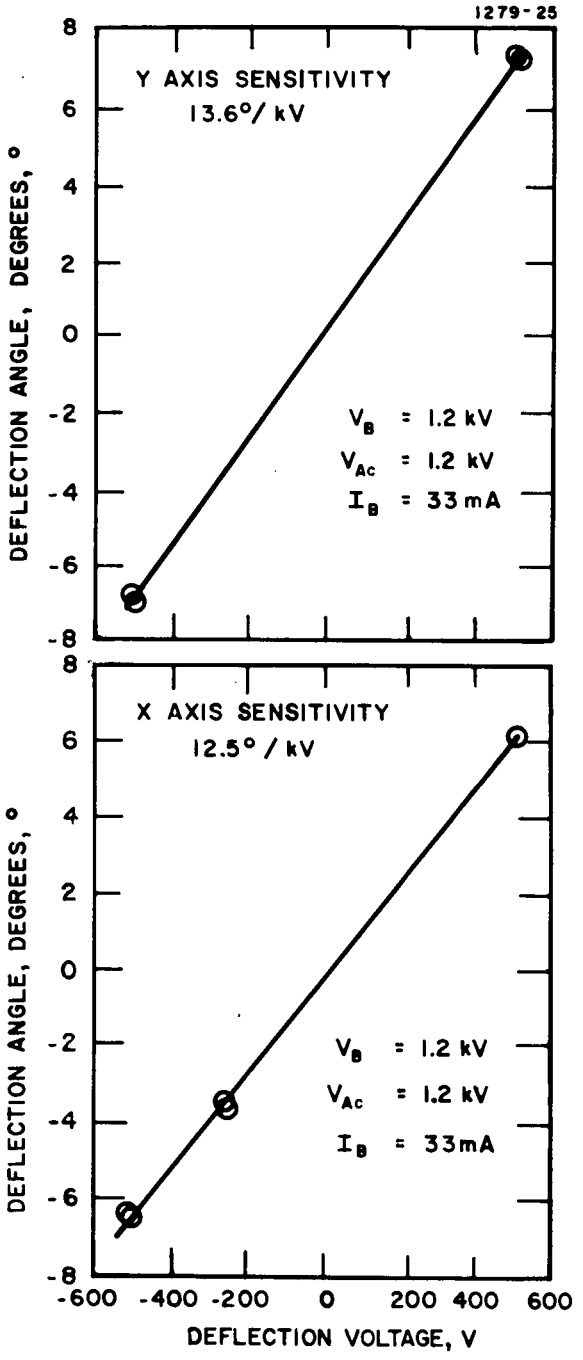

Fig. 40.
X- Y-Axis Deflection Sensitivities.

the X and Y axis of 13°/kV is identical with that reported under Contract NAS 3-14058; however, the individual sensitivities differ by about 10%. This difference is probably explained by the fact that the extraction grid was oriented for the current experiments such that the X and Y deflection plates were interchanged from their earlier orientation. Also the beam level for the current tests I_B = 33 mA exceeds the level I_B = 25 mA employed earlier. The integral over current density accounted for about two-thirds of the total beam current measured at the thruster screen electrode. Differences between the two measurements are attributed to beam plasma electrons reaching the unbiased electrodes of the beam probe.

d. Design Modifications — Inspection of the SIT-5 system before and after conclusion of the 100 hour durability test has uncovered definite patterns of ion beam erosion and material buildup which must be considered in planning design modifications for subsequent thruster systems. These patterns, indicated in Fig. 41, show the SIT-5 system after completion of the 100 hour test. Erosion patterns are apparent along the lip of the ground screen mask, on the beam side edge of the keeper electrode, and on the downstream edge of some of the deflection elements of the ion extraction system. The position of the aperture on the neutralizer-keeper electrode is also indicated; a decrease in aperture diameter was measured at this point.

The erosion pattern on the ground screen mask is shown in greater detail in Fig. 42. Well defined grooves are seen in the lip of the mask which correspond with the position of the outermost apertures of the ion extraction system. The appearance of these grooves was first noticed during the optimization tests. Rather than modify the mask at that

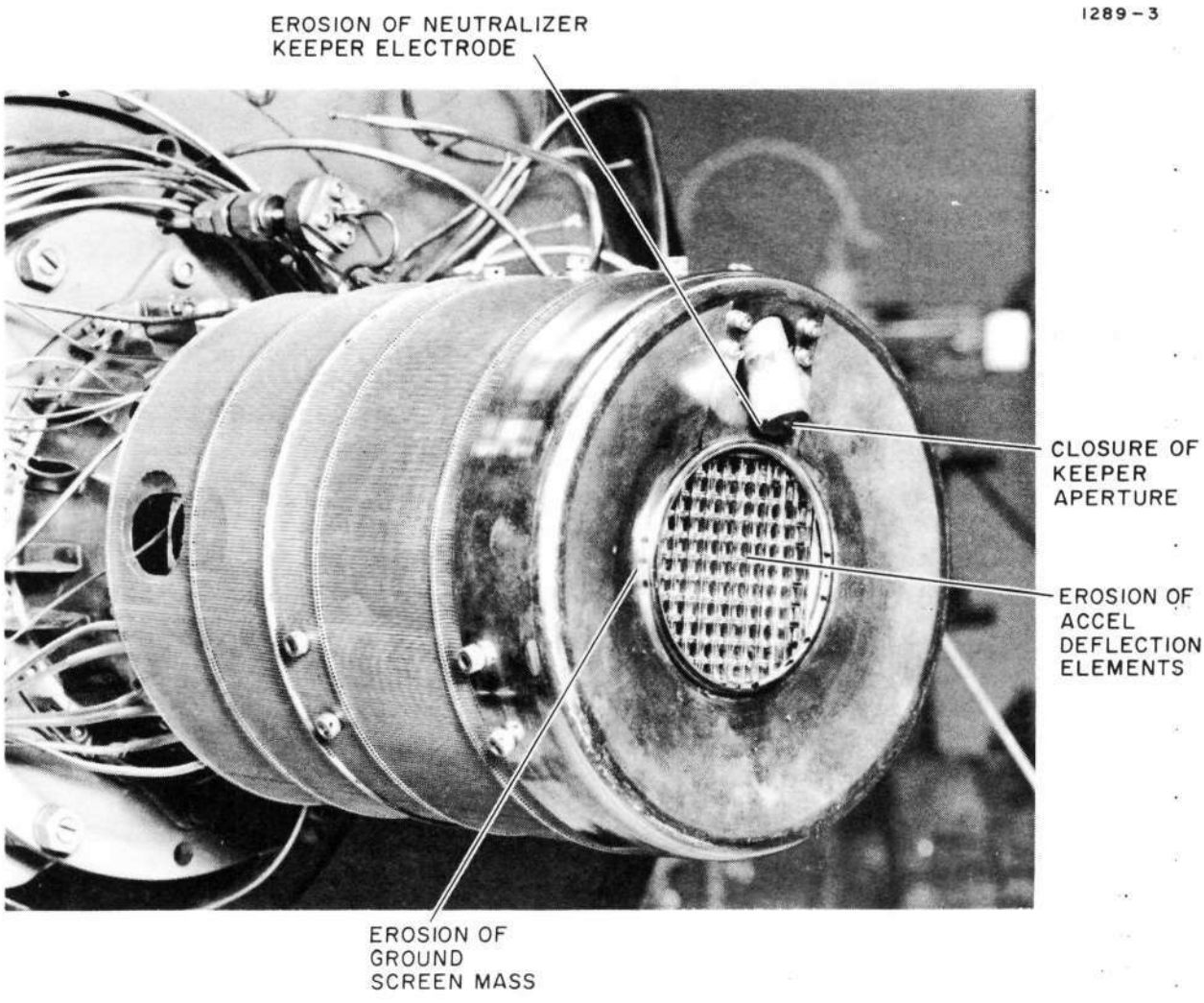

Fig. 41. SIT-5 System After 100 Hour Test.

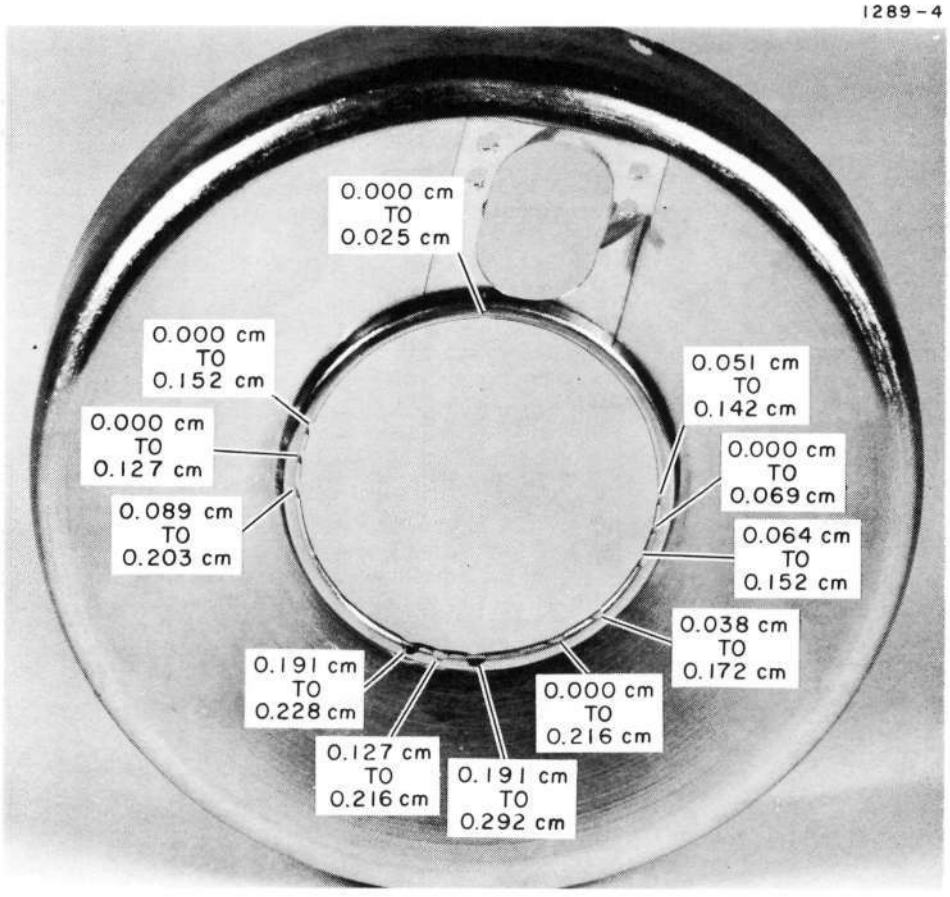

Fig. 42. Ground Screen Mask Erosion Change. (The Initial Erosion Resulted from Optimization Testing).

time, the decision was made to proceed with the 100 hour test in order to better assess the full extent of the erosion process. In Fig. 42, values are given for the maximum dimensions of the erosion openings as measured before and after conclusion of the 100 hour test. While each of the erosion marks was visible prior to commencement of the durability test, many points of erosion had not yet worn through the material; this is indicated by the dimension of 0.000 cm. The problem represented by this erosion process is considered to be minimal and will be avoided in subsequent designs by enlargement of the beam port in the ground-screen mask.

Erosion of the accel grid elements occurred at several locations mainly near the center of the discharge chamber. In Fig. 43, a series of notches is indicated on one deflection element near the center of regions where that element spans the beam apertures. These notches were first observed during early optimization tests and developed only slightly from their original dimensions to a final size of about 0.050 cm deep by 0.050 cm wide. Although the elements which suffered the most erosion were indexed by as much as 0.010 cm toward the screen apertures from their nominal location, most of this erosion may have resulted from thruster operation at low beam and accel voltages which occurred during the optimization period. It is likely that this erosion mechanism will not be a problem in the future so long as provisions are made to carefully index the deflection electrodes between the screen apertures* and care is exercised to avoid thruster operation

*More closely controlled alignment procedures have been incorporated in the assembly of grids produced under Contract NAS 3-15385.

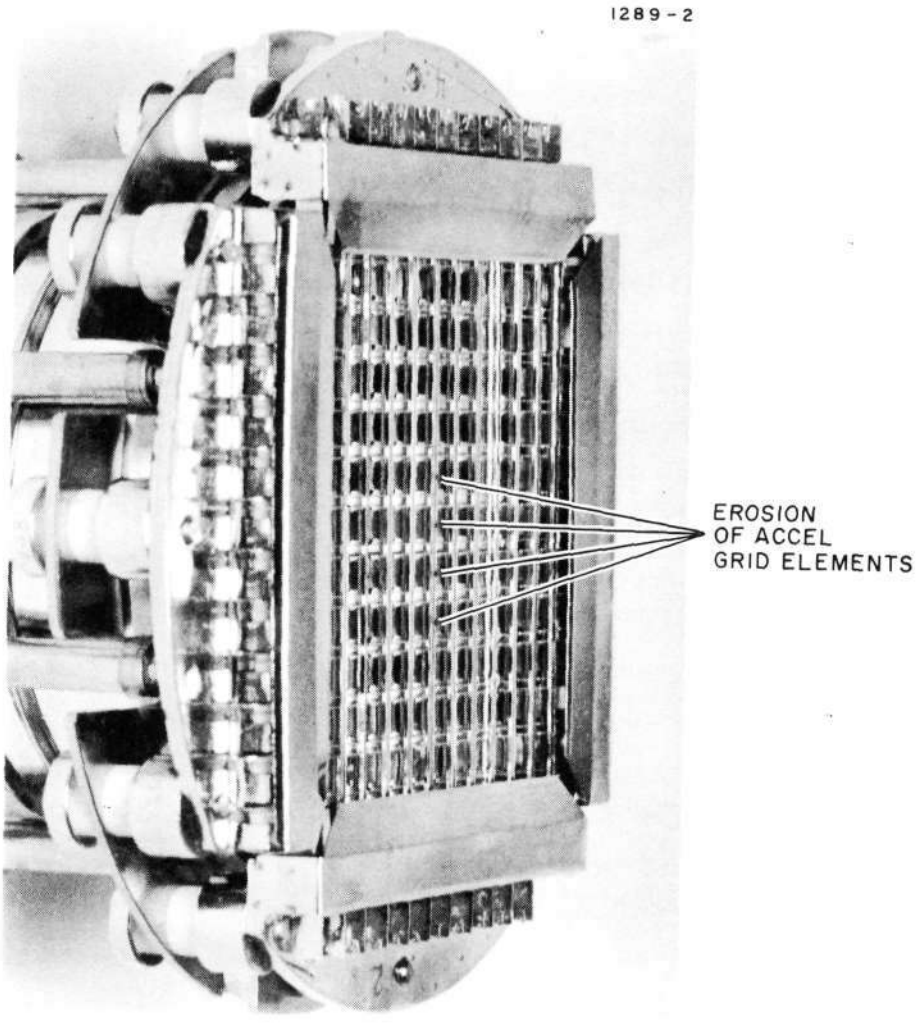

Fig. 43. Dual Grid System III-1-A.

which is far from optimal set points. No variation in beam deflection sensitivity was observed as a result of this erosion.

A plan view of the neutralizer-keeper electrode is shown in Fig. 44. Erosion of the keeper-aperture plate is evident in the upper right quadrant which was positioned closest to the ion beam during thruster operation. A sunburst pattern is also apparent, radiating outward from the keeper aperture. Measurements indicate that the aperture diameter was decreased from its original dimension of 0.076 cm to a value of 0.056 cm after completion of the 100 hour test.

During the 100 hour test, the neutralizer keeper was on occasion heated to white brightness by unstable operation which occurred prior to obtaining steady state operation in the high temperature discharge mode. At this time it is likely that the temperature of the aperture plate exceeded the recrystallization temperature for tantalum which occurs at 1200°C. It is not known whether or not this operation may be related to the evolution of the sunburst pattern or aperture closure, but these phenomena may be related since similar changes have not been noted in earlier operation of the neutralizer keeper. On the basis of the 100 hour test, the neutralizer design is felt to be generally satisfactory.

E. AREAS FOR CONTINUED DEVELOPMENT

In the analysis and design which preceded construction of the SIT-5 system, the unambiguous goal was that of avoiding catastrophic failure during the structural integrity test; a goal which has now been met. Whereas, the structural integrity of the SIT-5 thruster system is adequate to survive the environment of booster launch into earth

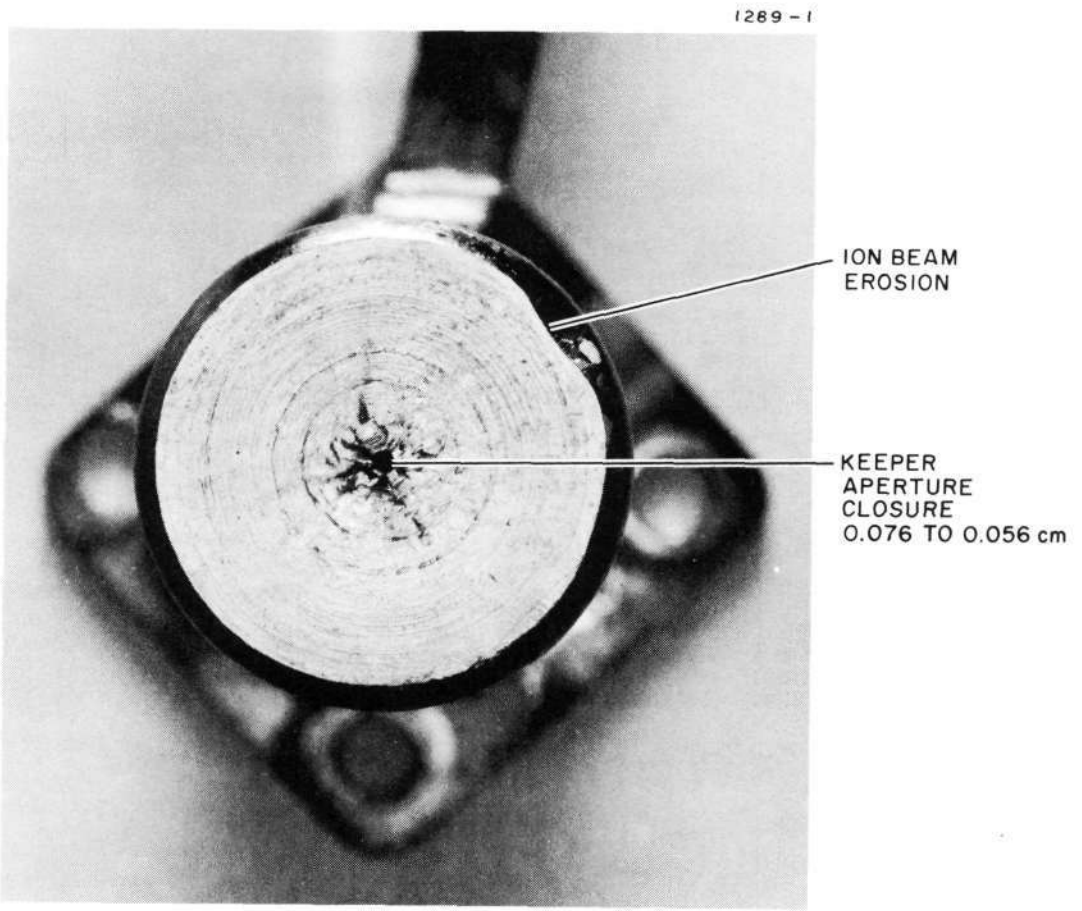

Fig. 44. Neutralizer Keeper Electrode After the 100 Hour Test.

orbit, opportunity must now be provided to optimize the structural design. Similarly further optimization of thruster operation with the thrust-vectorable optics is expected to result in significant advancement of thruster performance. These efforts are now being undertaken at HRL as part of a current contract NAS 3-15483.

1. Structural Analysis

To initiate the redesign process, accelerometer response data generated during the ealier vibration tests are being reduced. By comparing observed responses at a given location with the responses predicted by dynamic analysis, the analytical mathematical model can be improved and corrected, as required, to match prediction with observation. The revised mathematical model serves as a precision instrument to predict dynamic loads with a high degree of confidence. The dynamic loads derived from the analytical model provide a basis for precise evaluation of the strength of detailed features in the structural assembly. On the basis of this evaluation, structures will be identified where significant mass reduction is possible without compromising structural integrity. Similarly, areas of marginal integrity will be located for corrective design to increase structural reliability. In short, the knowledge of dynamic loads throughout the structure permits design optimization for minimum mass and maximum reliability.

a. Dynamic Modeling – Data obtained from the ion thruster structural integrity test conducted under Contract NAS 3-14129 will be used as initial input to evaluate the revised design. To facilitate this evaluation, all accelerometer response data from both the sinusoidal and random vibration tests will be reduced to plots of acceleration and

power-spectral-density versus frequency. Acceleration response data recently obtained from tests on the thrust vectorable grid assembly (under Contract NAS 3-15385) will also be used. The predicted frequencies of critical components in the model will be compared with measured frequencies of the test hardware. Differences will be reconciled by varying mass and stiffness elements of the mathematical model and the amount of critical damping used in the analysis.

The reduced data will be reviewed for applicability to the new 5 cm thruster design. In general, it is expected that sufficient similarities will exist to warrant the extensive use of the reduced test data in sizing structural elements of the new thruster. The mathematical model will be modified to reflect any major structural differences by a consideration of material similarities and structural weight for given components. Totally new design concepts can also be factored into the mathematical model, while retaining most of the benefits which are earlier obtained by matching predicted and observed dynamic responses. This is true, because the accuracy of the dynamic description of each of the structural elements depends not only on the matrix describing that particular element but also on the dynamic environment represented by all other elements with which it is coupled. Proceeding from an accurate model of an existing system, the effects of modifications in particular structural elements, can be evaluated accurately.

Details of the analytical procedure are outlined in the flow chart shown in Fig. 45. This procedure permits continuous updating of previously generated, lumped-mass dynamic mathematical models. Application of the information derived from the vibration tests through this procedure provides a basis for recommending new thicknesses for use with major

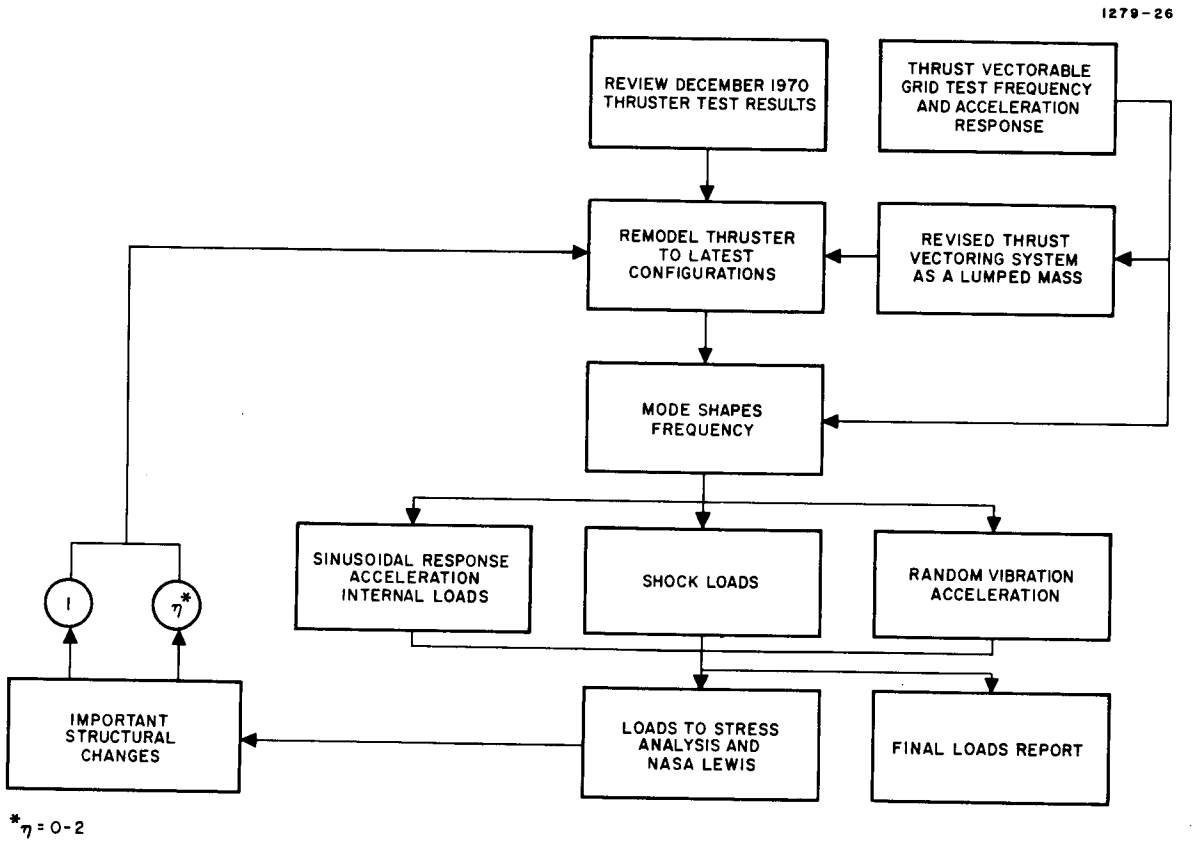

Fig. 45. Analysis Flow Chart for SIT-5 Redesign.

structural components. The new thicknesses, together with geometry, material and mass changes are incorporated as further revisions of the mathematical model.

As in the previous analyses under Contract NAS 3-14129, frequencies and mode shapes for the new thruster design will be generated. These mode shapes and frequencies will be examined to determine if any changes to the structure can be initiated before proceeding with the response loads portion of the analysis. Areas which exhibit low frequency (indicating lack of structural rigidity for critical components) will be changed at this point, and the mode shapes and frequencies will be calculated before the dynamic response is analyzed.

A dynamic response analysis will then be carried out using the calculated mode shapes and frequencies and the forcing functions of the contract specification. Sinusoidal and random vibration, as well as the shock spectrum environment, will provide the forcing functions. Response accelerations and displacements for all unrestrained degrees of freedom will be calculated for each mass station and used for stress analysis. In addition, internal loads on the flexible structural elements connecting the mass stations will be calculated for the sinusoidal as well as the random environments. A formal loads document will be published, containing a description of the model and all response information.

b. Stress Analysis – Stress analysis will be carried out to determine changes in the structure which are required for optimization with respect to strength, rigidity, and minimum mass. Any changes that are suggested as a result of this analysis will be a basis for modification to the mathematical model. New modes and frequencies will be obtained for the modified model and the entire above process

response analysis will be repeated. Primary considerations in the structural optimization of the ion thruster will be structural integrity and minimum mass within the limitations of the design loads, dynamic characteristics and environments, material behavior, thermal environment, and manufacturing requirements.

The basis of a satisfactory approach to structural analysis involves recognition of the problem for the particular design in terms of load, boundary conditions, and the permissible level of idealization. From this basis, a process of analysis is followed which involves the following:

- Use of basic mechanics: statics, dynamics, and material properties.
- Consideration of stress concentrations: stress raisers, geometric anomalies, and notch sensitivity.
- Fatigue considerations: minimizing fatigue effects, decreasing dynamic stress, and increasing dynamic integrity.

Computer programs will be used for analysis of complex structures such as the gas pressure vessel, the propellant reservoir, and the mounting flange. The HAC shell program is based on the finite element method for the determination of stresses, strains, and displacements developed in a laminated orthotropic shell of revolution with an arbitrary meridional configuration. The continuous shell structure is physically replaced by a system of conical shell elements interconnected at a finite number of nodal circles. The basis of the method is a consistently derived stiffness for each conical shell element, which is a relationship between the nodal circle forces and displacements quantities. The stiffness is determined by enforcing geometrical continuity

of displacements and rotations and maintaining equilibrium at each nodal circle. The mathematical expression of these requirements leads to a system of algebraic equations for the unknown nodal circle deformation quantities.

Application of the critical internal and external loads (resulting from the vibration and/or shock environments) to the structural load-carrying members will be investigated for the different mode of failures such as

Simple Overlaod

Material fracture (caused by excessive tensile, shear, compression stresses)

Excessive deformation

Overexcursion

Elastic instability

Repeated Loading

Fatigue rupture

Fatigue damage

The stress analysis effort anticipated during the contract period can be summarized by the following factors.

- Participate in preliminary structural design by the reconciliation of the specific critical acceleration loads from the vibration and shock test loads measured under Contracts NAS 3-14129 and NAS 3-15385.

- Perform stress analysis and structural flexibility analysis of the major structural elements for the critical design load as furnished from dynamic outputs.

- Provide technical support and analysis for accept/reject decisions arising in cases of nonconforming hardware.

- Monitor structural adequacy of all hardware supplied by vendors.

- Utilize HAC computer programs (shell and space-frame programs) where practicable in the performance of the structural or distortion analyses.

- Optimize the structure wherever possible to reduce mass and cost.

2. Redesign

The major redesign goals under the present contract are to reduce assembly difficulties encountered on SIT-5, reduce system mass, reduce fabrication problems, and integrate new parts with the thrust-vectorable accelerator grid. To achieve these goals, major changes are expected in the following components.

- Main Structure – The main structure will be redesigned to reduce its mass and to permit its removal without disconnecting fluid feed lines. As part of the mass reduction, the electrical terminal block will be replaced with individual terminals located along the circumference of the main structure.

- Propellant Storage Tank – The redesigned storage tank will have a similar over-all configuration with a modified mounting flange.

- Neutralizer – The redesigned neutralizer will be more compact and changed so that the keeper aperture lies, with relation to the outermost ion beam aperture, at an angle of 23° with respect to the axis of the thruster.

- Main Keeper Assembly – For ease of fabrication, the redesigned main keeper will use a swaged metal-to-ceramic joint instead of a metal-to-ceramic braze.

3. Thruster Optimization

In completion of the final goal under Contract NAS 3-14129, the SIT-5 thruster was operated in combination with the thrust-vectorable extraction system for a 100 hour durability test. In this configuration, the system operated at an electrical efficiency η_E = 46.8% with a propellant utilization efficiency η_m = 64% (including neutralizer losses). Hughes is confident that somewhat higher levels of efficiency can be met as a result of the program of discharge chamber optimization now in progress under NASA Contract NAS 3-15483.

In conjunction with continuing thruster development, development and optimization of the thrust vectorable system is also continuing under the follow-on NASA Contract NAS 3-15385. Thus far under the extraction grid program, a second generation system has been developed which has a deflection design identical to the one shown in Fig. 3, but which is believed to be far superior with respect to reliability and lifetime and to structural integrity in a launch environment. This system is presently undergoing operational testing at the NASA Lewis Research Center and in related testing at Hughes has demonstrated its structural integrity to dynamics levels in excess of those specified in Section A-2.

Optimization of steady state discharge chamber performance will continue along the lines already established under Contract NAS 3-14129 and continued in the current effort. The program of steady state performance optimization will determine the effects of changes in configuration of the following thrust chamber elements.

- Cathode pole-piece geometry
- Electron baffle size and location
- Hollow cathode geometry (enclosed and SERT-type configurations)

- Magnetic field configuration and intensity
- Discharge chamber length
- Accelerator open area fraction
- Accelerator open area diameter
- Neutralizer location

Changes in the cathode cup region, which encloses the main cathode with the cathode pole piece and the electron flow baffle, are believed to be most critical to further improvements in discharge chamber efficiency. This region is particularly sensitive in the SIT-5 thruster, because all of the propellant is introduced through the hollow cathode and passes into the cup region, contrary to the practice of precathode propellant diversion which is common to hollow cathode thrusters of larger diameter. This technique of propellant introduction can result in performance degradation, unless careful attention is paid to the design of the cathode cup region. There is a tendency for the discharge voltage to decrease as propellant flow through the cathode increases, if the geometrical parameters of the discharge chamber are held constant. Variations of discharge voltage can result in degradation of discharge performance. In the SIT-5 thruster, independent control over discharge voltage has been achieved through the use of post cathode propellant diversion. Ports are located in the walls of the cathode cup pole piece which permit reduction of the neutral particle density below the value which obtains when these ports are absent. For a given level of beam current, discharge voltage can be regulated by changing the transmission of the propellant diversion ports by the use of wire mesh of varying transparency.

SECTION IV

SUMMARY OF RESULTS

Under the subject program, the SIT-5 propulsion system has advanced from a predesign concept to a performance qualified prototype device. Dynamic analysis and vibration testing have confirmed the structural integrity of the design and established the system's capability to survive booster launch. Performance testing with a dielectric coated grid has demonstrated operation at very low specific impulse ($I_{sp,eff}$ = 1665 sec) with an over-all efficiency η_T = 26%. Similarly efficient operation (η_T = 29.8%) with high-angle (±10°) beam deflection grids at $I_{sp,eff}$ = 2220 sec demonstrates the systems capability for attitude control and station keeping of synchronous satellites.

SYMBOLS

MAJOR SYMBOLS

e	=	Charge on an electron, 1.6×10^{-19} coulombs
F	=	Mercury flow, mA/hour
G	=	Gravitational acceleration, 9.8 m sec^{-2}
I	=	Current, A
$I_{sp,eff}$	=	Effective specific impulse, sec
ℓ	=	Separation between the cathode and collector, cm
P	=	Power, W
t	=	Time, hr
T	=	Temperature, °C
V	=	Voltage, V
X Y Z	=	Spatial coordinates
η	=	Efficiency, a pure number

SUBSCRIPT REFERENCE SYMBOLS

Ac	=	Accel
B	=	Beam
C	=	Coupling
CH	=	Cathode Heater
D	=	Discharge
Disch	=	Discharge per beam ion
E	=	Electrical
H	=	Heater
Hg	=	Mercury

ISOL	=	Isolator
K	=	Keeper
m	=	Mass
M	=	Main CIV subassembly
N	=	Neutralizer NV subassembly
P	=	Vacuum pressure, Torr
T	=	Total
t	=	Tube
V	=	Vaporizer
VH	=	Vaporizer heater

REFERENCES

1. W.R. Kerslake, D.C. Byers, and J.F. Staggs, "SERT II Experimental Thruster System," AIAA Paper No. 67-700 (1967).

2. D.C. Byers and J.F. Staggs, "SERT II Flight-Type Thruster System Performance," AIAA Paper No. 69-235 (1969).

3. H.J. King, C.R. Collett, and D.E. Schnelker, Thrust Vectoring System Part I-5 cm Systems, Final Report, Contract NAS 3-14058 (NASA CR-72877) Hughes Research Laboratory, Malibu, California (1971).